Crosstalk and Signal Integrity in Ring Resonator Based Optical Add/Drop Multiplexers for Wavelength-Division-Multiplexing Networks

by

Riyadh Dakhil Mansoor, B.Eng, M.Sc, MIET.

School of Engineering and Sustainable Development

De Montfort University

A thesis submitted in partial fulfilment of the requirements for the degree of

Doctor of Philosophy

July 2015

***To my family*.**

ABSTRACT

With 400 Gbps Ethernet being developed at the time of writing this thesis, all-optical networks are a solution to the increased bandwidth requirements of data communication allowing architectures to become increasingly integrated. High density integration of optical components leads to potential 'Optical/Photonic' electromagnetic compatibility (EMC) and signal integrity (SI) issues due to the close proximity of optical components and waveguides. Optical EMC issues are due to backscatter, crosstalk, stray light, and substrate modes. This thesis has focused on the crosstalk in Optical Add/Drop Multiplexers (OADMs) as an EMC problem.

The main research question is: "How can signal integrity be improved and crosstalk effects mitigated in small-sized OADMs in order to enhance the optical EMC in all-optical networks and contribute to the increase in integration scalability?" To answer this question, increasing the crosstalk suppression bandwidth rather than maximizing the crosstalk suppression ratio is proposed in ring resonator based OADMs. Ring resonators have a small 'real estate' requirement and are, therefore, potentially useful for large scale integrated optical systems.

A number of approaches such as over-coupled rings, vertically-coupled rings and rings with random and periodic roughness are adopted to effectively reduce the crosstalk between 10 Gbps modulated channels in OADMs. An electromagnetic simulation-driven optimization technique is proposed and used to optimize filter performance of vertically coupled single ring OADMs. A novel approach to analyse and exploit semi-periodic sidewall roughness in silicon waveguides is proposed. Grating-assisted ring resonator design is presented and optimized to increase the crosstalk suppression bandwidth.

Approval Page

This is to certify that the work in this thesis consists of original work undertaken solely by myself. Information taken from the published work of others has been properly referenced. The material described in this thesis has not been submitted for the award of a higher degree or qualification in any other university.

Riyadh Mansoor

Leicester, 2015

ACKNOWLEDGEMENTS

First and foremost, I am grateful to Almighty God for enabling me to continue with this hard journey.

A debt of gratitude must be paid to my supervisor ***Prof. Alistair Duffy*** for his support during the course of my PhD and for knowing when to direct me and when to let me go my own way.

I would also like to thank Dr. Hugh Sasse, Dr. Mohammed Al-Asadi and Dr. Stephen Ison for their good humoured assistance throughout the course of the project. I want to extend my thanks to Prof. Slawomir Koziel from Reykjavik University for his wonderful collaboration and support for the optimization of vertical model. Thank and gratitude to Prof. Melloni and Dr. Daniele from the Politecnico di Milano/ Italy for sharing their simulator for validation.

I gratefully acknowledge the funding source that facilitated my PhD work. I would like to express my deep gratitude to the Ministry of Higher Education and Scientific Research/ Iraq, the Iraqi cultural attaché /London and the Ministry of Industry and Minerals /Iraq for their support.

Last, but not the least, I am very thankful to my parents, my wife (Shafaq) and my lovely kids for their support and patience throughout the duration of my PhD.

TABLE OF CONTENTS

ABSTRACT ..... **II**

ACKNOWLEDGEMENTS ..... **IV**

LIST OF TABLES ..... **IX**

LIST OF FIGURES ..... **X**

LIST OF ABBREVIATIONS ..... **XIV**

LIST OF PUBLICATIONS ..... **XVI**

CHAPTER ONE **INTRODUCTION** **1**

1.1. Motivations 1

1.2. All-Optical Networks 6

1.3. Aims and Objectives 9

1.4. New Contributions to Knowledge 10

1.5. Outline of the Thesis 11

CHAPTER TWO **CROSSTALK IN ALL-OPTICAL NETWORKS** **12**

2.1. Introduction 12

2.2. Optical Crosstalk 14

2.2.1. Classification of Crosstalk 14

2.2.2. Modelling of Crosstalk 17

2.3. Crosstalk In Optical Add/Drop Multiplexers 19

2.3.1. Array Waveguide Grating Based OADM 20

2.3.2. Fibre Bragg Grating Based OADM 21

CONTENTS **Page**

2.3.3. Ring Resonator Based OADM 23

2.4. Crosstalk Modelling in Ring Resonator Based OADMs 24

2.4.1. Inter-Band Crosstalk 24

2.4.2. Intra-Band Crosstalk 26

2.5. Mitigation of Crosstalk in Ring Resonator Based OADMs 30

2.6. Conclusion 34

CHAPTER THREE **OPTICAL RING RESONATORS 35**

3.1. Introduction 35

3.2. Ring Resonators 37

3.3. SOI Strip Waveguides 42

3.3.1. Dispersion, Effective Refractive Index and Group Index 43

3.3.2. Directional Coupler 44

3.4. CST Microwave Studio 47

3.5. Coupling in Ring Resonators 49

3.5.1. Lateral Coupling 49

3.5.2. Vertical Coupling 50

3.6. Cascaded Coupled Ring Resonators. 51

3.6.1. Series Coupling 51

3.6.2. Parallel Coupling 53

3.7. Optical Add/Drop Multiplexer 54

3.8. Conclusion 59

CHAPTER FOUR **OVER-COUPLED RING RESONATOR BASED OADM....60**

4.1. Introduction 60

4.2. Crosstalk Bandwidth in a Single Ring Resonator 63

4.2.1. CST Simulation 64

4.2.2. Analytical Calculations 65

4.3. Crosstalk Bandwidth in Double Ring Resonator 70

4.4. Conclusion 79

CHAPTER FIVE **CROSSTALK BANDWIDTH ESTIMATION OF PARALLEL COUPLED OADM.....81**

5.1. Introduction 81

5.2. Mason's Rule for Parallel Coupled Ring Resonators 83

5.3. CST Simulation 91

5.4. Analytical and Simulation Results 94

5.5. Conclusion 99

CHAPTER SIX **VERTICALLY COUPLED RING RESONATOR OADM 101**

6.1. Introduction 101

6.2. Crosstalk Suppression: Analytical and Simulation Model 103

6.2.1. Analytical Model 103

6.2.2. CST Simulation 106

6.3. Crosstalk Suppression Bandwidth 109

6.4. Optimization Method 110

6.5. Conclusion 116

CHAPTER SEVEN **GRATING-ASSISTED RING RESONATOR OADM 117**

7.1. Introduction 117

7.2. Coupled Mode Analysis 120

7.2.1. Time Domain Analysis 120

7.2.2. Space Domain Analysis 125

7.3. CST Validation 129

7.4. Controllable Reflectivity 134

7.5. Grating-Assisted Single Ring 140

7.6. Conclusion 144

CHAPTER EIGHT **CONCLUSIONS AND FUTURE WORK 145**

8.1. Conclusions 145

8.2. Suggestions for Future Work 150

REFERENCES 152

APPENDICES 173

Appendix A: **SFG METHOD FOR PARALLEL COUPLED OADMS** 173

Appendix B: **RUBY CODE FOR SIDEWALL ROUGHNESS GENERATION**. 176

LIST OF TABLES

TABLE **Page**

4-1. The relation between the inner and outer coupling coefficients for optimum coupling. 71

4-2. Inter-ring coupling coefficients for over-coupling. 77

6-1. Optimization results 113

LIST OF FIGURES

FIGURE **Page**

1-1. All-optical communication [27]..... 7

1-2. Size reduction of PLC's (series coupled ring resonator (left), PLC chip (centre) and a silicon wafer with hundreds of chips (right) [6]. 8

2-1. An explanation of crosstalk components in the cross connector [56]. 16

2-2. Crosstalk in OADM. 16

2-3. a. Array Waveguide Grating. b. The N channels AWG based OADM [66]. 21

2-4. Fibre Bragg Grating based OADM [54]. 22

2-5 a. Ring resonator add/drop filter. b. Racetrack resonator based OADM. 23

2-6. Drop port response for single (solid) and double (dashed) ring resonators. 26

2-7. Crosstalk suppression of a single ring resonator OADM. 28

2-8. Power penalty as a function of crosstalk suppression ratio. 29

3-1. A schematic diagram of a ring resonator based all-pass filter. 38

3-2. Different geometries of SOI directional couplers. 45

3-3. CST simulations of the fundamental TE like mode distribution at the input port of a single ring OADM 49

3-4. Laterally coupled ring resonator. 50

3-5. Vertical coupled ring resonator. 51

3-6. The schematic of N-series coupled ring resonator. 53

3-7. The schematic of N-parallel coupled ring resonator. 54

3-8 Schematic diagram of the ring resonator based OADM. 55

3-9 CST simulated frequency response of a single ring resonator based OADM. 59

FIGURE **Page**

4-1. Analytically calculated drop port response of a series coupled RR, with a study of the inter-ring coupling ($\boldsymbol{k_i}^2$) effect on the resonance splitting. 62

4-2. Schematic of a single ring add/drop filter with three NRZ of 10 Gbps modulated WDM signal. 64

4-3. Frequency response of a single ring resonator. 65

4-4. Bandwidth of crosstalk suppression and DPRR for a single ring resonator. 67

4-5. Bandwidth for asymmetric single ring resonator as a function of coupling coefficients. 69

4-6. Bandwidth of a symmetric single ring resonator as a function of coupling coefficient and losses. 69

4-7. The schematic of a series double ring resonator add/drop filter with 10 Gbps RZ WDM signal. 72

4-8. a) Frequency response for series double ring resonator. b) Spectrum splitting at resonance for series double ring resonator. 75

4-9. Bandwidth of crosstalk suppression and drop port rejection ratio for critical and over coupled double ring resonator (losses =4 dB/cm). 78

4-10. Bandwidth of the over coupled ring resonator as a function of losses for different coupling coefficient. 79

5-1. CST model of parallel coupled ring resonator. 84

5-2. Forward paths. 86

5-3. Closed loops. 87

5-4. Analytically calculated spectral response for a 0.05 coupling. 90

5-5. The model sensitivity for different coupling coefficients. 91

5-6. CST simulation of a symmetric parallel coupled ring resonator for optimum separation (a) and half resonator length (b). 93

5-7. The OBRR sensitivity to the coupling coefficients. 95

5-8. Coupling coefficient effects on the level of crosstalk suppression. 95

5-9. Crosstalk as a function of losses. 96
5-10. Crosstalk as a function of coupling coefficients. 97
5-11. Crosstalk bandwidth for an optimal coupling coefficient of 0.05, calculated using CST MWS. 98
5-12. Crosstalk bandwidth for a 0.06 coupling coefficient calculated using CST MWS. 99
6-1. (a) Vertical coupled ring resonator. (b) Cross section of the bent and bus waveguides. 104
6-2. CST model of a vertically coupled ring resonator OADM. 106
6-3. The spectral response of CST simulated ring resonator OADM. 107
6-4. Through port, Drop port, and out of band rejection ratio (OBRR) of the ring resonator as a function of vertical separation for optimized offset (a). 108
6-5. Analytically calculated crosstalk suppression bandwidth as a function of coupling coefficient. 110
6-6. Initial (thin lines) and optimized (thick lines) responses for design case (i) (two design variables): (a) |S21| and |S31| for 190.5 to 193.5 THz range, (b) magnification around 191 THz. Optimized 20dB-bandwidth is 19.8 GHz. 114
6-7. Initial (thin lines) and optimized (thick lines) responses for design case (ii) (four design variables): (a) |S21| and |S31| for 190.5 to 193.5 THz range, (b) magnification around 191THz. Optimized 20dB-bandwidth is 21 GHz. 115
7-1. Forward and backward modes in a rough-walled ring resonator add/drop filter. 121
7-2. The schematic diagram of a rough-walled ring resonator (a), and its equivalent structure (b). 126

FIGURE **Page**

7-3. a. Ring resonator response analytically modelled using time and space models. b. Experimental (line) and analytical (dot) results presented in [111]. 129

7-4. CST model of sidewall roughness in a single ring resonator add /drop filter. 130

7-5. CST frequency response of a rough-walled Ring Resonator. 131

7-6. CST (solid) and analytically (dotted) modelled spectral response for a rough-walled ring resonator. 132

7-7. The effect of back-reflection coefficient on the through and drop port response. 133

7-8. Single (a), and double (b) gratings. 134

7-9. Grating length effect on the reflectivity for L1=6500 nm, L2= 13000 nm and L3= 19500 nm. 136

7-10. The grating period effect on the reflectivity. 137

7-11. Changing the reflectivity with increasing the number of gratings. 138

7-12. Aspic model for three gratings (a), and the reflectivity as a function of wavelength (b) for single grating (blue), double gratings (green) and three gratings (red). 139

7-13. The effect of separation between gratings for three gratings. 140

7-14. a. The spectral response of a single ring resonator (using optimized parameters that maximize crosstalk bandwidth), b. Schematic of a grating-assisted OADM. 143

7-15. The three port response for a grating assisted ring resonator (ASPIC simulated results). 143

LIST OF ABBREVIATIONS

AWG	Array Waveguide Grating.
BER	Bit-Error-Rate.
CW	Continuous Wave.
EM	Electromagnetic.
EMC	Electromagnetic Compatibility.
FBG	Fibre Bragg Grating.
FD	Frequency Domain.
FSR	Free Spectral Range.
FWHM	Full Width at Half Maximum.
InP	Indium Phosphide.
NRZ	Non return-to-zero pulse.
OADM	Optical Add/Drop Multiplexer.
OEO	Optical –Electronic-Optical conversion.
OXC	Optical cross-connector.
PLCs	Planar Lightwave Circuits.
Q-factor	Quality factor.

ROAD	Reconfigurable Optical Add/Drop Multiplexer.
RZ	Return-to-zero pulses.
SI	Signal Integrity
Si	Silicon.
SiO_2	Silicon Dioxide.
SOA	Semiconductor Optical Amplifier.
SOI	Silicon On Insulator.
TD	Time Domain.
TE	Transverse electric.
TM	Transverse magnetic.
WDM	Wavelength Division Multiplexing.

LIST OF PUBLICATIONS

1. Journal papers

[P1] **R. D. Mansoor**, H. Sasse, M. A. Asadi, S. J. Ison and A. Duffy, "Over Coupled Ring Resonator-Based Add/Drop Filters," Quantum *Electronics, IEEE Journal Of*, vol. 50, pp. 598-604, 2014.

[P2] **R. D. Mansoor**, H. Sasse, S. Ison and A. Duffy, "Crosstalk bandwidth of grating-assisted ring resonator add/drop filter," *Optical and Quantum Electronics*, vol.47, no.5, pp.1127-1137, 2015.

[P3] **R. D. Mansoor**, S. Koziel*, H. Sasse, and A. Duffy,"Crosstalk Suppression Bandwidth Optimization of a Vertically Coupled Ring Resonator Add/Drop Filter," *IET Optoelectronics*, vol.9, no.2, pp.30-36, April, 2015.

[P4] **R. D. Mansoor**, H. Sasse, M. A. Asadi, S. J. Ison and A. Duffy, "Estimation of the Bandwidth of Acceptable Crosstalk of Parallel Coupled Ring Resonator Add/Drop Filters," *Transactions on EMC, IEEE Journal of, June, 2015*. DOI: 10.1109/TEMC.2015.2432914

[P5] **R. D. Mansoor**, H. Sasse and A. Duffy, "Optimization of Reflection Coefficient in Ring Resonator Add/Drop Filters", *International Journal of Numerical Modelling: Electronic Networks, Devices and Fields, 2015.* DOI: 10.1002/jnm.2080.

[P6] **R. D. Mansoor**, H. Sasse and A. Duffy, "Modified Crosstalk suppression bandwidth Single Ring Resonator Optical Add/Drop filter", *submitted for publication.*

- S. Koziel is a professor of engineering optimization at Reykjavik University; he helped with the preparing of the objective function and performing the optimization using fast computers in his lab. H.Sasse provided technical and research support. Other co-authors are with the supervision team.

2. Conference papers

[P7] **R. D. Mansoor**, S. Ison, H. Sasse and A. P. Duffy, "Impact of crosstalk in all optical networks," *Proceedings of the 61st IWCS Conference*, pp. 849-855, Rhode Island, USA, 2012.

[P8] **R. D. Mansoor**, H. Sasse and A. P. Duffy, "Analysis of Optical Ring Resonator Add/Drop Filters," *Proceedings of the 62nd IWCS Conference*, pp. 471-475, Charlotte, USA, 2013.

[P9] **R. Mansoor**, H. Sasse, S. Ison, and A. Duffy, "Modelling of Back Reflection in Optical Ring Resonators," *IEEE International Conference on Numerical Electromagnetic Modelling and Optimization for RF, Microwave, and Terahertiz Applications* (*NEMO*), Pavia, Italy, 2014.

[P10] **R. Mansoor**, H. Sasse, and A. Duffy, "Optimization of Vertically Coupled Add/Drop Ring Resonator Based Filter," *Proceedings of the Semiconductor and Integrated OptoElectronics (SIOE) Conference*, Cardiff, UK, 2014.

[P11] **R. Mansoor**, H. Sasse, and A. Duffy, "Modelling of A Roughened Sidewall Ring Resonator Add/drop Filter," *Proceedings of the XXII International Workshop on Optical Wave & Waveguide Theory and Numerical Modelling (OWTNM)*, Nice, France, 2014.

[P12] **R. Mansoor**, H. Sasse, and A. Duffy, "Enhancing the depth notch using a rough-walled SOI ring resonator" *IEEE Optical Interconnects*, San Diego, California, USA, 2015.

[P13] **R. Mansoor**, A. Duffy, "Review of Progress in Optical Ring Resonators with Crosstalk Modelling in OADMS" *the 64th IWCS conference*, Atlanta, USA, 2015.

[P14] **R. Mansoor**, M. Al-Asadi, and A. Duffy, "Optical Ring Resonator Add/Drop Filters", *Derby Electrical and Electronic Research Showcase (DEERS)*, Derby, UK, 2015.

CHAPTER ONE

INTRODUCTION

This chapter introduces the basic definition of 'Optical/Photonic' EMC and explains why it is of relevance in all-optical networks. Issues related to the performance of optical nodes and integration solutions are discussed; research outcomes and an outline of the rest of the thesis are provided.

1.1. Motivations

Optical Ethernet is a combination and extension of two existing technologies, Ethernet and Optical communication technology [1]. Ethernet started in 1973 with the aim of connecting personal computers, printers, and servers within copper local area networks LANs [2]. The optical Ethernet in the First Mile (EFM) was introduced in IEEE standard 802.3ah in 2001 for 1 Gbps transmission [3]. The Ethernet Passive Optical Network (EPON) was launched in 2010 as IEEE Standard 802.3av for 10 Gbps [4]. The IEEE Standard Project P802.3bs extending the bandwidth to 400 Gbps was proposed in 2013 and was intended to meet the increased requirements of multimedia communications and other data-dense applications such as large CAD file sharing [5].

Nowadays, telecommunications companies are increasingly focusing on more integrated solutions to cope with increased data transmission [6]. However, the integrated solutions to meet optical network requirements are subject to many factors that affect signal integrity, such as crosstalk and backscattering [7-10]. In view of this trend in all-optical networks, where competition in integration density and signal integrity is the driving force, there will be an increasing demand to address these issues of Optical/Photonic "EM Compatibility" especially in large scale integration technologies.

Electromagnetic Compatibility (EMC) is frequently described as being a "DC to light" phenomenon. EMC is defined by the International Electrotechnical Commission IEC as "The ability of a device, unit of equipment or system to function satisfactorily in its electromagnetic environment without introducing intolerable electromagnetic disturbances to anything in that environment" [11]. However, it is only with the move to increasingly all-optical networks that EMC of optical communications systems becomes a topic worth special attention in its own right. In this research, EMC is of relevance because add/drop multiplexers and filters are used to introduce and remove channels in Wavelength-Division Multiplexing nodes. Non-ideal behaviour can lead to the introduction of troublesome crosstalk between the dropped and added channels, with resulting increases in Bit Error Rate (BER) and loss of signal integrity [12]. By definition, "integrity" means "unimpaired and complete". Therefore, an optical signal with good integrity has a clean spectrum with a high suppression for unwanted channels.

Optical EMC issues are due to crosstalk, backscatter, stray light, and substrate modes that can no longer be regarded as negligible, especially in large scale integration technologies. Photonic integrated circuits are fabricated by combining optical waveguides closely in a single chip. Interconnections (optical waveguides) affect signal integrity due to light leakage between waveguides and are becoming a serious problem [13, 14]. Therefore, a high level of isolation is needed since all channels are processed simultaneously on chip [15], and just as in electronics, EMC issues that can disturb the operation of the PLC should be considered [7].

In this thesis, the topic of "Optical" EMC is approached by studying the crosstalk in all-optical networks; in the particular case of optical ring resonator based add/drop multiplexers (OADMs) and filters. Ring resonator based OADMs and filters are playing an important role in increasing the flexibility of Wavelength-Division Multiplexing (WDM) networks by allowing the insertion and dropping of wavelength channels [16, 17].

Ring resonators are key components in modern all-optical networks [18]. Their small size allows high density integration in optical/ Photonic circuits due to the use of high index contrast materials and the availability of CMOS fabrication facilities [19, 20]. Coupling a closed loop resonator with bus waveguides through the evanescent mode coupling leads to filter behaviour of the resulting structure. However, like any other optical filters, ring resonator based OADMs are prone to crosstalk. Inter and Intra-band crosstalk in ring resonator based OADMs result from the non-ideal dropping of channels [21]. The dropped

channel will be corrupted by the residual of a new added channel (intra-band crosstalk). Inter-band crosstalk also occurs due to the adjacent channels in a WDM signal [22].

Crosstalk in ring resonator based OADMs was mitigated by improving filter response using high order filters and increased notch depth in the through port response [23-26]. Increasing filter order (number of rings) or connecting different OADMs, giving a multi-stage structure, results in a reduction in the inter-band crosstalk. However, filter size will increase, conflicting with the goal of greater device density. While, increasing the notch depth by optimizing coupling coefficients (to mitigate the intra-band crosstalk) will only increase the crosstalk suppression ratio in a narrow band of frequencies at resonance. For modulated channels this implies that the side-bands will get different levels of suppression from that of the centre frequency. Each channel in WDM networks is modulated with different information [27]. For example, for 10 Gbps non return-to-zero (NRZ) transmission, the required bandwidth is 20 GHz [24]. Therefore, it is required to maintain a high level of crosstalk suppression ratio for a 20 GHz bandwidth in order to maintain signal integrity of the added/dropped channels.

Based on the calculations in [23, 28] it was shown that a level of $|20|$ dB for the crosstalk suppression ratio represents a sufficient level for acceptable BER and signal integrity. Therefore, this thesis suggests that increasing the crosstalk suppression bandwidth will allow for adding/dropping of modulated channels with equal level of crosstalk suppression over the whole side-bands and leading to an effective reduction in the crosstalk between the

channels in OADMs and filters. The crosstalk suppression bandwidth is defined as the bandwidth over which the level of crosstalk suppression is maintained at $\geq |20|$ dB.

In this thesis, a number of approaches are adopted in order to increase the crosstalk suppression bandwidth in small-sized OADMs. Analytical and numerical models are used to optimize coupling coefficients in laterally coupled rings (series and parallel double rings) and a vertically coupled (single) ring resonator based OADMs in order to achieve high crosstalk suppression bandwidth. Sidewall roughness in a single ring resonator is also exploited to improve signal integrity by increasing the crosstalk suppression bandwidth. A proper investigation of these methodologies is presented in the following chapters.

Hence, the motivations behinds this research can be summarised as follows:

1. Optical communication is an extremely fast growing technology, driven mainly by the increasing need for global expansion of the internet and, in particular, multimedia communications and other data-dense applications.

2. The need for high integration density and fabricating small components with high scalability to cope with increased demand for data transmission.

3. The integrated solutions to meet optical network requirements are prone to many factors that affect signal integrity, such as backscatter, crosstalk, stray light, substrate modes. The optical/Photonics community deals with many of the key issues, but do not specifically think of this as EMC and the EMC community has studied many of these issues, but not at optical frequencies. So, while this thesis presents a number of novel

contributions to the technology, it also aims to help provide a link between these discipline areas.

1.2. All-Optical Networks

Fibre optic communication systems can exploit the large bandwidth of optical fibres defined by the low propagation loss [29, 30] (14 THz at 1.33 μm and 15 THz at 1.55 μm). However, using a single wavelength channel to exploit this huge bandwidth is impractical due to amplifying and switching bottlenecks. The advent of Wavelength-Division Multiplexing (WDM) has had a major impact on the evolution of high transmission rates and low cost networks [31, 32]. WDM is a technique that employs many closely spaced optical-frequency wavelengths to transmit multiple data signals [27, 33].

In WDM networks, a number of nodes are required to provide switching, routing, and adding/dropping of channels [34]. Optical nodes in the first generation of WDM networks were based on Optical-Electrical-Optical (OEO) conversion for each wavelength, regardless of whether the wavelength would be dropped at this node or would pass through [29, 35]. The drawbacks of the OEO process are the cost, space requirements, and power consumption, especially for long distances and high capacity networks [31].

The fabrication of new optical components such as Optical Add/Drop Multiplexers (OADM) [16], Optical Cross-Connecters (OXC) [36] and amplifiers [37] had led to the second generation of WDM networks (All-optical or transparent networks) as shown in Figure 1-1. All-optical networks have emerged as a solution to keep up with the increasing

throughput demand. With all-optical networks, the transmitted signals are treated completely in the optical domain [38]. Therefore, bottlenecks presented by OEO conversion have been eliminated, allowing for higher data rate transmission using different signal formats [33, 39].

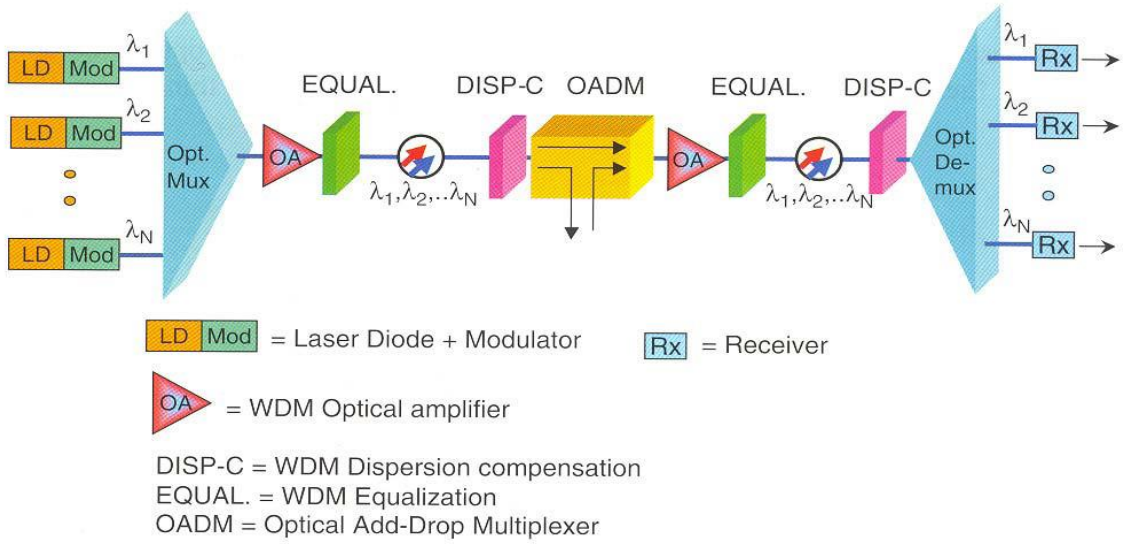

Figure 1-1. All-optical communication [27].

Optical nodes in the early all-optical networks were realized by using a hybrid technology, where each component was fabricated separately and then connected together [40, 41]. This resulted in large size and high cost optical nodes. The second generation of optical nodes combined a high number of optical functions in a single integrated device. A similar approach to that used for electronic integrated circuits was suggested [42]. This approach had a lot of advantages over the hybrid one, especially in terms of functionality and cost reduction. A number of devices per chip were fabricated [43, 44]. The drawback of this

technology was the integration complexity and the difficulty of scaling to meet the network growth.

Planar Lightwave Circuits PLCs were introduced [6] to reduce cost and complexity and, at the same time, improve the scalability of optical networks. Silicon-On-Insulator (SOI) technology [45] offers strong confinement of light in a small size optical waveguide, which makes it of great interest in the fabrication of PLCs. Figure 1-2 shows the size reduction obtained with PLCs made using SOI and explains how a large number of optical devices are integrated in a single silicon wafer. However, the increasing levels of integration, greater data rate and greater bandwidth requirements mean that the limiting factors are getting similar to those faced in electronic circuits and, hence, "Photonic EMC" is worthy of study and interest.

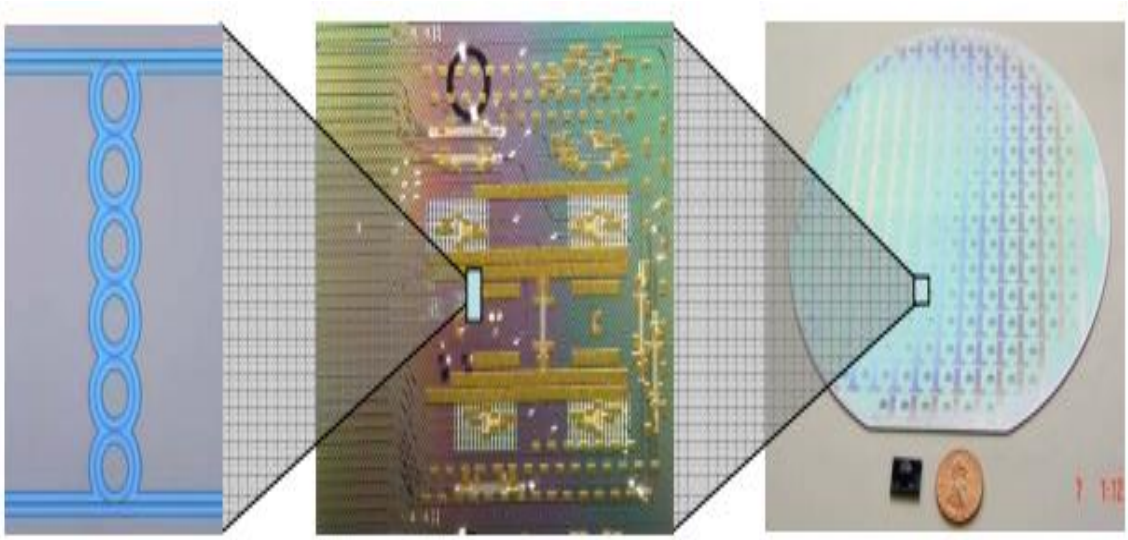

Figure 1-2. Size reduction of PLC's (series coupled ring resonator (left), PLC chip (centre) and a silicon wafer with hundreds of chips (right) [6].

1.3. Aims and Objectives

- This thesis aims to:

1. Introduce "Photonic" EM Compatibility.

2. Mitigate the crosstalk effect and improve signal integrity in ring resonator based OADMs by increasing the crosstalk suppression bandwidth.

3. Reduce filter size and contribute to the increase in integration scalability.

- The objectives are:

1. To exploit the resonance splitting that occurs due to the inter-ring coupling coefficients in a series coupled OADM.

2. To enhance the crosstalk suppression bandwidth by optimizing ring parameters in a parallel coupled OADM.

3. To optimize ring parameters of a vertically coupled OADM in order to increase the crosstalk suppression bandwidth in a small-sized OADM.

4. To exploit the resonance splitting induced by sidewall roughness in rough-walled ring resonators to maximize the crosstalk suppression bandwidth.

By following the above objectives, a number of novel designs and models are obtained, as listed in the next section.

1.4. New Contributions to Knowledge

The main contributions of this thesis are as follows:

1. The over-coupling condition between the inter-rings in series coupled ring resonators OADMs is proposed. Over-coupling, simultaneously, improves the bandwidth and the level of inter-band crosstalk suppression, and allows for high data rate signal dropping compared to critically coupled OADMs.

2. A general form of the transfer function of parallel coupled ring resonator OADMs is derived using the Signal Flow Graph method (based on Mason's rule). The use of Mason's rule in this regard is novel and useful. The derived model provides an accurate starting point for design and analysis and, in doing this, provides a better insight into the filter performance.

3. An electromagnetic simulation-driven optimization technique is proposed and used to improve the crosstalk suppression bandwidth of a vertically coupled ring resonator based OADM.

4. A novel design of grating-assisted ring resonator is proposed to increase the crosstalk bandwidth compared to the smooth-walled ring OADM. A general model for a rough-walled ring resonator is derived using the time and space domain Coupled Mode Theory.

1.5. Outline of the Thesis

The remainder of this thesis is organised as follows:

Chapter 2 investigates crosstalk in all-optical networks; emphasis is given to the crosstalk in ring resonator based OADMs.

Chapter 3 provides a general background of optical ring resonators and presents their features in WDM networks.

Chapter 4 looks into crosstalk issues in series coupled ring resonator OADMs and examines the crosstalk performance as a function of the inter-ring coupling coefficients.

Chapter 5 examines the performance of parallel coupled ring resonators OADMs and focuses on the optical signal integrity perspective.

Chapter 6 proposes a design of small size vertically coupled ring resonator OADMs that provides an increased crosstalk suppression bandwidth.

Chapter 7 proposes a general solution for rough-walled ring resonators modelling, as well as a particular solution to maximize the crosstalk suppression bandwidth.

C**hapter 8** concludes the thesis with a summary of its main findings and recommendations for future work.

CHAPTER TWO

CROSSTALK IN ALL-OPTICAL NETWORKS

In this chapter, crosstalk and signal integrity issues in all-optical networks are introduced and discussed. A mathematical definition of crosstalk in optical cross-connectors and add/drop filters is presented. Two main topics are discussed: First, to increase the integration density in optical integrated circuits, ring resonators are good candidates due to their small size. Second, to improve the crosstalk performance in WDM networks, the crosstalk suppression ratio should be kept $\geq |20|$ *dB over a wide range of frequencies (covering the entire bandwidth of modulated dropped channels). This frequency range will be defined as the "crosstalk suppression bandwidth" throughout this thesis.*

2.1. Introduction

Wavelength-Division Multiplexing (WDM) systems transmit a number of channels at data rates of 10 Gbps or higher in each wavelength channel [27]. The number of transmitted channels is limited by the bandwidth of the optical devices used, such as optical amplifiers. In order to meet the required information capacity, these channels are allocated close to

each other (within the optical amplifier bandwidth). Passing the closely-spaced wavelength channels through optical devices such as filters and multiplexers will result in the occurrence of system impairments (linear crosstalk) [46, 47]. Other impairments, however, will occur due to the nonlinearity of the medium induced by the combined optical power of individual channels (nonlinear crosstalk). As a result, optical crosstalk represents a major limiting factor in WDM networks [48, 49].

Optical add/drop multiplexers OADMs and filters that drop one channel of WDM signal, without disturbing other channels, are essential elements in all-optical networks [50]. Ring resonator based OADMs are shown to be good candidates to realize integrated add/drop filters for WDM networks [24]. However, ring resonator based OADMs are prone to crosstalk. This chapter aims to:

1. Study the crosstalk in all-optical networks
2. Model the crosstalk in ring resonator based OADMs.

This chapter is organized as follows:

1. Crosstalk in all-optical networks is discussed and classified. A mathematical definition of the corrupted channels is presented.

2. Different OADMs structures are discussed and compared in terms of their size and crosstalk performance.

3. Crosstalk in ring resonator based OADMs is modelled and an overview of the current state of knowledge about mitigating crosstalk is presented.

This chapter suggests that maintaining an adequate level of crosstalk suppression ratio for a wide bandwidth (covering the side-bands of modulated channels) is of substantial importance to improve the overall performance in WDM networks.

2.2. Optical Crosstalk

2.2.1. Classification of Crosstalk

Crosstalk in all-optical networks can be classified as linear or nonlinear depending on the network topology and components used. In metropolitan and long-haul networks, optical fibre characteristics are strongly affected by the power and frequency of propagated WDM channels. Although the power in each channel of the WDM signal may be below that needed to produce fibre non-linearity, the total power summed over all channels can quickly become significant [51]. Nonlinearity causes inter-channel effects such as Self Phase Modulation (SPM) [52], Cross Phase Modulation (XPM) and Four Wave Mixing (FWM) [53].

In local area networks (LANs), which are used to transmit data over short distances, the effect of nonlinearity is less challenging. Linear crosstalk is the dominant type. Linear crosstalk results from non-ideal performance of WDM nodes. Two types of linear crosstalk are defined depending on the spectral location of crosstalk channels with respect to the pass-band of optical filters: In-band and out-of-band crosstalk [25]. Optical out-of-band crosstalk usually results from channels with spectra located out of the optical filter pass-band. It is also called inter-band crosstalk and appears between channels of different

wavelengths. The ability to suppress this type by using narrow-band filters makes it less harmful [24].

In-band (also called intra-band) crosstalk results from the residual of closely spaced channels (separated by Δf), where Δf is within the optical filter bandwidth. This type of crosstalk is more problematic and causes serious degradation of system performance due to the difficulty of removing it using optical filters. Furthermore, it will propagate with WDM channels along the network and the destructive effect of this type of crosstalk will be accumulated within each node it passes through [33, 47].

At the receiver side, the electrical filter bandwidth (B) will determine whether the intra-band crosstalk is electrically in-band ($\Delta f \leq B$), or out-of-band ($\Delta f > B$). The major limitation in the system performance in the presence of crosstalk will result mainly from electrical in-band crosstalk [34]. If $\Delta f = 0$ (the signal and crosstalk have the same nominal frequency), then the crosstalk will be homodyne [47]. Otherwise, if the signal and crosstalk have a closely spaced frequency, i.e. $\Delta f \neq 0$ but still less than the electrical bandwidth, the crosstalk will be heterodyne [54].

Optical cross-connectors [36, 55] and OADMs are essential elements in all-optical networks. Cross-connectors consist of channel selective components (multiplexers/de-multiplexers) and switching elements. Crosstalk in optical cross-connectors results from adjacent WDM channels (inter-band) and from the delayed version of the channel itself after travelling through different paths in the switching matrix (intra-band) as shown in

Figure 2-1. In OADMs, intra-band crosstalk results from the new added channels, while the inter-band crosstalk results from adjacent WDM channels as shown in Figure 2-2.

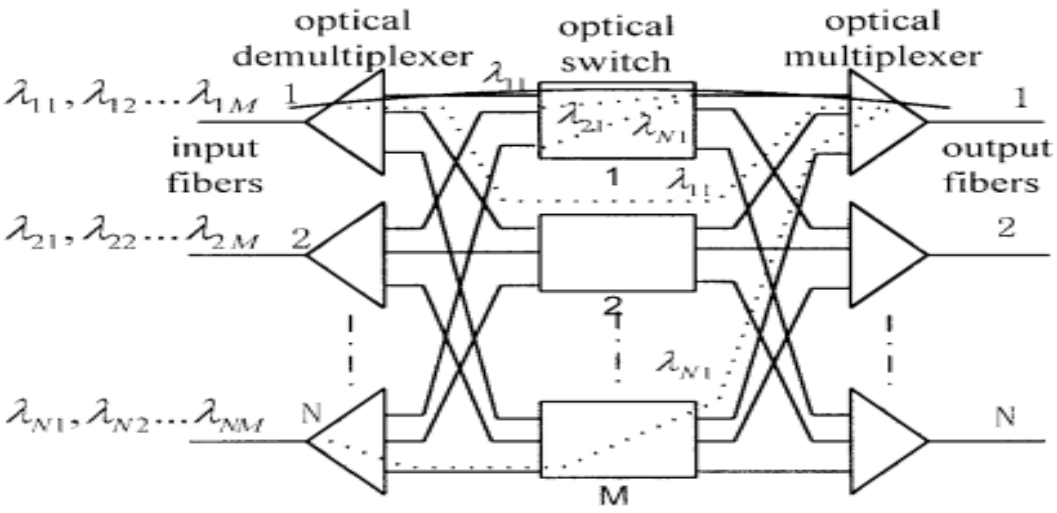

Figure 2-1. An explanation of crosstalk components in the cross connector [56].

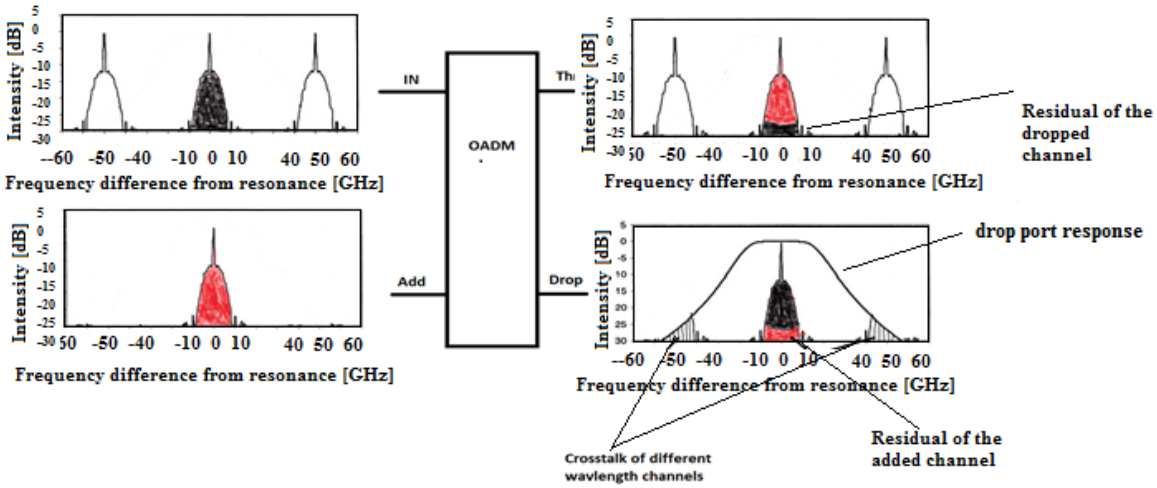

Figure 2-2 Crosstalk in OADM.

2.2.2. Modelling of Crosstalk

In this section, an optical system that uses on/off keying transmission is studied for crosstalk modelling [57]. The optical field can be considered as a continuous wave (CW) of the form:

$$\boldsymbol{E_s}(t) = \hat{\boldsymbol{r}}_s\sqrt{P_s}\, e^{(\mathrm{j}\omega_s \mathrm{t}+\mathrm{j}\emptyset_s(\mathrm{t}))} \qquad 2\text{-}1)$$

where, P_s the optical power, $\hat{\boldsymbol{r}}_s$ represents the state of polarization, ω_s is the CW frequency, and $\emptyset_s(t)$ is the instantaneous optical phase.

After the propagation of an optical signal in an all-optical network, many crosstalk terms will disturb it. The corrupted an optical field at the receiver input will be a combination of the desired signal and the intra-system noise and can be expressed as:

$$\boldsymbol{E_{ph}}(t) = \boldsymbol{E_s}(t) + \sum_k \boldsymbol{E_k}(t)$$

$$= \hat{\boldsymbol{r}}_s\sqrt{P_s}\, b_s(t)e^{(\mathrm{j}\omega_s \mathrm{t}+\mathrm{j}\emptyset_s(\mathrm{t}))} + \sum_{\mathrm{k}=2}^{\mathrm{N}} \hat{\boldsymbol{r}}_{\mathrm{k}}\sqrt{\epsilon_k P_s}\, b_k(t)e^{(\mathrm{j}\omega_{\mathrm{k}} \mathrm{t}+\mathrm{j}\emptyset_{\mathrm{k}}(\mathrm{t}))} \qquad (2\text{-}2)$$

where, $\epsilon_k = \frac{P_k}{P_s}$ is the power ratio of the kth crosstalk component to the dropped channel power, and N is the total number of channels in a WDM signal. $b_s(t)$ and $b_k(t)$ represents the binary symbols forming the amplitude modulating signal $\in \{0,1\}$.

The receiver in such systems consists of a photo-detector followed by an electrical filter and a decision (threshold) circuit [58, 59]. The photo-detector output current is proportional

to the square of the incident optical field. The output of an electrical filter is then compared with a decision threshold level (I_D) to decide whether a "1" or "0" state was sent. The power leakage from unwanted channels may lead to a "1" state at the receiver side while the transmitted signal is "0" or vice versa, with resulting increases in Bit Error Rate (BER) and loss of signal integrity.

The receiver photo-current can be written as:

$$i_{ph}(t) = \rho\left|\boldsymbol{E}_{ph}(t)\right|^2 = \rho\left|\boldsymbol{E}_s(t) + \sum_{k=2}^{N}\boldsymbol{E}_k(t)\right|^2 \tag{2-3}$$

where ρ represents the photodiode responsitivity and it will be considered equal to unity for simplicity. The general form of the photo-current will consists of four terms [58], as below:

1. Signal power term $[P_s b_s(t)]$.
2. Crosstalk power term $[\, P_s \sum_{k=2}^{N} b_k(t)\, \epsilon_k]$.
3. Signal-crosstalk beating term

$$\left[2P_s \sum_{k=2}^{N} \hat{\boldsymbol{r}}_s \cdot \hat{\boldsymbol{r}}_k \sqrt{\epsilon_k}\, b_k(t) b_s(t) \cos[(\omega_s - \omega_k)\mathrm{t} + \emptyset_s(\mathrm{t}) - \emptyset_k(\mathrm{t})]\right]$$

4. Crosstalk-crosstalk beat noise term, which is of less importance in the study of the system performance in terms of crosstalk impairment [60].

$$\left[2P_s \sum_{k=2}^{N-1} \sum_{l=k+1}^{N} \hat{\boldsymbol{r}}_k \cdot \hat{\boldsymbol{r}}_l \sqrt{\epsilon_k \epsilon_l}\, b_k(t) b_l(t) \cos\big((\omega_k - \omega_l)t + \emptyset_k(t) - \emptyset_l(t)\big)\right]$$

The total current can be written as in (2-4) below:

$$i_{ph}(t) = P_s \Bigg[b_s(t) + \sum_{k=2}^{N} \epsilon_k b_k(t) + 2 \sum_{k=2}^{N} \hat{\boldsymbol{r}}_s \cdot \hat{\boldsymbol{r}}_k \sqrt{\epsilon_k}\, b_k(t) b_s(t) \cdot \cos[(\omega_s - \omega_k)\mathrm{t} + \emptyset_s(\mathrm{t}) - \emptyset_k(\mathrm{t})] + 2 \sum_{k=2}^{N-1} \sum_{l=k+1}^{N} \hat{\boldsymbol{r}}_k . \hat{\boldsymbol{r}}_l \sqrt{\epsilon_k \epsilon_l} \cdot b_k(t) b_l(t) \cos[(\omega_k - \omega_l)t + \emptyset_k(\mathrm{t}) - \emptyset_l(\mathrm{t})] \Bigg] \quad (2\text{-}4)$$

The most important crosstalk contribution is the signal-crosstalk beating term which can be considered as a random variable in term of the phase [61].

2.3. Crosstalk In Optical Add/Drop Multiplexers

Optical add/drop multiplexers OADMs can be found either in a fixed or reconfigurable mode of operation [62]. In a Reconfigurable-OADM (ROADM), the dropped wavelength can be adjusted based on the network requirements [63]. The crosstalk in ROADM results from the presence of switches that perform the reconfiguration. Passive or fixed OADMs are used to add/drop a preselected wavelength in the WDM node. No switches are required, and each node will be used to add/drop a specific wavelength. Crosstalk in this configuration results from the non-ideal separation between channels. Different types of OADM are used in WDM nodes [64]. A comparison between the three major structures, in terms of signal integrity and integration scalability, is presented in this section.

2.3.1. Array Waveguide Grating Based OADM

Array Waveguide Gratings (AWGs) [65], shown in Figure 2-3 a, are planar devices with an array of waveguides that perform multiplexing and de-multiplexing of WDM channels. Crosstalk in the AWG based OADM results from incomplete suppression of neighbouring channels during de-multiplexing (in the first free propagation region− input slab) and multiplexing (second free propagation region−output slab). An optical add/drop multiplexer based on AWG is shown in Figure 2-3 b.

In Figure 2-3 b, m channels are added/dropped and n channels are passed ($m + n = N$), where N is the total number of channels in the input fibre. In this design, an AWG is used to perform both de-multiplexing and multiplexing functions in the OADM [66]. In this structure, each dropped channel λ_d will be corrupted by three different crosstalk contributions:

1. $(N - 1)$ channels from the network (inter-band crosstalk)

2. m −added channels (intra-band crosstalk).

3. n −pass channels (this will be a combination of inter and intra-band crosstalk).

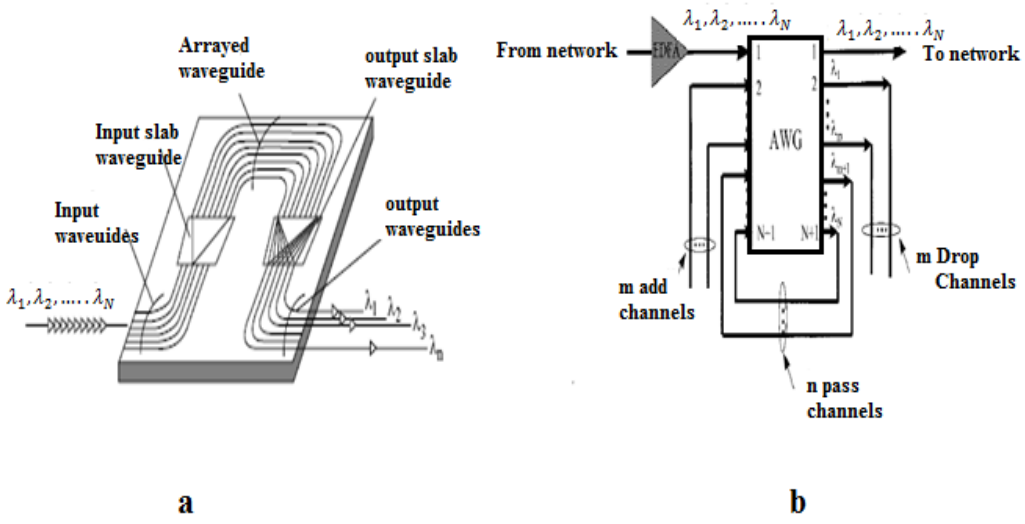

Figure 2-3. a. Array Waveguide Grating. b. The N channels AWG based OADM [66].

The delayed versions of the dropped channel, which are leaked to the n pass signals, will be added again with the dropped channel and this will lead to an increase in the intra-band crosstalk [66]. The drawbacks of AWG based OADMs can be summarized as:

1. Integration scalability is limited by the leakage between channels due to the close spacing between waveguides.
2. Crosstalk calculations in AWG [67, 68] have shown that the performance of OADMs degrades as either or both m or N are increased.

2.3.2. Fibre Bragg Grating Based OADM

Another possible structure to perform add/drop functionality in WDM networks is the Fibre Bragg Gratings based OADMs [69]. Bragg gratings are a periodic perturbation in the effective refractive index of an optical waveguide [70]. Changing the refractive index will

make the waveguide acts as a filter centred on a specific wavelength. Therefore, a wavelength that propagates in a FBG will be reflected back if it satisfies the Bragg condition ($\lambda_{Bragg} = 2 \cdot n_{eff} \cdot \Lambda$) [71], where, n_{eff} is the effective refractive index of the fibre, and Λ is the grating period. More discussion on Bragg gratings is presented in Chapter seven.

Figure 2-4 shows a schematic diagram of a FBG based OADM [54]. Crosstalk in this structure results from the leakage of added channels in the Bragg gratings which leads to the presence of unwanted signals at the drop port [72]. Therefore, the dropped channel will be a combination of the reflected channel (λ_2) and the leakage of added channels. Crosstalk in this structure depends on fibre Bragg reflectivity and, in general, it is less than that on the AWG [73]. However, the optical circulators will increase the filter size and this affects the integration scalability.

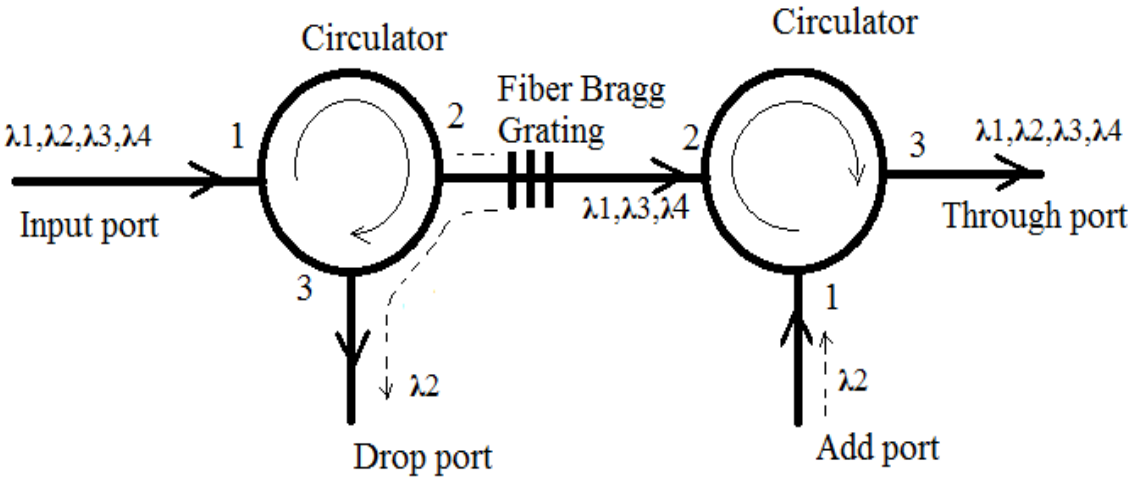

Figure 2-4. Fibre Bragg Grating based OADM [54].

2.3.3. Ring Resonator Based OADM

Figure 2-5 shows the schematic diagram of a first order (single) ring resonator based OADM. In its simplest form, it consists of a pair of bus waveguides evanescently coupled to a closed loop waveguide (ring or racetrack shape) [18]. More discussion on the ring resonators will be presented in Chapter three.

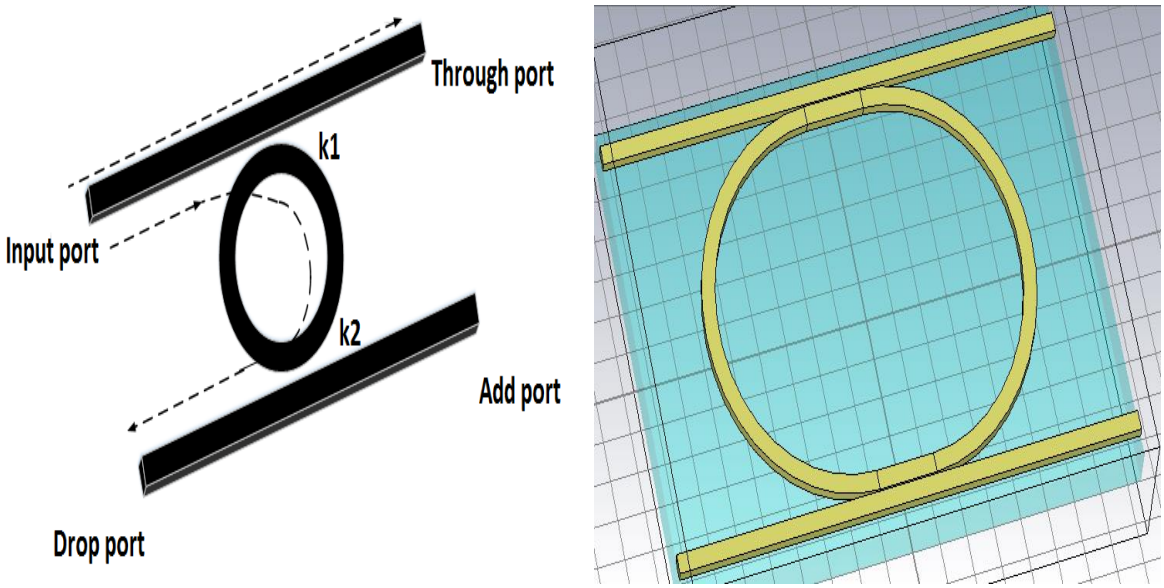

a **b**

Figure 2-5 a. Ring resonator add/drop filter. b. Racetrack resonator based OADM.

Crosstalk in ring resonator based OADMs results from the non-ideal dropping of channels [21]. The dropped channel will be corrupted by the residual of a new added channel (intra-band crosstalk). Inter-band crosstalk also occurs due to the adjacent channels in a WDM

signal [22]. Ring resonators have a small 'real estate' requirement and are therefore potentially useful for large scale integrated optical systems compared to their AWG and FBG counterparts [74, 75].

2.4. Crosstalk Modelling in Ring Resonator Based OADMs

2.4.1. Inter-Band Crosstalk

Considering that the OADM (shown in Figure 2-5) is used to drop a single channel from a WDM signal at the input port, the dropped channel will be corrupted by the residual of $(N-1)$ adjacent channels. The drop port photo-current will consist of two terms (as in (2-5)), i_s is the receiver current due to the dropped channel, and i_n is the summation of crosstalk currents resulting from the leaked power of (N-1) adjacent channels.

Based on equation (2-4), equation (2-5) can be derived:

$$i_{ph} = i_s + i_n = P_s \left[b_s(t) + \sum_{k=2}^{N} b_k(t)\, \epsilon_k \right] \tag{2-5}$$

The third and fourth terms of equation (2-4) are small and neglected due to the frequency difference between the dropped and unwanted channels.

The level of crosstalk current, i_n, depends on:

1. Bit pattern of the $(N-1)$ channels $b_k(t)$. i_n becomes maximum when all channels are in a "1" state simultaneously, which represent the worst case.
2. Suppression ratio (ϵ_k) for each adjacent channel (drop port response).

Figure 2-6 shows the suppression ratio (ϵ_k) for three channels in a single and double ring resonator based OADM separated by 50 GHz (as specified by the ITU-T G.694.1 telecommunication standards [22]).

For a single ring OADM, based on the drop port response (solid line in Figure 2-6), the suppression ratio is:

1. For the first adjacent channel (50 GHz from the resonance), $\epsilon_k = -5\ dB$.
2. For the second channel (100 GHz from the resonance), $\epsilon_k = -10\ dB$.
3. For the third channel (150 GHz from the resonance), $\epsilon_k = -12\ dB$.

However, the drop port response depends on the coupling coefficients and also on the number of resonators used (multiple rings). Increasing the order of the filter (the number of rings) will lead to a sharp transition in the spectral response as shown in Figure 2-6 (dashed line). Hence, a reduction in the inter-band crosstalk can be achieved. The suppression ratio for adjacent channels in a double ring resonator OADM are: -14.5 , -26.5 and -32.7 dB for 50, 100 and 150 GHz spaced channels, respectively. Reducing the effect of inter-band crosstalk requires enhancing the drop port response shape by using multiple rings (increasing the order of the filter) [76, 77], but at the expense of increasing filter size. More discussion on cascaded ring OADMs is presented in Chapter three.

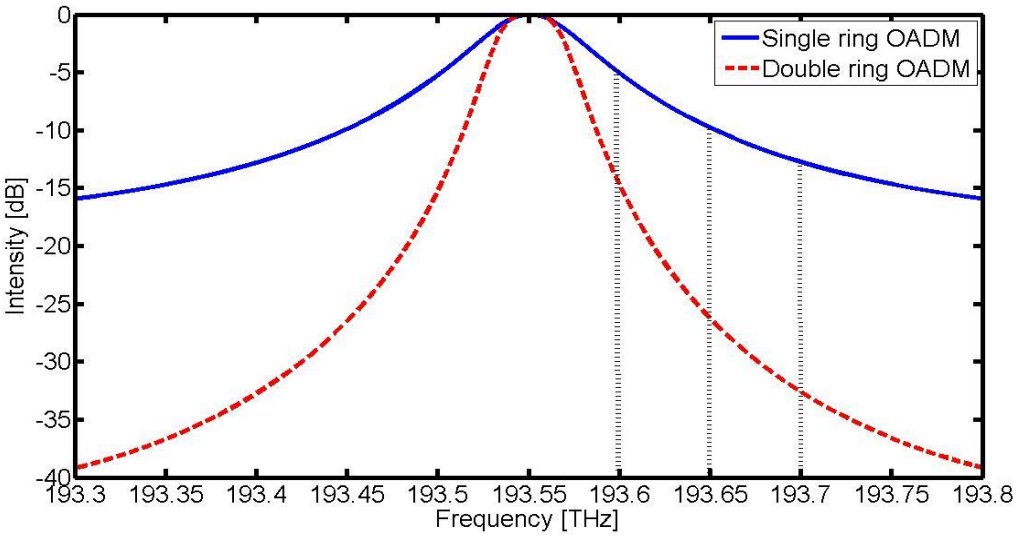

Figure 2-6. Drop port response for single (solid) and double (dashed) ring resonators.

2.4.2. Intra-Band Crosstalk

Intra-band crosstalk is the main source of system performance degradation in all-optical networks [24]. It occurs due to power leakage from a new added channel $\boldsymbol{E}_a(t)$ of a similar wavelength to that of the dropped channel $\boldsymbol{E}_d(t)$.

The receiver photo-current can be expressed as:

$$i_{ph}(t) = \rho\left|\boldsymbol{E}_{ph}(t)\right|^2 = \rho|\boldsymbol{E}_d(t) + \boldsymbol{E}_a(t)|^2 \quad (2\text{-}6)$$

Equation (2-4) can be re-written as in [78]:

$$i_{ph}(t) = \left[P_d + P_a + 2\sqrt{P_d P_a}\,\cos\left(\phi_d(t) - \phi_a(t)\right)\right] \quad (2\text{-}7)$$

Equation (2-7) consists of three terms:

1. Dropped channel photo-current.
2. Added channel photo-current, which is small due to the crosstalk suppression.
3. Crosstalk current that results from the beating between $\boldsymbol{E}_a(t)$ and $\boldsymbol{E}_d(t)$. The worst case is studied where the crosstalk term and the dropped signal are in phase [30].

Following the calculations of [67], the BER at the receiver is:

$$BER = \frac{1}{4} erfc\left(\frac{1}{\sqrt{2}} \cdot \frac{i - I_D}{\delta_1}\right) + \frac{1}{4} erfc\left(\frac{1}{\sqrt{2}} \cdot \frac{I_D}{\delta_0}\right) \tag{2-8}$$

1. The first term of this equation represents the BER for a "1" state where the receiver's current is i, while the second term is for a "0" state.
2. I_D is the threshold level.
3. $erfc$ is the complementary error function [79].
4. δ_0 is the receiver noise which exists in the absence of crosstalk (it is mainly due to thermal noise) for the "0" state.
5. δ_1 represents the sum of the beating term of crosstalk and receiver noise ($\delta_1 = \sqrt{{\delta_0}^2 + \gamma i^2}$) for the "1" state [68].
6. $\gamma = \frac{P_a}{P_d}$ is the crosstalk suppression ratio at resonance as shown in Figure 2-7.

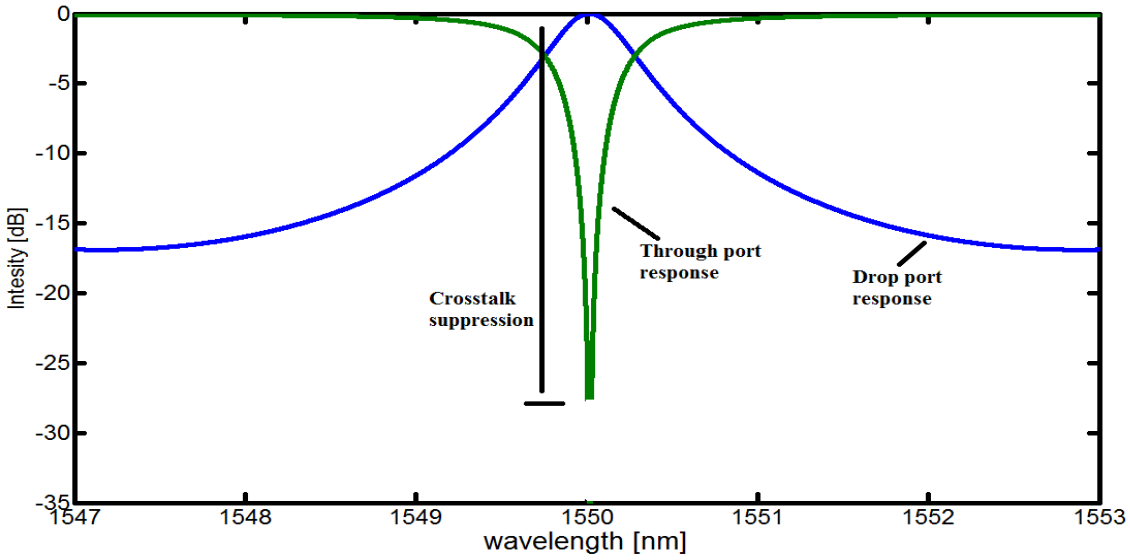

Figure 2-7. Crosstalk suppression of a single ring resonator OADM.

Using the optimum threshold value of I_D given by [67]:

$$I_D = \frac{i}{\delta_0 + \sqrt{{\delta_0}^2 + \gamma i^2}}$$

BER is:

$$BER = \frac{1}{2} erfc\left(\frac{1}{\sqrt{2}} Q\right)$$

where, $Q = \frac{i}{\sqrt{{\delta_o}^2 + \gamma i^2}}$.

To evaluate the effect of intra-band crosstalk, power penalty should be considered. Power penalty is defined as the amount of power to be added to overcome the effect of crosstalk and maintain same BER in the absence of crosstalk.

The power penalty (x) is [67]:

$$x = -10\log[1 - \gamma\, Q^2] \tag{2-9}$$

For a BER=10^{-9}, Q = 6 [73].

The power penalty required to counteract the intra-band crosstalk effect depends on γ (crosstalk suppression ratio) which in ring resonator based OADMs represents the difference between the drop and through port responses at resonance (Figure 2-7). Equation (2-9**)** is plotted in Figure 2-8 to show the relation between the crosstalk suppression ratio (γ) and the required power penalty to obtain BER=10^{-9}.

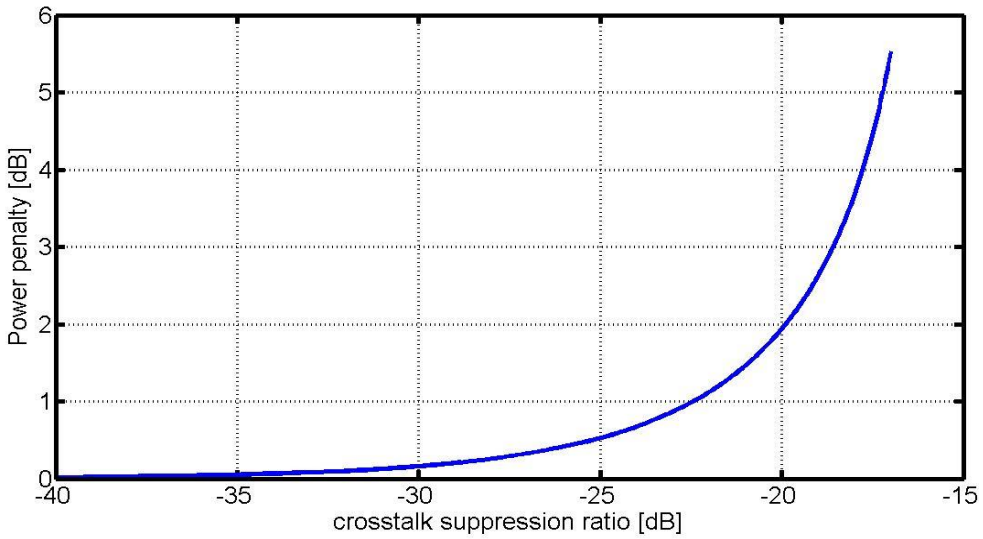

Figure 2-8. Power penalty as a function of crosstalk suppression ratio.

Crosstalk analysis shows that the level of crosstalk in ring resonator based OADMs is lower than that in AWG based OADMs with less dependence on the number of channels in the WDM signal. Also, ring resonator based OADMs are of small size and allow for high scale integration compared to FBG based OADMs. Crosstalk mitigation techniques in ring resonators were based on increasing the crosstalk suppression ratio as will be discussed in the next section. In Figure 2-8, for the crosstalk suppression ratio being higher than $|20|$ dB, a high reduction in the imposed power penalty can be achieved. Allowing for high values of crosstalk suppression ratios (at resonance) will reduce the required power penalty for a narrow band of frequencies. However, for WDM networks, the crosstalk suppression ratio should be kept high, $\geq |20|$ dB, over the whole frequency range of modulated channels in order to ensure a reduced power penalty. Increasing the "crosstalk suppression bandwidth" rather than the "crosstalk suppression ratio" allows adding/dropping modulated channels in WDM networks with improved signal integrity and mitigated level of crosstalk, and this is the main aim of this thesis.

2.5. Mitigation of Crosstalk in Ring Resonator Based OADMs

The crosstalk effect in ring resonator based OADMs was studied numerically in [24, 25]. The intra-band crosstalk effects were estimated by calculating the eye opening penalty at the receiver side. The drop port rejection ratio at a wavelength of the adjacent channel was used to estimate the inter-band crosstalk effect. In [24], a numerical investigation of the

presence of input and add signals in a ring resonator OADM was performed. Modulated signals at both the input and add ports were used to investigate the filter performance. The analysis showed that, at high bit rate add/drop operations, the levels of induced intra-band crosstalk and the wavelength selectivity are strongly dependant, even in higher order filters. Multi-stage topology was suggested to reduce the effect of crosstalk for different data rates. In this topology, the first stage is optimized for low crosstalk in the drop port channel, while another stage is used for the added channel crosstalk mitigation. However, this required an increase in the filter size.

The operation of OADMs based on active ring resonators was investigated in [25] with high bit-rate return-to-zero (RZ) input channels at both the input and the add port. The use of an active ring resonator was suggested in order to eliminate the intra-band crosstalk between the incoming channels. A double-stage topology that addresses the inefficiencies of the single stage OADM was proposed. However, the amplified spontaneous emission (ASE) effect of the semiconductor optical amplifier was not considered.

In [23], lossy single ring and series coupled double ring OADMs were investigated analytically and numerically in order to select appropriate coupling coefficients that reduce the crosstalk at a given level of loss. Symmetric and asymmetric coupled ring resonators were examined and the range of the appropriate coupling coefficients was estimated. Limitations constraining the single ring OADM were addressed with the series coupled double-ring OADM design. Vertical coupling was suggested as an alternative to the

standard coupled resonator layout, which allows greater flexibility in the choice of coupling coefficients.

Series coupling between ring resonators was proposed to increase the filter order [26, 80]. Increasing the filter order leads to an improvement in the spectral response and allows high suppression of the adjacent channel crosstalk (inter-band crosstalk). However, the sub-micrometre gap between the rings (inter-ring coupling coefficient) has a great effect on the overall response. In [26], the inter-ring coupling effect was addressed either by selecting the optimum coupling or by proper physical arrangement of the rings. The optimum condition for coupling coefficients to improve the crosstalk suppression ratio (only) was proposed and a formula that calculates the optimum coupling coefficient of different order filters was analytically derived. The optimum coupling coefficients for a second order series coupled ring resonator in the presence of losses was studied (as will be discussed in Chapter four).

In [80], the optimal arrangement for a high order series coupled ring resonator was suggested. The dependence of the filter response of four series-coupled rings with two different ring radii on the arrangement of ring radii was investigated. An analytical study to calculate the effect of using rings with different radii on the inter-band crosstalk and how these arrangements work with high bit rate signals was presented. However, this analysis was applicable for the case of four rings resonators.

Parallel coupling between ring resonators was also proposed to mitigate the crosstalk [81, 82]. In this coupling configuration, the spectral response depends on the phase relationship

between rings (also controlled by the separation between rings). In [81], it was shown that a number of ring resonators in parallel-coupled configurations provide an improvement in the filter performance and reduce the inter-band crosstalk. Most attention was given to the out-of-band rejection ratio (OBRR) and how to reduce the inter-band crosstalk by controlling the separation between rings. In [82], the phase relationship between rings that affects the spectral response of the filter was studied experimentally. A box-like response was achieved, and high out of band rejection ratio was obtained. However, filter size was increased.

A cross-grid architecture (using a vertical coupled ring resonator) was proposed to increase the scalability. Cross-grid technology for crosstalk reduction was examined experimentally in [10, 17]. In [10], the performance of a ring-resonator based OADM was evaluated through the BER measurements in single channel 10 Gb/s and 3-channel 10 Gb/s WDM configurations. The performance of three output ports with respect to a specified input one was experimentally estimated. The robustness of this design was assessed with respect to crosstalk effects when several channels propagate together. The drawback of this technology is the intersection between optical waveguides that can lead to further crosstalk.

In [17], the role of cascaded OADMs for crosstalk reduction and spectrum clean-up in add/drop filters were addressed experimentally for ring resonator cross-grid technology. An add/drop node using a 2×2 cross-grid array and three ring resonators, to reduce the output port crosstalk values, was proposed. In this design, the first ring was used to drop the required channel, while the second and third rings were used to clean up the drop and

through port, respectively. The intersection between optical waveguides also represents the drawback of this design.

A "Racetrack" model of the resonator was used in [83] to increase the through port notch and improve the drop port response by using asymmetric coupling. In a racetrack resonator based OADM, the coupling region length is longer than that of a ring resonator. This permits better control of the spectral response. An increase in the crosstalk suppression ratio was obtained. Increasing the filter order and also using a multi-stage structure were proposed in [84], but at the expense of filter size.

2.6. Conclusion

In this chapter, crosstalk in all-optical networks was discussed and mathematically defined. Optical add/drop multiplexers OADMs were taken as the main components of interest due to their importance in accessing networks. Different structures of OADM were presented and the crosstalk in each type was explained. An overview of the already existing contributions to mitigate the crosstalk effect in ring resonator based OADMs were presented. Increasing the "crosstalk suppression bandwidth" rather than the "crosstalk suppression ratio" allows adding/dropping modulated channels in WDM networks with improved signal integrity and mitigated level of crosstalk. Therefore, proposing solutions to improve signal integrity by increasing the crosstalk suppression bandwidth in ring resonator OADM is the main focus in the following chapters. However, an understanding of ring resonators as a building block is required first, which is presented in Chapter three.

CHAPTER THREE

OPTICAL RING RESONATORS

In this chapter, Silicon-on-Insulator ring resonators are investigated and their add/drop functionality is explained. Silicon waveguides and the coupling between evanescent modes in directional couplers are discussed. Coupling schemes, cascaded coupling and coupling coefficient effects on different port responses are discussed and explained. OADM spectral characteristics are shown to be highly dependent on the coupling regions' geometry. This chapter provides the necessary background for the following chapters.

3.1. Introduction

Wavelength-Division Multiplexing (WDM) using Silicon-on-Insulator (SOI) waveguides has become an attractive area of research to enable high integration density of photonic components as well as to ensure high speed data transmission [16]. In SOI technology, high index contrast between core and cladding materials allows for light propagation in small cross-section silicon waveguides with very little optical leakage [7]. Therefore, SOI is suitable for integrating photonic components in a micrometre transverse length scale [85].

WDM communication networks require optical components which can separate closely spaced channels effectively and allow for the flexible addition and dropping of channels [86]. Ring resonator based OADMs for WDM networks are considered as one example of SOI technology [85]. Their small size allows for high density integration in optical photonic circuits by exploiting the availability of the Complimentary-Metal-Oxide Semiconductor (CMOS) fabrication facilities [19].

Ring resonators are promising devices for different applications in all-optical networks [87-89]. Coupling a closed loop resonator with a bus waveguide leads to a modified structure with a filter-like behaviour. Careful choice of coupling coefficients between ring and bus waveguides has a great effect on the filter performance. Crosstalk analysis in Chapter two suggested that ring resonator based OADMs have a superior performance over their FBG and AWG counterparts. Therefore, this chapter aims to provide a general background of optical ring resonators and present their features in WDM networks.

This chapter is organized as follows:

1. An explanation of ring resonators and their add/drop functionality in WDM networks is presented. Directional couplers between ring and bus waveguides are discussed and mathematically modelled.

2. The simulation software which is used throughout this thesis is introduced and discussed.

3. Coupling schemes (vertical and lateral), cascaded coupling (series and parallel) and the main criteria that define the usability of ring resonators as an OADMs, all are discussed and explained.

3.2. Ring Resonators

Ring resonators were first proposed by Marcatili [90] to support travelling wave resonant modes. A re-entrant waveguide with a perimeter of several μm was used to construct an optical resonator. The resonator was coupled to an external waveguide to get a transfer of the optical energy. The resultant structure (shown in Figure 3-1) supports a number of circulating wavelengths that satisfy the resonance condition $N \cdot \lambda_{res} = n_{eff} \cdot l$, where N, an integer representing the mode number, l is the average resonator perimeter, and n_{eff} is the effective refractive index. The difference between two consecutive resonances is called the Free Spectral Range (FSR), which is of great interest in WDM systems.

If a WDM signal is launched at the input port in Figure 3-1, wavelengths that satisfy the resonant condition will be coupled to the ring. The constructive interference after each round trip results in an increase of the optical power in the resonator. The transfer of optical power is realized by exploiting the coupling between the evanescent modes in the ring and the bus waveguide. This structure represents a ring resonator based all-pass filter which is used for dispersion compensation in WDM networks [91].

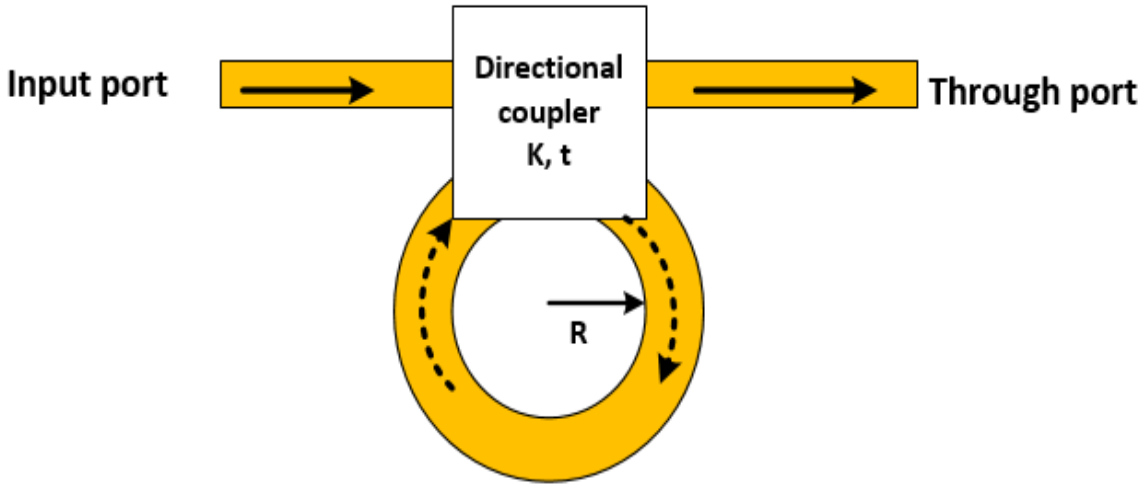

Figure 3-1. A schematic diagram of a ring resonator based all-pass filter.

In a ring resonator based OADM structure (Figure 2-5), there is another bus waveguide coupled to the resonator. Therefore, the stored energy will be coupled to the output waveguide leading to a build-up of optical power at the drop port and resulting in a notch in the through port response (due to coupling) [92, 93]. The resonant wavelength is determined by the resonator length and effective refractive index, whereas, the coupling and loss coefficients are responsible for deciding the spectral response shape. Coupling coefficients are dependent on the coupling region characteristics (separation gap and coupling length), while losses are related to the type of materials used and the length of resonator, as well [94]. Ring resonator based OADMs can be used to drop multiple channels from a WDM signal to increase the flexibility of the network [95-97]. A four channel dropping structure was proposed based on a compact parent-sub micro-ring

resonator [98]. Series and parallel coupled ring resonators have been proposed and used to enhance the spectral characteristics of OADMs by increasing the Out-of-Band Rejection Ratio and obtaining a sharp roll-off from pass-band to stop-band [21, 99-102].

Light propagation in any bounded medium is based on the refractive index contrast [30]. Low Index Contrast (LIC) materials were used first for optical waveguide fabrication where the difference between core and cladding refractive indices is low. A reduction of the propagation loss was achieved using the conventional LIC devices [103]. However, large radius resonators were required to reduce leakage of the light. This means large components with a small FSR (FSR is inversely related to the radius). The FSR is required to be as high as possible to accommodate a wide bandwidth in the C-window ($1535 - 1565\ nm$). Therefore, a number of rings (with different radii) were coupled in series to increase the FSR using the Vernier effect [104-106]. The Vernier effect extends the FSR by reducing all resonances which are not an integer multiple of the FSR of each individual ring. The new FSR is related to the FSR of each ring as [107]:

$$FSR_{extended} = n_1 FSR_1 = n_2 FSR_2$$

Where, n_1 and n_2 are integers.

The advancement in fabrication technologies has enabled the construction of small radii resonators using high index contrast material (HIC) [108]. High index contrast between core and cladding refractive indices results in a strong confinement of light even with a small bend radius. Polycrystalline silicon (poly Si) waveguides were proposed in [109] with radii of $3\,, 4$, and $5\ \mu m$ and a FSR about $20 - 30\ nm$. The disadvantage of this design was

the presence of a high insertion loss in the through port. Silicon nitride SiN was also used in [84] and a ring of radius 8 μm was fabricated to achieve 20 nm FSR. Recently, Silicon-On-Insulator (SOI) has been used which allows for the fabrication of small radius rings (using CMOS technology) with low bending and scattering losses [20]. A large FSR (up to 32 nm) with a low level of bending loss has been achieved [85].

Silicon-On-Insulator (SOI) waveguides are a promising technology for integrated photonic devices in WDM networks [110]. In this technology the propagation loss is relatively low [111]. However, the back reflection effect due to sidewall roughness is of great importance [112, 113]. Sidewall roughness is usually considered as a random perturbation and back reflection is treated as a stochastic variable [113]. The analytical calculations in [107] showed that the performance of a resonator is strongly affected by the characteristics of the surface roughness. The statistics of back reflection induced sidewall roughness were investigated experimentally, first, in uncoupled optical waveguides [114]. It was shown that the intensity of back reflection follows the distribution of a single scattering system with a strong dependence upon waveguide length. Secondly, the change in back reflection characteristics when a ring resonator is coupled to an optical waveguide was examined in [115] and showed that after a multiple round trip in the ring resonator, back reflection increases coherently and can affect the behaviour of the filter even at moderate quality factors (high coupling coefficients). In rough-walled ring resonators, back reflection is a well-known cause of resonance splitting due to mutual coupling between forward and backward propagating modes [18, 107, 116-118]. This effect has been exploited to improve

the extinction ratio by increasing the depth of the through port at resonance [116] and is further investigated in Chapter seven.

SOI ring resonators are receiving an increased level of attention from many research groups. IMEC (Belgium) is one of the centres that work on the use of SOI single mode optical waveguides [8, 18]. They fabricated a ring resonator with 5 μm radius [119] with losses ranging from $2.5 - 3$ dB/cm and FSR of 13.7 *nm*. Other groups such as the Institute fur Halbeitertechni (Germany) [16, 120], California Institute of Technology [121], the University of Wisconsin-Madison (USA) [122], and the Politecnico di Milano (Italy) [10, 115, 118], have fabricated ring and race track SOI resonators for different applications. Reducing ring radius leads to an increase in the coupling coefficient sensitivity to fabrication process (due to close proximity between ring and bus waveguides). To reduce the coupling coefficient sensitivity, a straight waveguide section was introduced to increase the coupling region. The resulting shape is a racetrack-like resonator (as shown in Figure 2-5 b) [123]. However, this will increase the resonator perimeter and results in a reduced FSR. Racetrack resonators with improved FSR were designed using the Vernier effect [98, 124].

SOI ring resonators are a key building block to implement WDM schemes on CMOS compatible platform and realizing monolithic integrated photonic circuits [19]. They have found wide applications in all-optical networks such as add/drop multiplexers, delay lines, and bio-sensors [87, 89, 118]. However, integration of optical components leads to potential crosstalk and signal integrity (SI) issues due to the close proximity of optical

components and waveguides. In this thesis, a number of approaches are adopted to effectively reduce the crosstalk between the channels in optical ring resonator based add/drop multiplexers (OADMs) and filters in order to enhance the overall performance, and, moreover, allow for increased integration.

3.3. SOI Strip Waveguides

Optical waveguides are the fundamental elements that interconnect different devices in PLCs [125]. They have a similar function to that performed by metallic strips in an electrical integrated circuit. However, unlike electrical signals that require a high conductivity region to flow, optical signals require a high refractive index contrast medium to propagate. SOI waveguides consist of a high refractive index material made of Si on the top of lower refractive index SiO_2 cladding layer on a silicon substrate [16], and fabricated using UV or electron e-beam lithography technology [126]. Lithography is the process of transferring patterns from mask to wafer [127].

Different optical modes travel in an optical waveguide with lateral and transverse confinements. The optical mode is a spatial pattern of electromagnetic field in one or more dimensions that remains constant in time. The number of transmitted optical modes depends on the waveguide geometry and the choice of the materials [20]. To ensure single TE mode propagation around 1.55 μm, the cross section of an SOI strip waveguide should be between 200 nm to 250 nm in height and between 400 nm to 500 nm in width [18]. The most common way to couple light between optical waveguides is to place them close

to each other through a directional coupler. Coupling characteristics are affected by geometrical dimensions of the coupling region, effective refractive index, and material dispersion [125], as will be discussed in the following subsections.

3.3.1. Dispersion, Effective Refractive Index and Group Index

The resonance condition of ring resonators depends mainly on the waveguide effective refractive index (n_{eff}). In order to perform a proper analytical modelling of coupling coefficients, optical dispersion should be considered. Dispersion represents the rate of change of the group delay with respect to wavelength. There are mainly two sources of dispersion in optical waveguides:

1. Inter-modal dispersion: it is caused by the mixing of modes in a multi-mode system, and it is of no concern under single-mode operation.
2. Chromatic dispersion: which includes:
    i. Material dispersion, which comes from the wavelength-dependent index of a material.
    ii. Waveguide dispersion, which occurs when the speed of a wave or its effective index in a waveguide depends on its operating wavelength.

The total dispersion ($\frac{\partial n_{eff}}{\partial \lambda}$) of a guided mode is the sum of the material dispersion and waveguide dispersion.

The wavelength dependence of silicon and silicon dioxide refractive index (material dispersion) has been determined in [128]. In both cases (Si and SiO_2), the slope is negative within the wavelength range of $1300\ nm$ to $1700\ nm$.

$$n(Si) = (-2.95 \times 10^{16})\lambda^3 + (2.244 \times 10^{11})\lambda^2 - (5.75 \times 10^5)\lambda + 3.938 \quad (3\text{-}1)$$

$$n(SiO_2) = (-1.7 \times 10^9)\lambda^2 - (7 \times 10^3)\lambda + 1.459 \quad (3\text{-}2)$$

The wavelength dependency of the effective refractive index for a single TE mode waveguide shows a negative slope. Based on the curve-fitting results presented by [129], the change of the effective refractive index is:

$$n_{eff}(\lambda) = (-1.269 \times 10^6)\lambda + 4.36 \quad (3\text{-}3)$$

The group index is the partial derivative of the effective refractive index [124].

$$n_g(\lambda) = n_{eff}(\lambda) - \lambda \frac{\partial n_{eff}}{\partial \lambda} \quad (3\text{-}4)$$

Equations (3-3) and (3-4) represent the effective and group refractive indices dependence on the wavelength which will be used in the mathematical analysis through this thesis.

3.3.2. Directional Coupler

Typically, directional waveguide couplers consist of two waveguides with close proximity that permit a power exchange from one waveguide to the other [50, 125]. The length of coupling region (L_c), distance between waveguides (g), and index profile of the coupler (n_1, n_2 and n_3) affect the amount of the coupled power. For the SOI directional coupler shown in

Figure 3-2, silicon dioxide (SiO_2) of refractive index $n_2 = 1.47$ is used as a lower clad for silicon (Si) waveguides with refractive index $n_1 = 3.47$; the upper cladding is air with refractive index $n_3 = 1$.

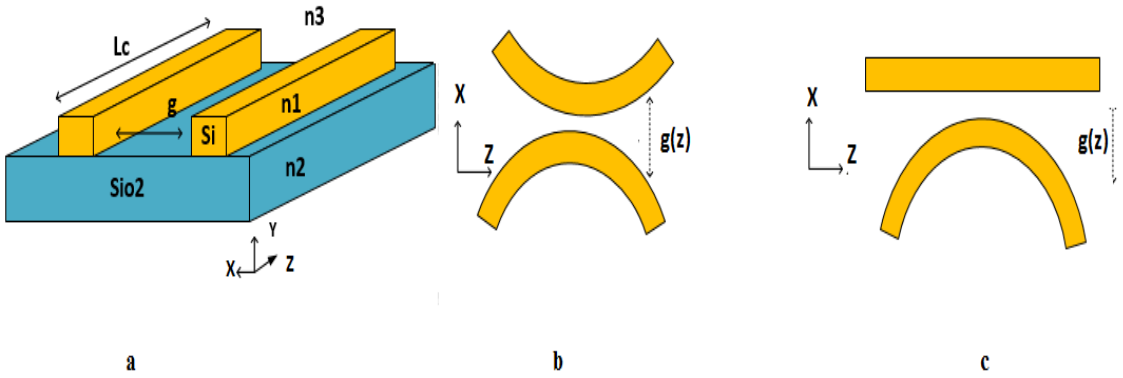

Figure 3-2. Different geometries of SOI directional couplers.

The coupling coefficient k is calculated based on the directional coupler geometry, as below:

1. For a parallel bus waveguide directional coupler (Figure 3-2 a), the coupling of light can be expressed in terms of the superposition of the supermodes [130]. The term "Supermode" was used in [131, 132] to describe modes in a system of parallel coupled optical waveguides. To ensure a 100% power transfer, the length of coupling region should be equal to L_π, where L_π is the length over which the phase difference between odd and even supermodes is equal to π.

The coupling region L_π can be expressed as [16]:

$$L_\pi = \frac{\pi}{(\beta_e - \beta_o)} = \frac{\lambda}{2\left({n_{eff}}^e - {n_{eff}}^o\right)} \tag{3-5}$$

${n_{eff}}^e$, and ${n_{eff}}^o$ are the effective refractive indices for even and odd supermodes, respectively, which can be calculated using a numerical code, in [133, 134] (using the semi-vectorial mode solver [135]).

Increasing the distance between waveguides (g) will reduce the difference $\left({n_{eff}}^e - {n_{eff}}^o\right)$ and leads to an increase in L_π [83, 133]. The coupling coefficient k depends on L_π (which is a function of g) and the actual length of coupling region L_C (Figure 3-2) as in (3-6) [16]:

$$k = \sin\left(\frac{\pi L_c}{2L_\pi}\right) e^{\left(-\left(\frac{\beta_e+\beta_o}{2}\right)L_c\right)} \tag{3-6}$$

2. For a directional coupler with two bent waveguides (Figure 3-2 b), (3-6) is not applicable due to the change of the separation gap along the coupling region. The instantaneous coupling strength is expressed in as (3-7) [50]:

$$k\big(\mathrm{g}(z)\big) = \frac{\epsilon_o \omega}{4} \iint ({n_1}^2 - {n_3}^2) f_1(x,y) {f_2}^*(x,y) dxdy \tag{3-7}$$

Where, $f_1(x)$ and ${f_2}^*(x)$ are the power normalized modal fields in the two bent waveguides, ω is the angular frequency and $\mathrm{g}(z)$ is the separation width (centre to centre of bent waveguides). The net coupling coefficient k is:

$$k = \int_{-\infty}^{\infty} k\big(\mathrm{g}(z)\big) dz \tag{3-8}$$

where, g(z) depends on the waveguide width w_r and the direction of propagation z. It can be approximated to a parabola as in (3-9) [50]:

$$g(z) = (g + w_r) + \gamma z^2 \tag{3-9}$$

$$\gamma = \frac{1}{2R} = \frac{R_1 + R_2}{2R_1 R_2}$$

R_1 and R_2 are the radii of the bent waveguides.

3. For a bus and bent waveguide directional coupler (Figure 3-2 c). The coupling coefficient can be calculated using (3-7) and (3-8) by substitute the radius R_2 of the bus waveguide as $R_2 \to \infty$.

Based on the above analysis, the coupling between the evanescent tails of modes in both waveguides depends on the field profile which is difficult to estimate theoretically. Therefore, 3D simulation software is used throughout this thesis for modelling and estimating of coupling coefficients from the obtained frequency responses.

3.4. CST Microwave Studio

Analytical calculations, using Coupled Mode Theory, are not sufficient to provide the required accuracy for OADM design. They do not account for multiple reflections very easily, nor scattering and delay. Therefore, photonic CAD tools are needed for modelling and validation. A wide variety of simulation algorithms (using Beam Propagation Method (BPM), Eigenmode Expansion Method (EME), and Finite Difference Time Domain Method (FDTD)) have been developed for modelling passive photonic devices [136-138].

In this thesis, CST Microwave Studio (MWS) [139] is used as a simulation engine to simulate light propagation. It allows for both the validation of final designs and the analysis through the design process (using the optimization options).

The full-wave discrete method used in CST MWS requires a mesh generation process to specify the mesh cell size (by defining the Lines per Wavelength ratio (LPW)). Increasing the LPW ratio will increase the accuracy of results, but at the expense of simulation time and memory. A grid convergence test was carried out in this thesis to specify an acceptable LPW ratio with a reasonable simulation time. The results showed that LPW$=15$ to 20 is within the acceptable range. Increasing the LPW ratio above 20 will result in a long simulation time with little or no improvement in results. The CST simulation of the fundamental mode profile is shown in Figure 3-3.

The CST MWS provides a simulation-driven optimization option which allows for obtaining the optimized design parameters at a low computational cost. A proper formulation of the objective function with a trust-region-based optimization algorithm [140] will result in an optimum design for the OADM [141], as will be discussed in chapter six.

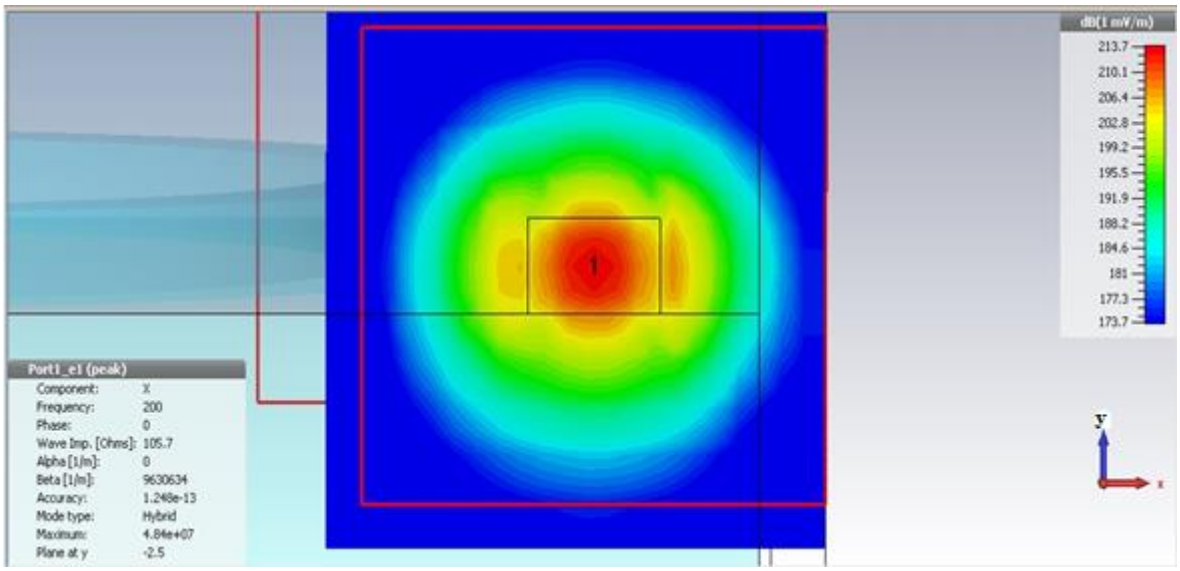

Figure 3-3. CST simulations of the fundamental TE like mode distribution at the input port of a single ring OADM

3.5. Coupling in Ring Resonators

There are two main approaches in which the coupling of light between the bent and bus waveguides is achieved: lateral and vertical coupling. The waveguide cross section in each scheme is different in order to support the required mode for each case. The TE like mode is the dominant mode for the lateral coupling and for vertical coupling, the TM like mode is dominant.

3.5.1. Lateral Coupling

If the bus and bent waveguides are placed in the same plane, as shown in Figure 3-4, the coupling will take place horizontally. This is the lateral coupling configuration. The

coupling strength is controlled by the gap width between waveguides. The small gap size required to ensure strong coupling in a HIC material makes this scheme of high sensitivity to the lithography and etching procedures [127].

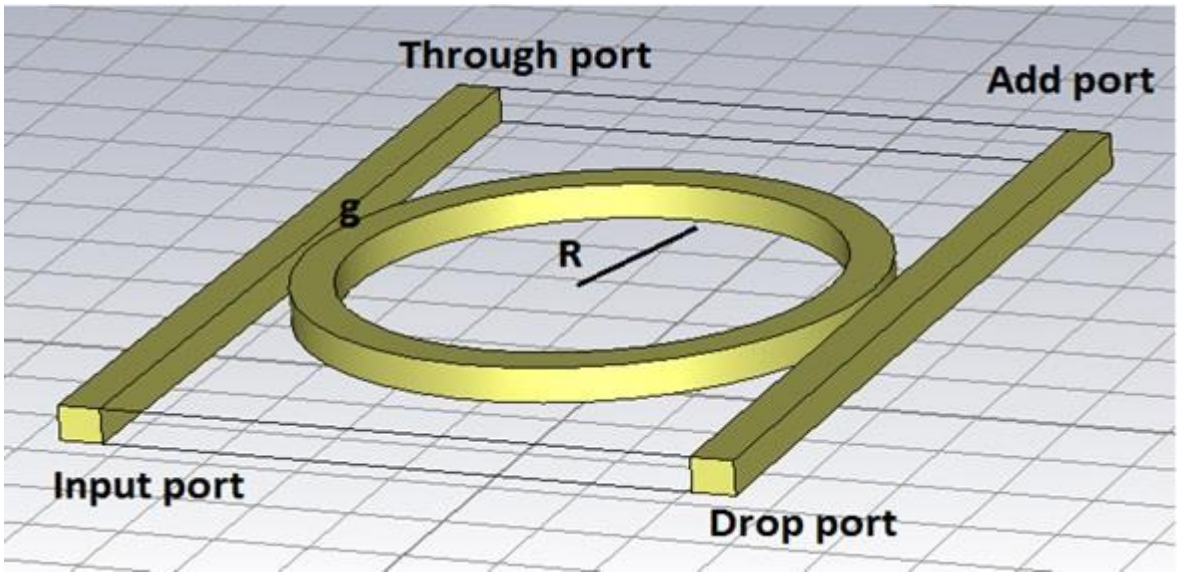

Figure 3-4. Laterally coupled ring resonator.

3.5.2. Vertical Coupling

In a vertical coupling configuration, bus and bent waveguides are etched in different layers (as shown in Figure 3-5). From the design point of view, this means increased flexibility because the ring and bus waveguides can be optimized separately [142]. The separation layer thickness (*d*) and the lateral deviation between bus waveguides and the ring will affect the coupling strength in this scheme [143]. Enhancing the crosstalk performance of a vertical coupled OADM, by optimizing the ring parameters, will be the main aim of chapter six.

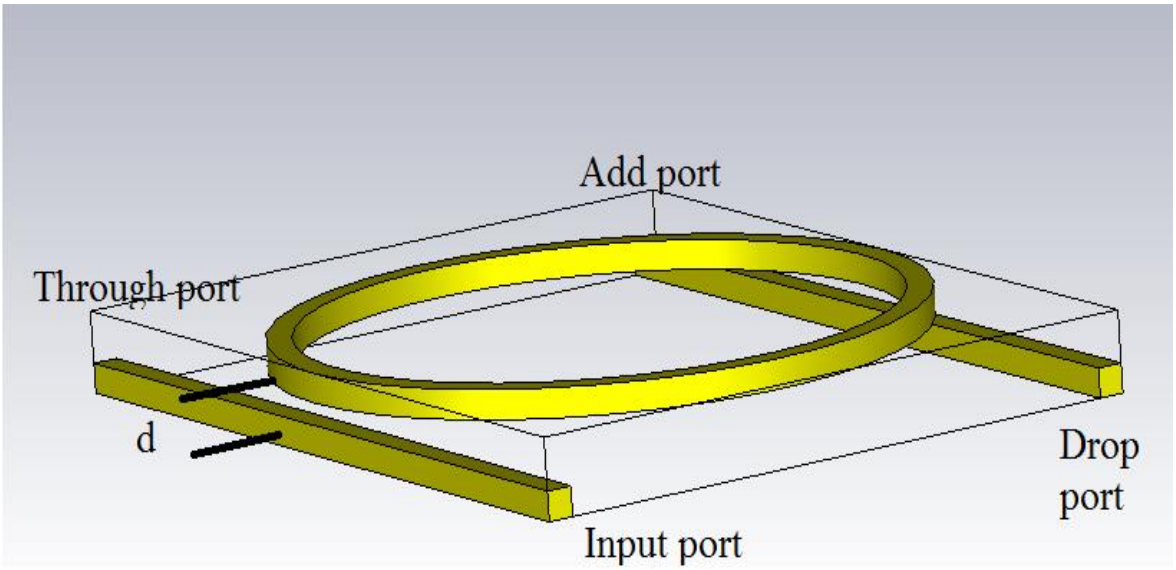

Figure 3-5. Vertical coupled ring resonator.

3.6. Cascaded Coupled Ring Resonators.

Improved spectral characteristics such as flat pass band response, high out-of-band rejection ratio and sharp step function can be obtained by using multiple (series or parallel) coupled ring resonators.

3.6.1. Series Coupling

Figure 3-6 shows the schematic of series coupled double ring resonators. Several rings can be placed between input and output bus waveguides. The outer coupling coefficients (between bus waveguides and outer rings) and the coupling between inter-ring are modelled

by directional couplers with coupling coefficients, κ_n, and transmission coupling coefficient t_n. More explanation about the effect of inter-ring coupling is presented in Chapter four.

If a defined WDM signal is injected as a source at the input port (port 1 in Figure 3-6), the frequency response will be as follows:

1. Off-resonance, the fraction of light, which has completed a single round trip in the first ring, interferes destructively with the light that has just coupled to the ring. There will be no build-up of the power inside the resonator. Only a small amount of light will couple to the second ring. The light remains mainly in the bus waveguides and propagates to the through port.

2. At resonance, the fraction of light that has just completed one round-trip in the first ring interferes constructively with the light coupled to the ring resulting in a coherent build-up of the power inside the ring resonator. After multiple coupling between inner-rings, the light will be dropped at port 3 (Figure 3-6) if the number of rings is odd, or it will be dropped at port 4 (opposite to port 3) if the number of rings is even.

Ring radii are either of the same size to support similar resonance wavelengths or with different sizes arranged to support a specific wavelength based on the Vernier effect [98, 124].

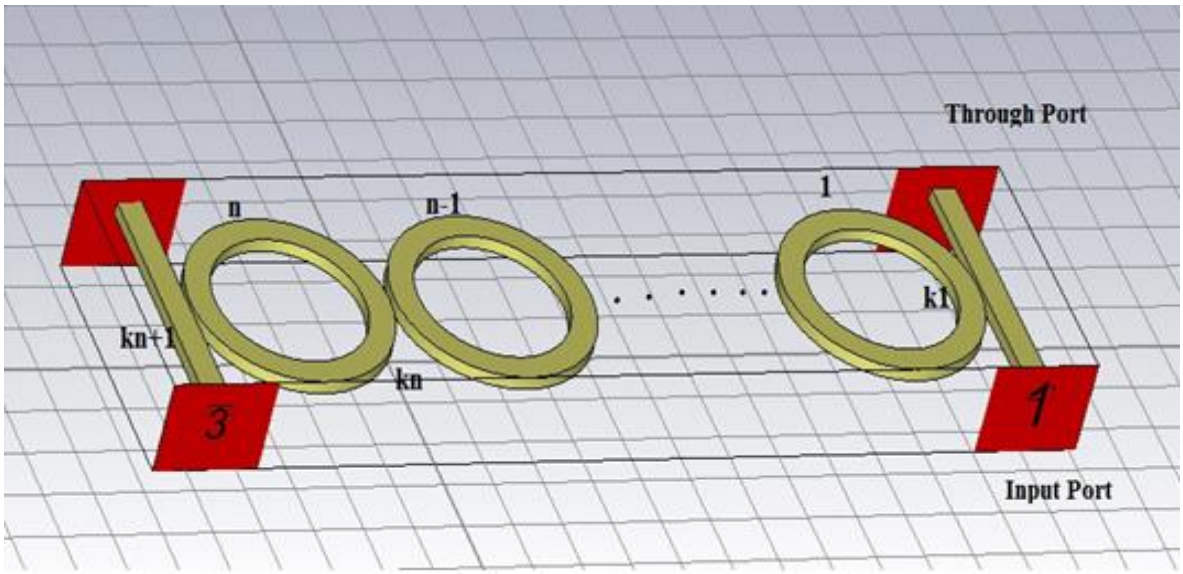

Figure 3-6. The schematic of N-series coupled ring resonator.

3.6.2. Parallel Coupling

In this configuration, rings are arranged in such a way that there is no direct coupling between the nearest neighbouring rings (as shown in Figure 3-7). Therefore, it offers more flexibility in the fabrication process compared to the serial configuration (no inter-ring coupling). The centre-to-centre separation between the nearest neighbour rings (L_p) will determine filter response. Therefore, this distance should be chosen carefully to obtain the desired interference at a specified wavelength range. The useful wavelength range is rather limited due to the phase change that occurs due to the separation (L_p) between the rings. Outside this range the drop port response will vary in an undesirable way due to the interference of light coming from the individual resonators. More explanation of the

separation L_p effect on the crosstalk performance of this type of filters will be presented in Chapter five.

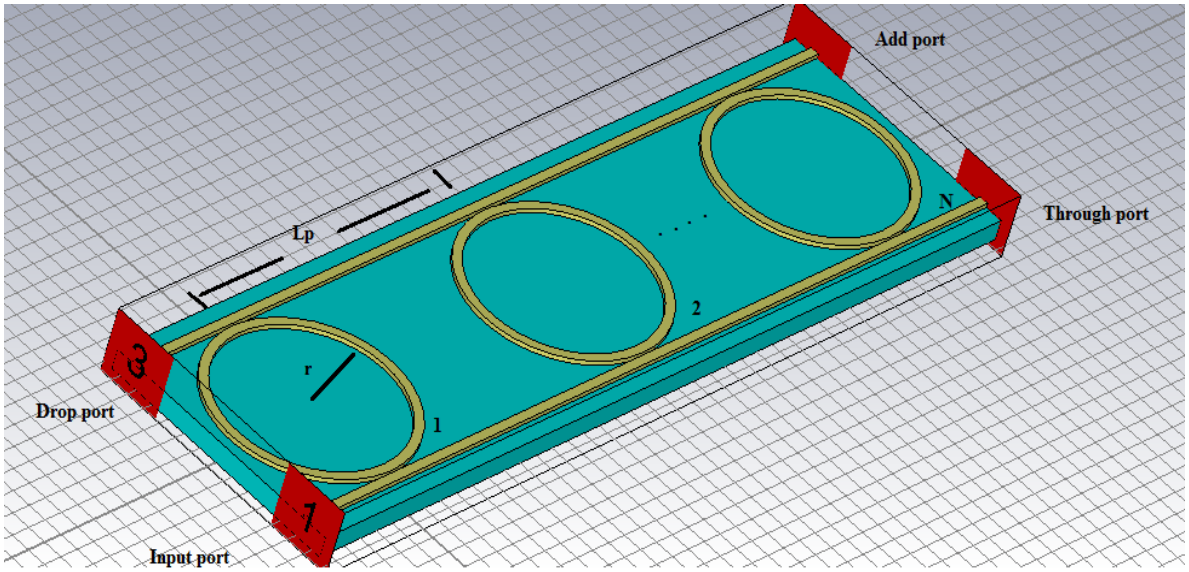

Figure 3-7. The schematic of N-parallel coupled ring resonator.

3.7. Optical Add/Drop Multiplexer

In this configuration, two directional couplers are formed as shown in Figure 3-8. Directional couplers are defined by the coupling coefficient (k^2), and the transmission coefficient (t^2) [144]. The values of k^2 and t^2 are determined by the length of coupling region, gap width and refractive index profile. For lossless coupling, $k^2 + t^2 = 1$.

However, the coupling losses are included in the loss coefficient α of the ring which determines the wave reduction after one round trip.

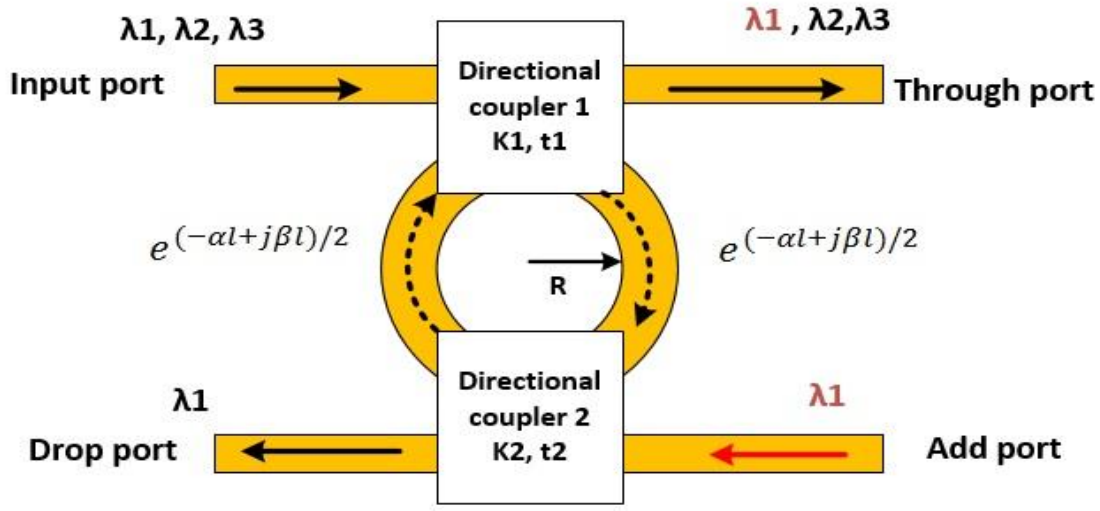

Figure 3-8 Schematic diagram of the ring resonator based OADM.

The spectral response of ring resonator based OADMs is highly affected by the coupling region's characteristics. Symmetrical coupled OADMs are realised by similar directional couplers (i.e $k_1 = k_2$). OADMs are said to be asymmetrically coupled if $k_1 \neq k_2$ which is physically realized by a different separation gap in each side of the ring [102, 145]. The drop and through port transfer functions of a single ring resonator OADM are calculated using the space domain Coupled Mode Theory (CMT) [19, 94, 146], as in (3-10) and (3-11), respectively:

$$G_d = \frac{-k_1 k_2 x^{1/2}}{1 - t_1 t_2 x} \tag{3-10}$$

$$G_{th} = \frac{(t_1 - t_2 x)}{1 - t_1 t_2 x} \tag{3-11}$$

where, $x = e^{-\alpha l - j\beta l}$ is the round trip propagation coefficient and l is the ring perimeter. Coupling and loss coefficients affect all the filter parameters, starting from the insertion loss to finesse as shown in equations (3-12) to (3-19) below [146]:

1. Through port response (Insertion loss):

$$IR = |G_{th}|^2 = \frac{{t_2}^2 e^{-2\alpha l} - 2t_1 t_2 e^{-\alpha l} cos\beta l + {t_1}^2}{1 - 2t_1 t_2 e^{-\alpha l} cos\beta l + {t_1}^2 {t_2}^2 e^{-2\alpha l}} \tag{3-12}$$

At resonance (through port notch):

$$IR_{res} = \frac{(t_2 e^{-\alpha l} - t_1)^2}{(1 - t_1 t_2 e^{-\alpha l})^2} \tag{3-13}$$

The ratio between maximum and minimum values of the through port response represents the extinction ratio, $\mathrm{ER_{th}}$:

$$ER_{th} = \frac{IR_{max}}{IR_{res}} = \left[\frac{(1 - t_1 t_2 e^{-\alpha l})(t_2 e^{-\alpha l} + t_1)}{(t_2 e^{-\alpha l} - t_1)(1 + t_1 t_2 e^{-\alpha l})}\right]^2$$

2. Drop port response:

$$DR = |G_d|^2 = \frac{{k_1}^2 {k_2}^2 e^{-\alpha l}}{1 - 2t_1 t_2 e^{-\alpha l} cos\beta l + {t_1}^2 {t_2}^2 e^{-2\alpha l}} \tag{3-14}$$

At resonance:

$$DR_{res} = \frac{{k_1}^2 {k_2}^2 e^{-\alpha l}}{(1 - t_1 t_2 e^{-\alpha l})^2} \tag{3-15}$$

The ratio between maximum and minimum values of the drop port response represents the Out-of-Band Rejection Ratio, OBRR:

$$OBRR = \frac{(1 + t_1 t_2 e^{-\alpha l})^2}{(1 - t_1 t_2 e^{-\alpha l})^2}$$

3. Free spectral range (FSR): the frequency separation between two consecutive resonances [18].

$$FSR = \lambda_{res+1} - \lambda_{res} \cong \frac{{\lambda_{res}}^2}{n_g l} \tag{3-16}$$

4. Full width at half maximum FWHM:

$$FWHM = \frac{(1 - t_1 t_2 e^{-\alpha l}){\lambda_{res}}^2}{\pi n_g l \sqrt{t_1 t_2 e^{-\alpha l}}} \tag{3-17}$$

5. Q-*factor*, measures the number of round trips of the stored energy before it drops to 0.367 ($= 1/e$) of its initial value; mathematically it can be expressed as:

$$Q_{factor} = \frac{\lambda_{res}}{FWHM} = \frac{\pi n_g l \sqrt{t_1 t_2 e^{-\alpha l}}}{\lambda_{res}(1 - t_1 t_2 e^{-\alpha l})} \tag{3-18}$$

6. Finesse: is a measure of the ratio between the resonances' sharpness to their spacing; mathematically, it can be expressed as [18]:

$$Finesse = \frac{FSR}{FWHM} = \frac{\pi\sqrt{t_1 t_2 e^{-\alpha l}}}{(1 - t_1 t_2 e^{-\alpha l})} \quad (3\text{-}19)$$

7. Crosstalk suppression: is defined as the difference between the drop and through port intensities at the resonance. It represents the level of suppression of the unwanted channels; mathematically it can be expressed as the difference between equations (3-12) and (3-15).

8. Losses: the losses can be caused by different factors such as: coupling losses and round trip losses (propagation losses, sidewall roughness and fabrication mismatch of waveguide width). All the losses are included in the attenuation term (α), and appear in all equations as $e^{-\alpha l}$.

The key factors to assess the OADM performance are the through port notch depth, maximum power dropped and the crosstalk suppression ratio at resonance. Equations (3-12) to (3-19) show that a careful choice of the coupling coefficient will result in substantial performance enhancement. A typical frequency response of a single ring resonator OADM is presented in Figure 3-9. It was calculated using CST MWS. The through and drop port responses are shown in this figure. Free spectral range (FSR) and Out-of-Band Rejection Ratio (OBRR) are illustrated in this diagram.

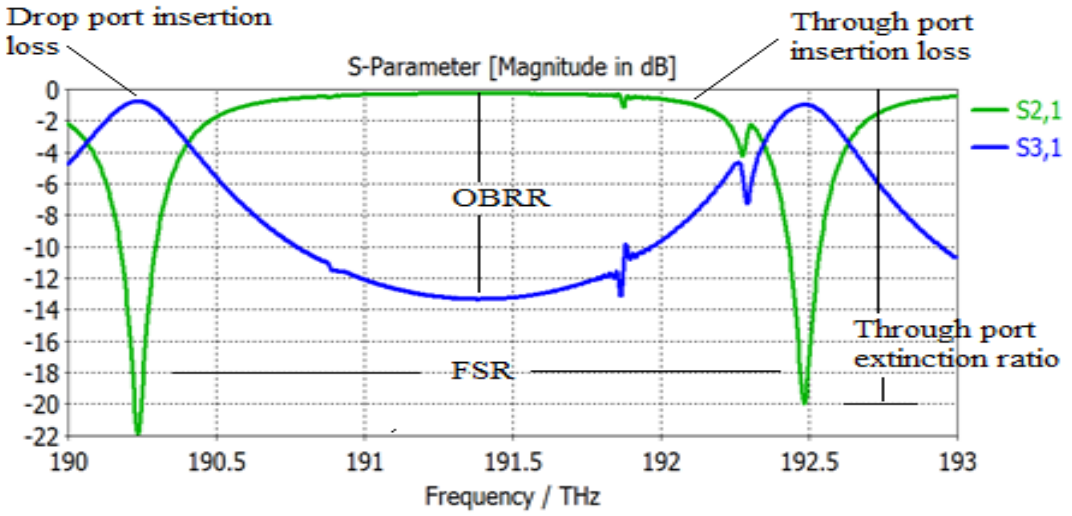

Figure 3-9 CST simulated frequency response of a single ring resonator based OADM.

3.8. Conclusion

This chapter has presented an overview of the ring resonator operation principle, fabrication and applications. Emphasis was given to their add/drop functionality in WDM networks. Directional couplers in SOI waveguides were explained and the coupling coefficients were mathematically defined. CST Microwave Studio (MWS) simulation software was introduced and proposed to be used for numerical validation throughout this thesis. Through and drop ports transfer functions were derived analytically using the space domain CMT. The crosstalk suppression ratio (which is defined as the difference between the drop and through port responses at resonance) was shown to be highly affected by coupling coefficients. Controlling coupling coefficients through the waveguide cross section, separation gap, and the length of coupling region allows for increased crosstalk suppression ratio.

CHAPTER FOUR

OVER-COUPLED RING RESONATOR BASED OADM

This chapter looks into crosstalk issues in (series) coupled ring resonator OADMs. It examines the crosstalk performance as a function of the inter-ring coupling coefficients. The over-coupling condition is proposed as a solution to improve the crosstalk suppression bandwidth. The simulation results show that, in an over-coupled double ring resonator, the crosstalk suppression bandwidth is increased in comparison with that of a critically coupled OADM. Over-coupling improves filter performance by providing wider bandwidth over which high crosstalk suppression is maintained.

4.1. Introduction

Series coupled ring resonators were proposed to enhance OADMs performance by increasing the crosstalk suppression ratio and improving the spectral shape compared to single ring based OADMs [124, 147]. Inter and intra-band crosstalk in series coupled OADMs are highly affected by the inter-ring coupling coefficients. In [26] a formula to calculate the optimum coupling coefficients that increase the crosstalk suppression ratio was proposed, the resulting filter was said to be a critically coupled OADM. Inter-ring

coupling is responsible for the occurrence of a response splitting at resonance since the coupling section will behave like a perturbation point in the ring [19]. Exploiting the resonance splitting to increase the crosstalk suppression bandwidth is the main aim of this chapter.

In an ideal resonator (smooth-walled ring and without a coupling section) each mode can travel in two directions, the forward propagating mode (deliberately excited by the bus waveguide) and the backward propagating mode; the forward and backward travelling modes are uncoupled [18]. However, any small perturbation which can be felt by the optical mode can lead to couple these two modes. When there is coupling, this will result in a net power transfer between modes, and causes resonance splitting.

The outer coupling coefficients (between rings and bus waveguides) and inter-ring coupling coefficients play an important role to control the resonance splitting. Figure 4-1 shows the effect of inter-ring coupling coefficient in a series double ring resonator. The outer coupling coefficient k^2 is chosen to be 0.24. Different values of the inter-ring coupling coefficients ${k_i}^2$ are examined (${k_i}^2 = 0.016, 0.05, 0.1, and\ 0.15$) to show how the resonance splitting is changed with the increase of inter-ring coupling. For 0.016 inter-ring coupling, the drop port response shows no splitting. However, for a 0.15 coupling coefficient (decrease of the gap separation between rings), the splitting becomes strong with a single minimum at resonance of -5dB. At the same time, the through port response will also have resonance splitting and a single maximum will appear at resonance. Physically, that can be interpreted as: if the time to deplete the ring due to counter directional coupling (depending on the back

reflection coefficient) becomes shorter than the time to charge up the ring, the resonance splitting will exist [50].

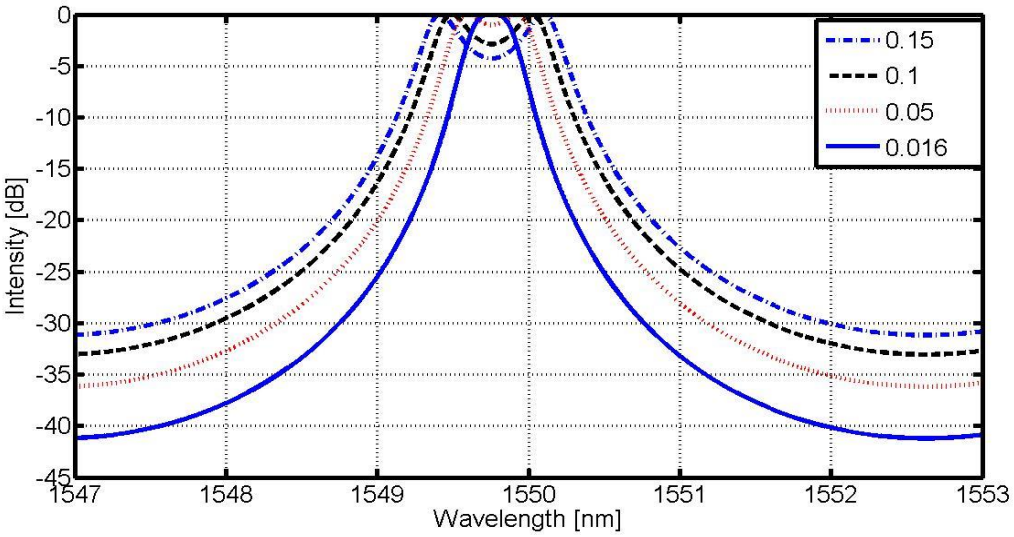

Figure 4-1. Analytically calculated drop port response of a series coupled RR, with a study of the inter-ring coupling (k_i^2) effect on the resonance splitting.

Keeping the difference between this single minimum at the drop port and the single maximum of the through port (at resonance) exceeds an adequate level of suppression for a wide range of wavelengths allows for high crosstalk suppression bandwidth and improves filter performance. This chapter aims to:

1. Derive an expression for the crosstalk suppression bandwidth in single and double ring resonators OADM.
2. Maximize the crosstalk suppression bandwidth by exploiting the resonance splitting induced by the inter-ring coupling.

This chapter is organized as follows:

1. Analytical models of the crosstalk suppression bandwidth in a single and double ring resonator are derived and validated using CST MWS.

2. The inter-ring coupling coefficient effect on the crosstalk suppression bandwidth is modelled and optimized.

3. An over-coupling condition between inter-ring is proposed and simulated.

This chapter concludes with the design of an over-coupled OADM that provides 40 GHz crosstalk suppression bandwidth compared to 28 GHz in the critically coupled OADM. Increasing the bandwidth means that higher data rate channels can be added/dropped with improved signal integrity.

4.2. Crosstalk Bandwidth in a Single Ring Resonator

Figure 4-2 shows a schematic diagram of a single ring resonator based OADM. It indicates that a single ring resonator is coupled with two bus waveguides via two coupling regions. In this section, the crosstalk performance of a single ring resonator based OADM is analysed analytically and modelled using CST MWS to estimate the crosstalk suppression bandwidth.

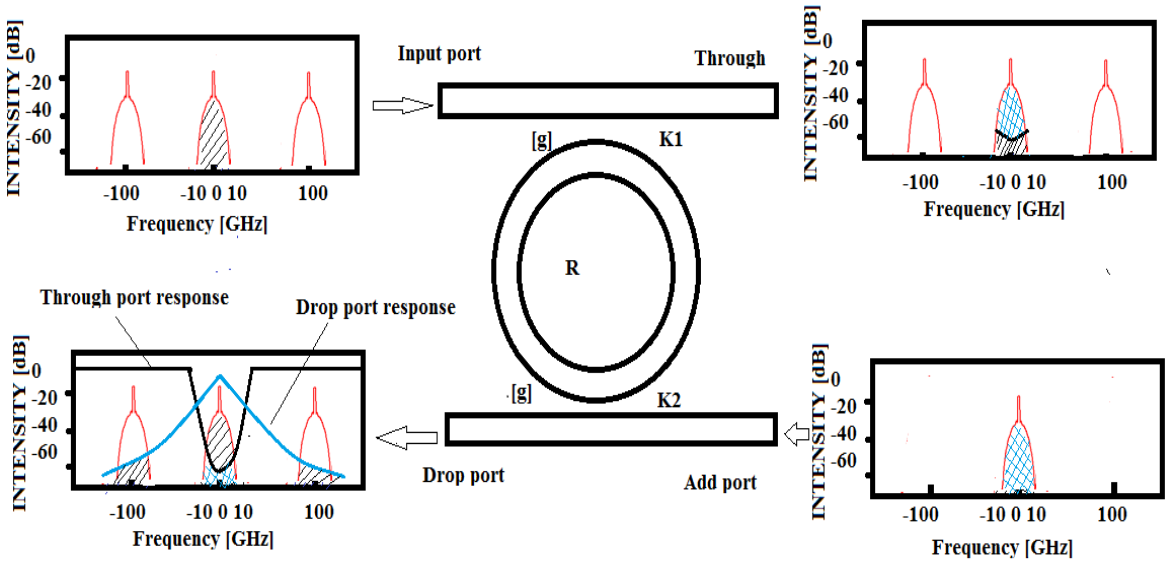

Figure 4-2. Schematic of a single ring add/drop filter with three NRZ of 10 Gbps modulated WDM signal.

4.2.1. CST Simulation

The time domain solver results using CST MWS [139] for the single ring resonator (illustrated in Figure 4-2) are shown in Figure 4-3. An SOI ring resonator was modelled using the following parameters: ring radius equal to 16 μm (corresponding to a 5.5 nm free spectral range), a silicon waveguide with a core refractive index ($n_{core} = 3.47$), and a silicon dioxide lower cladding with a core refractive index ($n_{clad} = 1.47$). The upper clad refractive index was equal to 1 (air). The cross section of silicon waveguide was chosen to ensure a single mode propagation (width= 460 $nm \times$ height= 250 nm). In Figure 4-3, S_{21} and S_{31} represent through port and drop port frequency responses, respectively, while, S_{11} and S_{41} are the normalized power reflection at input port and add port respectively. The

separation between bus and ring waveguides [g] was 40 *nm* which corresponds to a power coupling coefficient ($k_1{}^2 = k_2{}^2 \approx 0.4$). For this value of coupling, the through port attenuation at resonance is -20.7 dB and the maximum drop port is about -1.05 dB, which means that it is difficult with this coupling value to maintain a useful bandwidth. Different coupling coefficients are examined by changing the separation between the bent and straight waveguides to maximize the crosstalk suppression bandwidth.

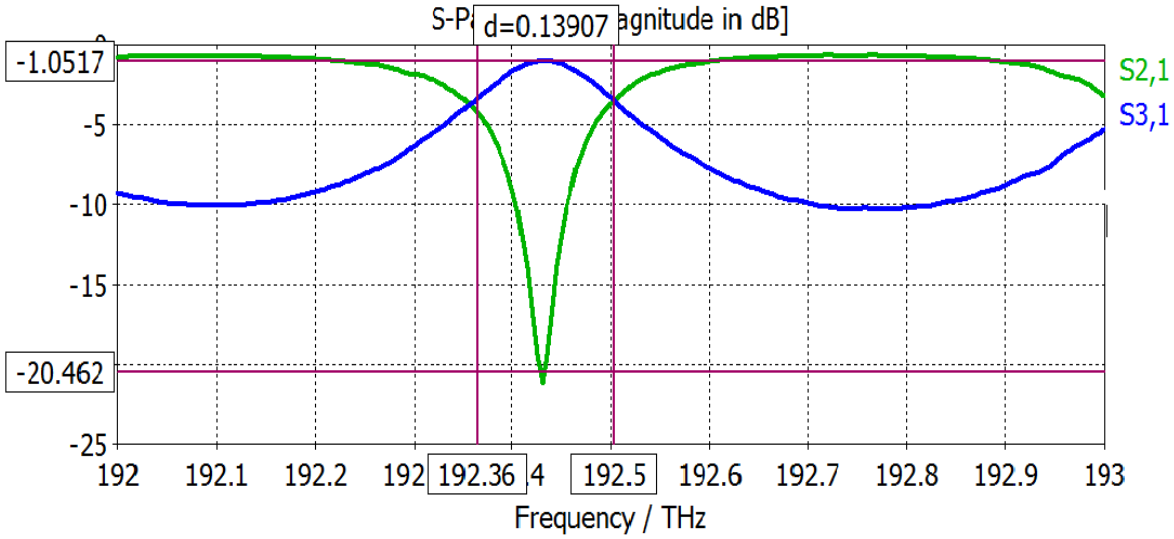

Figure 4-3. Frequency response of a single ring resonator.

4.2.2. Analytical Calculations

The inter-band crosstalk level is obtained from (3-14) by calculating *DR* at 100 GHz, which is called the 'Drop Port Rejection Ratio' DPRR. However, this value depends on the

data rate. For example, it should be calculated at 200 GHz when the transmission rate is 40 Gbps since the channel separation is 200 GHz. The intra-band crosstalk is calculated by taking the difference between the through port intensity and drop port intensity at resonance and it should be high to ensure high crosstalk suppression ratio. To obtain a high suppression of crosstalk in a single ring resonator, the through port intensity should vanish at resonance to ensure that the required channel is completely dropped. This implies that (3-12) should be equal to zero. In a symmetric ring resonator it is difficult to get the numerator of (3-12) equal to zero except in the case of a lossless resonator which is simply impractical. An asymmetric ring resonator with different coupling coefficients was used to maximize crosstalk suppression by choosing t_1 and t_2 in such a way that (3-12) equals zero. These values of coupling coefficients represent "critical" coupling [18].

The other important factor is to calculate the bandwidth over which the crosstalk suppression value is more than the minimum acceptable level of $|20|$ dB [23]. By taking the difference between (3-14) and (3-12), the crosstalk suppression XT is given as:

$$XT = 10\ \log DR - 10 \log IR \tag{4-1}$$

$$XT = 10\log \frac{{k_1}^2 {k_2}^2 e^{-\alpha L}}{1 + {t_1}^2 {t_2}^2 e^{-2\alpha L} - 2t_1 t_2 e^{-\alpha L} \cos \beta L} - 10\log \frac{{t_1}^2 + {t_2}^2 e^{-2\alpha L} - 2t_1 t_2 e^{-\alpha L} \cos \beta L}{1 + {t_1}^2 {t_2}^2 e^{-2\alpha L} - 2t_1 t_2 e^{-\alpha L} \cos \beta L} \tag{4-2}$$

The shape of XT suppression is symmetric around the resonance frequency and the wavelength shift from resonance for each value of XT is calculated using (4-3):

$$\mathrm{Cos}\,\beta L = \frac{{t_1}^2 + {t_2}^2 e^{-2\alpha L} - {k_1}^2 {k_2}^2 e^{-\alpha L} \times 10^{-XT/10}}{2t_1 t_2 e^{-\alpha L}} \tag{4-3}$$

For example, for the required value of $|20|$ dB, the bandwidth of crosstalk suppression is found from:

$$\Delta f = \frac{c}{\pi n_{eff} L}\left[2\pi N + \cos^{-1}\frac{{t_1}^2 + {t_2}^2 e^{-2\alpha L} - 0.01 \times {k_1}^2 {k_2}^2 e^{-\alpha L}}{2t_1 t_2 e^{-\alpha L}}\right] \tag{4-4}$$

where, N is the mode index of the resonator, and *c* is the speed of light in free space.

Figure 4-4 shows the crosstalk bandwidth and the DPRR as a function of coupling coefficients for a symmetric single ring resonator. Changing coupling coefficients will affect filter selectivity through the change of quality factor (3-18).

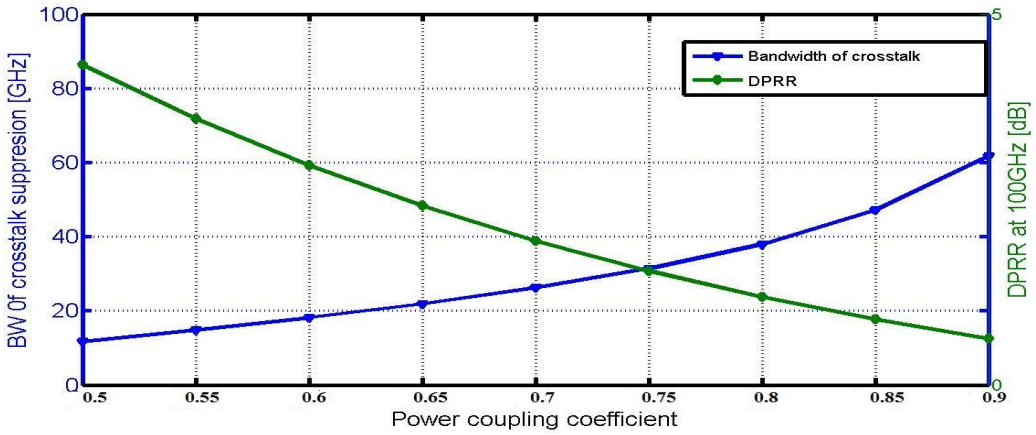

Figure 4-4. Bandwidth of crosstalk suppression and DPRR for a single ring resonator.

The bandwidth of modulated channels is mainly affected by the data rate and the transmission technique. For a given data rate, the bandwidth of RZ is twice that of NRZ. 10

Gbps of NRZ transmission requires 20 GHz bandwidth. Thus, the crosstalk suppression bandwidth should be more than 20 GHz to ensure a dropping of this channel with a reduced level of crosstalk. For a symmetric ring resonator, and from (4-4), the value of the coupling coefficient to attain the required bandwidth for 10 Gbps NRZ is $|k|^2 = 0.625$. For this high coupling coefficient, the DPRR at 100 GHz can be calculated from (3-14) and it is found to be equal to 2.4 dB, which is very low and means that a high level of inter-band crosstalk will be added to the dropped signal. If a 10 Gbps RZ signal is used, the single ring resonator filter is unable to support this signal since it requires a high coupling coefficient (about 0.8) which gives a 1.8 dB DPRR (high inter-band crosstalk).

Asymmetric coupling may represent a better alternative where the coupling coefficient of the second coupling region (t_2), can be chosen to satisfy the critical coupling condition $t_1 = t_2 e^{-\alpha L}$. Using these coupling coefficients for both coupling regions, the through port response at resonance is equal to zero (notch filter). This gives maximum crosstalk suppression ratio. The limitation of the critical coupling ring resonator is that it is asymmetric, which means that the signal entering from the input port is subjected to a different coupling value from the signal entering the adding port. This result in a different behaviour for the add and drop ports of the filter. This limitation has been addressed in [81] by suggesting a series-cascaded ring resonator pair in which the coupling coefficients are adjusted to reduce the crosstalk in the added and dropped signals simultaneously. The effect of coupling coefficients in an asymmetric ring resonator is shown in Figure 4-5.

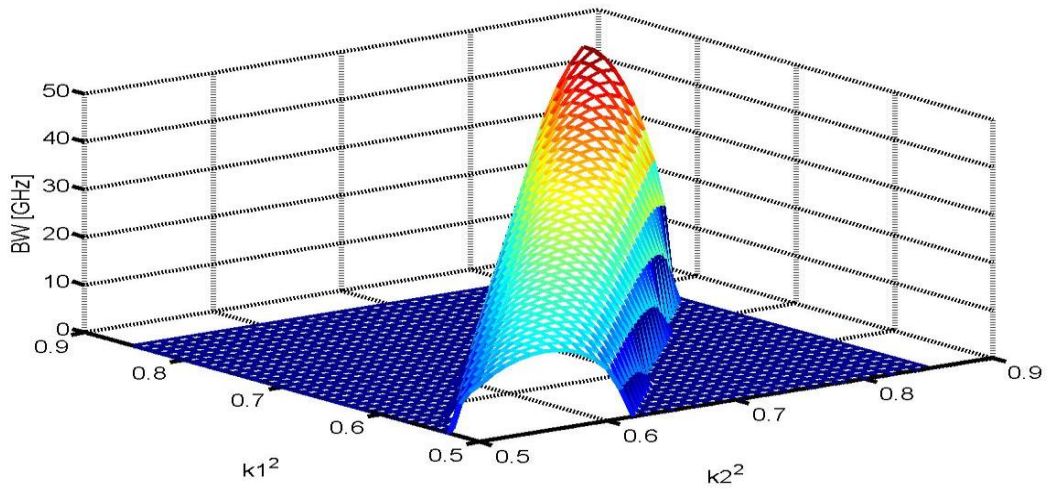

Figure 4-5. Bandwidth for asymmetric single ring resonator as a function of coupling coefficients.

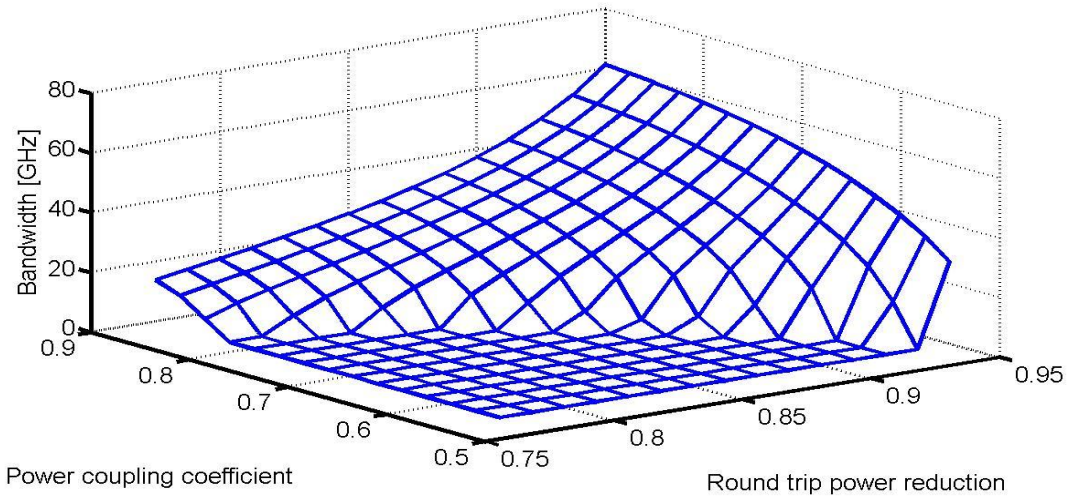

Figure 4-6. Bandwidth of a symmetric single ring resonator as a function of coupling coefficient and losses.

The surface plot presented in Figure 4-5 shows that an asymmetric single ring resonator requires a high coupling coefficient to ensure a wide bandwidth. High through port attenuation is possible in a critical coupled single resonator. However, the bandwidth over

which this suppression occurs is narrow. To increase this bandwidth the coupling coefficient should be high, which would act to increase the level of inter-band crosstalk. The presence of losses in ring resonators also affects the useful bandwidth, as shown in Figure 4-6. Increasing losses in the ring will reduce the bandwidth of crosstalk suppression, resulting in a high inter- and intra-band crosstalk.

4.3. Crosstalk Bandwidth in Double Ring Resonator

An improved spectral response can be obtained when multiple ring resonators are coupled in series. A high DPRR will result from increasing the filter order and this in turn will improve the inter-band crosstalk suppression. However, the study of intra-band crosstalk in second order ring resonators shows a high dependence on the coupling coefficients between the rings (inter-ring coupling k_i). The outer coupling coefficients (between bus waveguides and rings) are considered symmetric (identical separation of outer coupling regions). Hence, the crosstalk performance will depend on the choice of the inter-ring coupling value relative to the outer coupling value. The calculations of the optimum values of inter-ring coupling coefficient k_i for different orders of series coupled ring resonator were shown to follow the formula [$k_i = \frac{k^2}{(2-k^2)}$] [26], where k is the coupling coefficient of the outer rings. It was shown in [25] that the optimum value of coupling coefficient calculated using the above formula yields a higher through port attenuation at resonance and maximizes crosstalk suppression ratio. Table 4-1 shows the values of inter-ring coupling coefficients corresponding to the outer coupling coefficients for a symmetric double ring resonator.

Table 4-1. The relation between the inner and outer coupling coefficients for optimum coupling.

Outer-coupling coefficient $[\|k\|^2]$	0.5	0.55	0.6	0.65	0.7	0.75	0.8
Inter-coupling coefficient $[\|k_2\|^2]$	0.113	0.145	0.18	0.23	0.29	0.36	0.444

The optimum values in Table 4-1 maximize crosstalk suppression ratio, but do not give the maximum bandwidth (required to ensure a high bit rate transmission in the network). An analysis of the spectral response of a higher order ring resonator shows that the response exhibits a "splitting" at resonance, which depends on the inter-ring coupling coefficient, and the number of splits is dependent upon the order of the filter [18].

The analysis given in this section focusses on the calculation of crosstalk suppression bandwidth in a second order ring resonator and the values of coupling coefficient that maximize it. The aim is to find the value of the inter-ring coupling coefficient that produces a splitting of the response at resonance with a level that satisfies the crosstalk suppression requirements over as wide bandwidth as possible. The drop port response will have a double maximum near the resonant frequency and a single minimum at resonance. The through port will have a single maximum at resonance and a double minimum near resonance. By keeping the difference between the single minimum of the drop port response and the single maximum of the through port within the accepted level of suppression, the bandwidth will be increased. To operate the filter in a "splitting" spectral

region the inner coupling coefficient should be higher than the optimum coupling values given in Table 4-1, and hence these are described as "over-coupled" ring resonators.

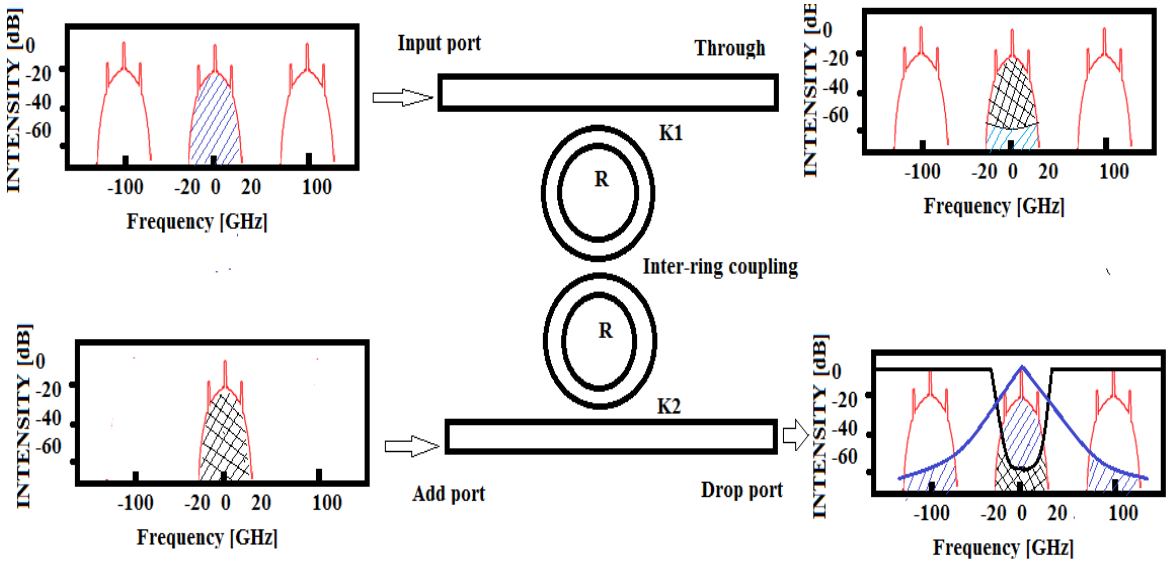

Figure 4-7. The schematic of a series double ring resonator add/drop filter with 10 Gbps RZ WDM signal.

Following the analysis given in section 4.3, for the second order ring resonator shown in Figure 4-7, the drop port and through port transfer functions and the intensity responses are given as below [23]:

The drop and through ports transfer functions are:

$$T_{through} = \frac{t_1 - t_2 x - {t_1}^2 t_2 x + t_1 x^2}{1 - 2t_1 t_2 x - {t_1}^2 x^2} \tag{4-5}$$

$$T_{drop} = \frac{j{k_1}^2 k_2 x^2}{1 - 2t_1 t_2 x - {t_1}^2 x^2} \tag{4-6}$$

The intensity responses for drop and through ports are:

$$IR = \frac{A_1 - A_2 \cos \beta L + A_3 \cos 2\beta L}{B_1 - B_2 \cos \beta L + B_3 \cos 2\beta L} \tag{4-7}$$

$$DR = \frac{D}{B_1 - B_2 \cos \beta L + B_3 \cos 2\beta L} \tag{4-8}$$

where,

$$A_1 = {t_1}^2 + 2e^{-2\alpha L}{t_1}^2{t_2}^2 + e^{-2\alpha L}{t_2}^2 + e^{-2\alpha L}{t_1}^4{t_2}^2 + e^{-4\alpha L}{t_1}^2 \tag{4-9.a}$$

$$A_2 = 2e^{-\alpha L}t_1 t_2 + 2e^{-3\alpha L}t_1 t_2 + 2e^{-\alpha L}{t_1}^3 t_2 + 2e^{-3\alpha L}{t_1}^3 t_2 \tag{4-9.b}$$

$$A_3 = 2e^{-2\alpha L}{t_1}^2 \tag{4-9.c}$$

$$B_1 = 1 + 4e^{-2\alpha L}{t_1}^2{t_2}^2 + e^{-4\alpha L}{t_1}^4 \tag{4-9.d}$$

$$B_2 = 4e^{-\alpha L}t_1 t_2 + 4e^{-3\alpha L}{t_1}^3 t_2 \tag{4-9.e}$$

$$B_3 = A_3 \tag{4-9.f}$$

$$D = e^{-2\alpha L}[1 - {t_2}^2 - 2{t_1}^2 + 2{t_1}^2{t_2}^2 + {t_1}^4 - {t_1}^4{t_2}^2] \tag{4-9.g}$$

Figure 4-8.**a** shows the frequency response of a critical coupled double ring resonator obtained using the time domain solver modelled in CST MWS. S_{41} represents the drop port frequency response in the double ring resonator. The coupling coefficient was (≈ 0.4) and the inter-ring separation was 90 *nm*. The crosstalk bandwidth of about 28 GHz is shown in this Figure. However, Figure 4-8.**b** is the response of the same filter with a different separation between the rings. Changing the inter-ring separation to 85 *nm* will lead to the occurrence of frequency splitting at resonance. This splitting comes from the mutual coupling between the forward and backward modes propagated inside the ring (as discussed in section 4.1). However, this process could be interpreted as a useful effect to increase the bandwidth of crosstalk suppression as shown in Figure 4-8.b. Figure 4-8.**b** shows an increase in the useful bandwidth over which higher crosstalk suppression is obtained.

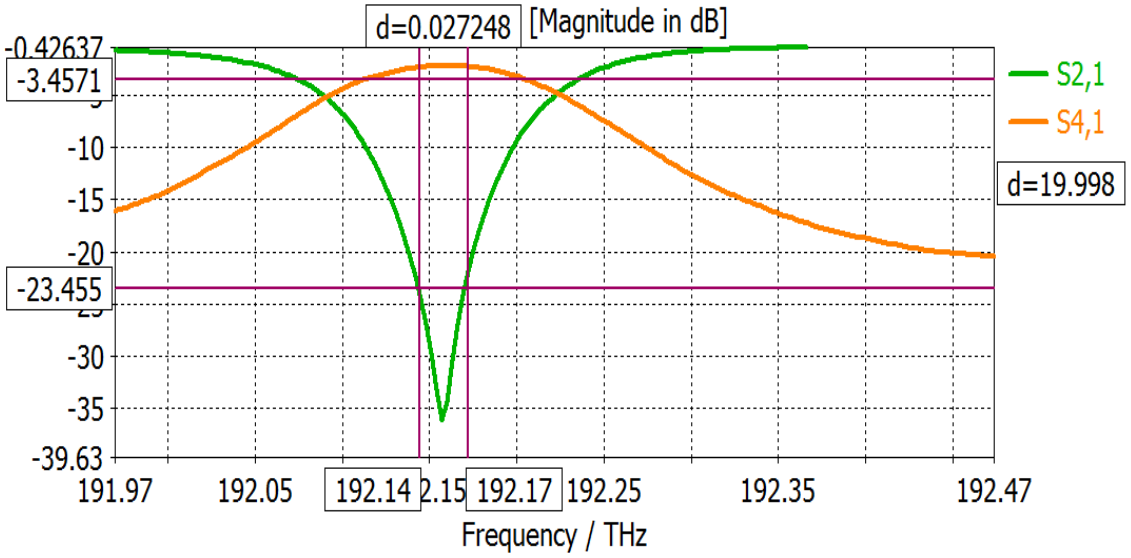

(a)

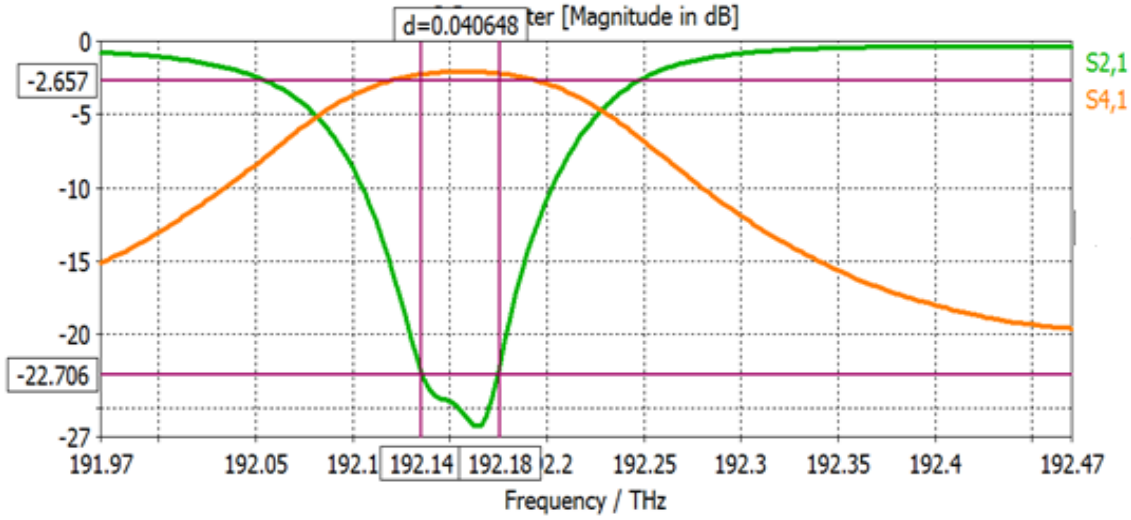

(b)

Figure 4-8. a) Frequency response for series double ring resonator. b) Spectrum splitting at resonance for series double ring resonator.

Analytically, using the same approach used in the case of a single ring resonator, the crosstalk suppression bandwidth is calculated as in (4-1). The difference here is the presence of a single maximum and minimum in the through and drop response respectively. To examine the effect of changing the inter-ring coupling coefficient on the spectral response, the second derivative of the drop port response given in (4-8) with respect to the phase will be taken. At resonance, the value of k_i that gives the second derivative a value equal to zero (maximally flat) is calculated and designated as k_{flat}. To maximize the bandwidth, the value of inter-ring coupling is chosen to be greater than k_{flat} and should satisfy (4-1) where the value of XT should be held at $|20|$ dB or more.

From (4-1) and using (4-7) and (4-8), (4-10) is obtained

$$XT = 10\log\frac{D}{A_1 - A_2\cos\beta L + A_3\cos 2\beta L} \tag{4-10}$$

For the required level of crosstalk suppression:

$$A_1 - A_2\cos\beta L + A_3\cos 2\beta L = 0.01D \tag{4-11}$$

In order to calculate the bandwidth of crosstalk suppression from (4-11), this equation should first be solved to obtain the value of inter-ring coupling that ensures the required level of suppression at resonance frequency (where the single maximum and minimum of through and drop response occurs). At resonance, (4-11) results in a second order equation for ${t_2}^2$ and the solution of this equation will result in two values of t_2. The value of inter-ring coupling ($k_2 = \sqrt{1 - {t_2}^2}$) that results in an over-coupling between rings should be greater than k_{flat} as in Table 4-2.

Table 4-2. Inter-ring coupling coefficients for over-coupling.

Outer-coupling coefficient $[\|\boldsymbol{k}\|^2]$	$\mathbf{0.5}$	$\mathbf{0.55}$	$\mathbf{0.6}$	$\mathbf{0.65}$	$\mathbf{0.7}$	$\mathbf{0.75}$	$\mathbf{0.8}$
Inter-coupling coefficient $[\|\boldsymbol{k_2}\|^2]$	$\mathbf{0.131}$	$\mathbf{0.170}$	$\mathbf{0.217}$	$\mathbf{0.273}$	$\mathbf{0.34}$	$\mathbf{0.41}$	$\mathbf{0.512}$

Equation (4-11) should be solved again as a second order equation in terms of $cos\,\beta L$ in order to calculate the bandwidth. Using (4-12), the bandwidth can be calculated in terms of coupling coefficients

$$\cos\beta L = \frac{A_2}{2A_3} + 0.5\sqrt{\left[\left(\frac{A_2}{A_3}\right)^2 - 4\frac{(A_1 - 0.01D)}{A_3}\right]} \tag{4-12}$$

The values for A_1, A_2, A_3 and D are calculated from (4-9.a).

Figure 4-9 shows the difference in the crosstalk suppression bandwidth for critical coupling (Table 4-1) and that computed using (4-12). It is noted that for RZ at 10 Gbps, where the required bandwidth is 40 GHz, the power coupling coefficient in the case of critical coupling is 0.58, while in the case of an over-coupled ring resonator it is 0.46. The DPRR in the case of an over coupled ring resonator is 13 dB. This is compared to 7 dB for critical coupling which means an enhancement of inter-band crosstalk suppression.

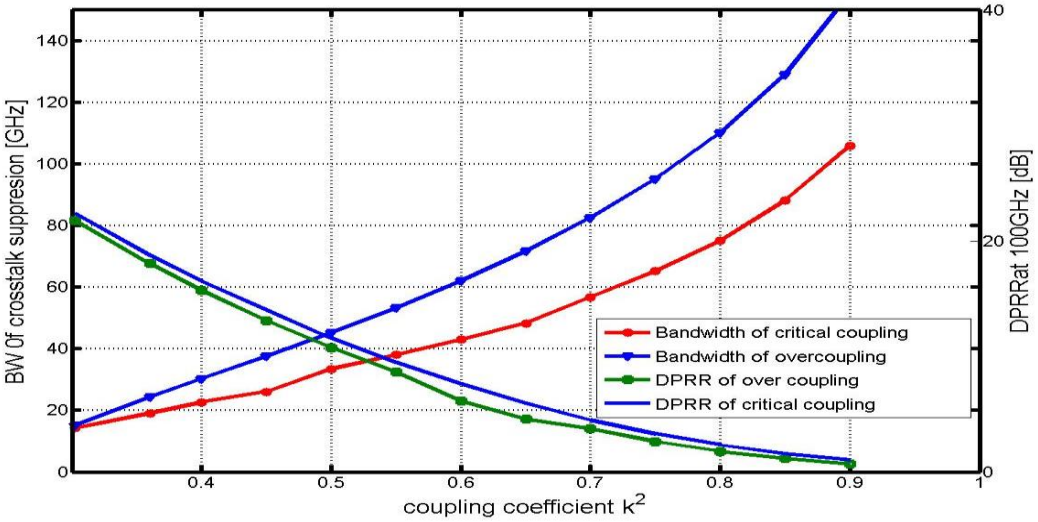

Figure 4-9. Bandwidth of crosstalk suppression and drop port rejection ratio for critical and over coupled double ring resonator (losses =4 dB/cm).

The effect of ring losses in the over-coupled ring resonators is shown in Figure 4-10. Different values of round trip losses are used, and for each value of loss the inter-ring coupling coefficient is calculated to obtain the required level of crosstalk. Then the bandwidth of crosstalk suppression is calculated as a function of both the losses and coupling coefficients. For some levels of losses it is difficult to acquire the accepted level of crosstalk suppression. This is represented as a bandwidth equal to zero in Figure 4-10.

From the results shown in Figure 4-9 and Figure 4-10 it can be seen that an over-coupled ring resonator provides a wider bandwidth to accommodate higher data rate signals with low crosstalk compared to a critical coupled ring resonator filters. Optimising the value of inter-ring coupling to operate in the over coupled region gives a better spectral response in terms of intra-band and inter-band crosstalk simultaneously.

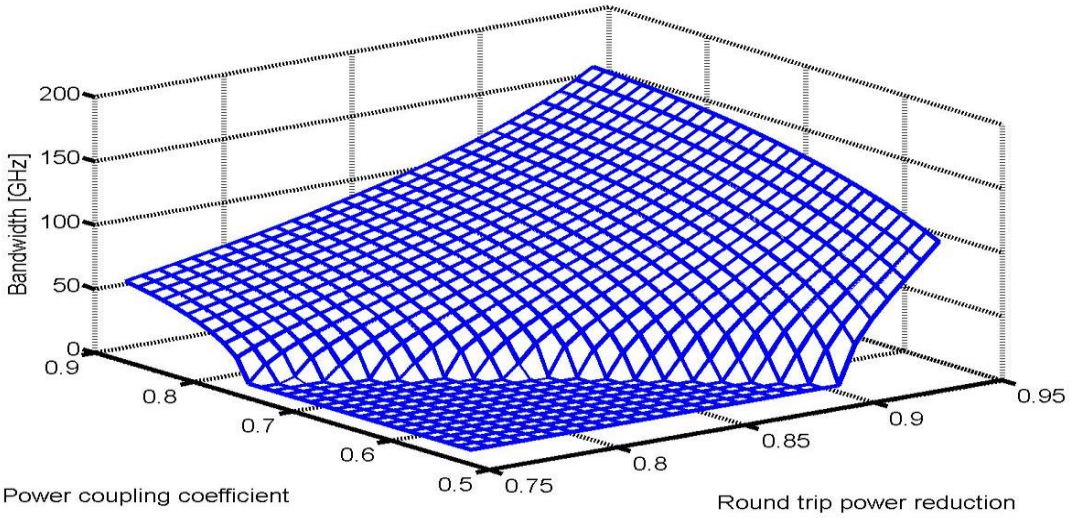

Figure 4-10. Bandwidth of the over coupled ring resonator as a function of losses for different coupling coefficient.

4.4. Conclusion

In this chapter, increasing the crosstalk suppression bandwidth in a series (double) ring resonator based OADM was the main aim of interest. Inter and intra-band crosstalk effects in single and double ring resonator filters were investigated for intensity modulated RZ and NRZ signals. It was shown that for a double ring resonator based filter, with a power coupling coefficient of 0.46, the bandwidth of crosstalk suppression in the case of critical coupling is 28 GHz, while for the over coupled condition the bandwidth is 40 GHz. This means that a critically coupled filter will add more crosstalk if used with a 10 Gbps RZ signal. Physically, that means, for the same separation gap between the rings and bus waveguides, it is possible to enhance the bandwidth of the model by more than 40% by

adjusting the inter-ring coupling. Over coupling in a series coupled OADM improves the bandwidth and the level of inter-band crosstalk simultaneously and allows for high data rate channel dropping.

CHAPTER FIVE

CROSSTALK BANDWIDTH ESTIMATION OF PARALLEL COUPLED OADM

This chapter investigates crosstalk issues in (parallel) coupled optical ring resonators. It examines the performance of a well-known optical device (an OADM based on parallel coupled ring resonators realized in SOI technology) but focusses on the optical signal integrity perspective. The Signal Flow Graph approach (based on Mason's rule) is used to identify filter performance in terms of crosstalk suppression bandwidth and EMC. The use of Mason's rule in this regard is novel and useful. The good agreement between analytical and simulation results suggests that using the derived analytical model is a faster and easier approach for filter design and provides a better insight into the signal integrity performance of the filter.

5.1. Introduction

Parallel coupled ring resonators were proposed to enhance the overall response of OADM in WDM networks [81, 82, 102]. High Out-of-Band Rejection Ratio (OBRR) and improved crosstalk suppression ratio are shown to be achieved by optimizing coupling coefficients and the separation distance between rings. However, optimizing the resonator parameters,

in order to enhance the crosstalk performance, requires a simple and direct form for the OADM transfer function.

Different techniques have been proposed for the analysis of cascaded photonic devices. The most elementary analytical method is to write out explicit node and loop equations and extract the overall transfer function from them. Despite the fact that this method provides the required characteristics (such as phase, group delay and dispersion) it is complicated and cumbersome [20]. The transfer matrix based method has been used for transfer function derivation by calculating the scattering matrix of each ring. The overall transfer matrix is calculated by using matrix multiplication [148]. The complexity of this approach increases with the number of coupled rings.

The graphical approach, also called Signal Flow Graph (SFG) method proposed by Mason [149] was also used to provide a faster and easier approach for multipath (series coupled) ring resonators [124]. This approach showed a reduction of calculation time from 1/3 to 1/20 compared to the transfer matrix method, depending on the complexity of the filter (number of rings) [150]. The group delay and dispersion characteristics of the filter are difficult to calculate directly by the SFG method. However, in [151] this method was used to calculate the transfer function of a single ring resonator OADM including the group delay. This chapter aims to:

1. Derive the transfer function of a parallel coupled ring resonator OADM using the SFG method.

2. Optimize filter parameters (based on the derived transfer function) in order to improve the crosstalk suppression bandwidth.

This chapter is organized as follows:

1. The SFG method based on Mason's rule is presented and a general form of the transfer function of N rings coupled in parallel is derived.
2. The validity of the proposed analytical model is examined against CST MWS simulation results.
3. Coupling coefficients, centre-to-centre separation and ring losses effects are studied and optimized to improve the crosstalk suppression bandwidth.

This chapter concludes with a simple and direct form for the transfer function. This form is used to study the effect of different parameters on the filter performance and, moreover, to improve the crosstalk suppression bandwidth.

5.2. Mason's Rule for Parallel Coupled Ring Resonators

Consider the parallel coupled ring resonator based filter shown in Figure 5-1. If a WDM signal enters at port 1, only the channels that satisfy the resonance condition will be coupled to port 3, the designated drop port. Channels with different wavelengths from resonance will pass (ideally) unaffected to the through port. A new channel can be added at port 4 (the opposite side of the system to port 3).

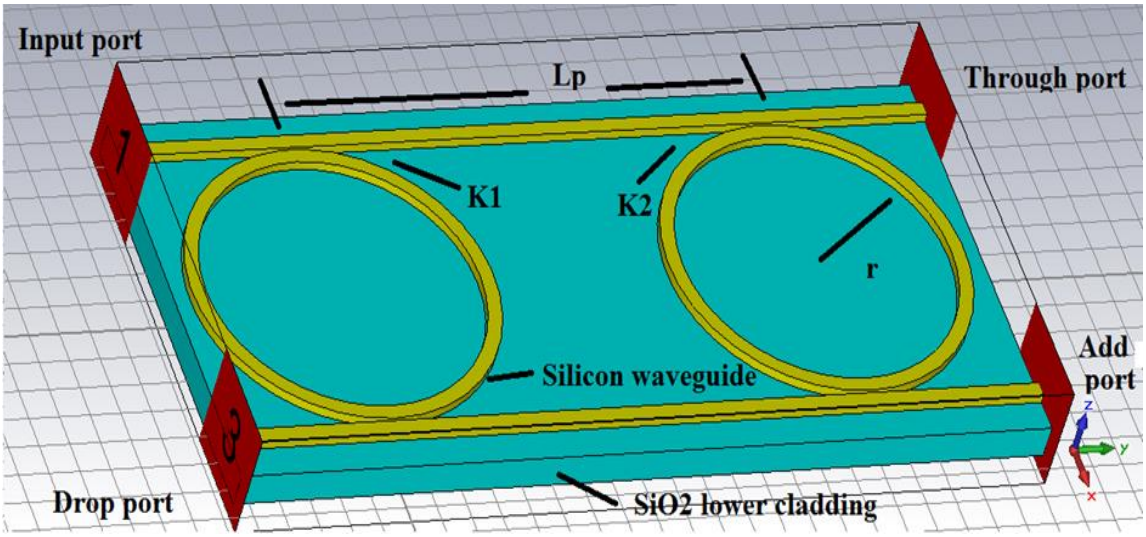

Figure 5-1. CST model of parallel coupled ring resonator.

The coupled light in each ring will be subjected to a transmission coefficient x_1 given in (5-1) after one round trip, while the light propagating from the first ring to the second ring will have a magnitude and phase change depending on x_2 given in (5-2), which represents the waveguide loss and propagation phase change.

$$x_1 = e^{-\alpha L_r - j\beta L_r} \tag{5-1}$$

$$x_2 = e^{-\alpha L_p - j\beta L_p} \tag{5-2}$$

In (5-1) and (5-2), β is the phase constant, L_r is the ring perimeter, L_p is the separation distance between the rings and α is the loss coefficient measured in cm^{-1}.

There are a number of assumptions on which this analysis is based:

1. Losses in the bus waveguides are small, so the approximation can be made as $e^{-\alpha L_p} \approx 1$.
2. Propagation constants in the ring and bus waveguides are the same.
3. No back reflection propagation occurs in the rings.
4. Equal radii rings, $L_r = L_{r_1} = L_{r_2}$.
5. Symmetric coupled rings are used.

Mason's rule [149] was used to determine the transfer function of a linear system by first finding the forward paths between input and output and then defining the closed loop gains. The total gain is then calculated by taking the summation of the forward gain of each path multiplied by a quantity representing the gain of non-touching loops of that path. This quantity is called the cofactor. The result is divided by a term representing the total gain of closed loops plus the gain product of non-touching loops. The two loops are said to be non-touching if they do not share any node.

In Figure 5-2, there are two forward paths: G_1 represents the path for light coupled to the first ring, propagating around the half length of this ring and coupled to the drop port. The remaining light will propagate in the second path G_2, which is twice the distance between rings plus half of the second ring length.

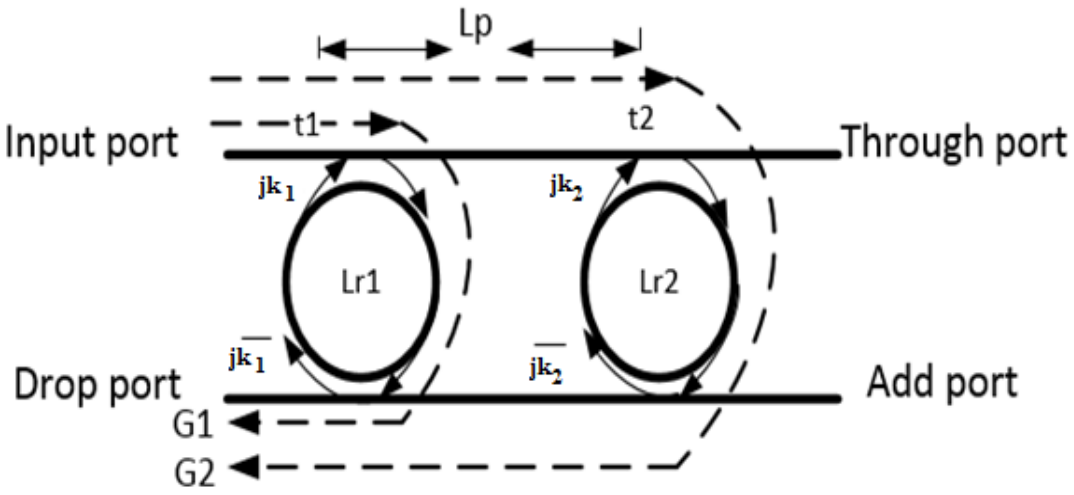

Figure 5-2. Forward paths.

$$G_1 = -k_1{}^2 x_1{}^{1/2} \tag{5-3}$$

$$G_2 = -t_1{}^2 k_2{}^2 x_2{}^2 x_1{}^{1/2} \tag{5-4}$$

There are two closed loops as shown in Figure 5-3 resulting from the light circulating in each ring ($T_1$and T_2), and extra closed loop resulting from the path containing half of each ring and the separation between them (T_3).

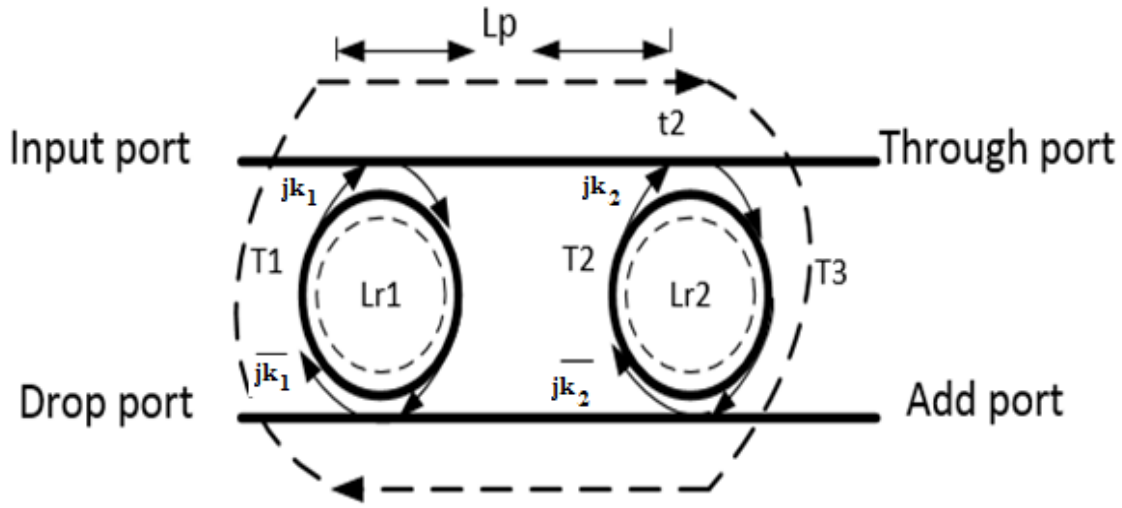

Figure 5-3. Closed loops.

$$T_1 = t_1^2 x_1 \tag{5-5.a}$$

$$T_2 = t_2^2 x_1 \tag{5-5.b}$$

$$T_3 = k_1^2 k_2^2 x_1 x_2^2 \tag{5-5.c}$$

The gain product of non-touching loops (T_1 and T_2) is given by:

$$T_{21} = t_1^2 t_2^2 x_1^2 \tag{5-6}$$

Applying Mason's rule:

$$G = \frac{\sum G_i \Delta_i}{\Delta} \tag{5-7}$$

where, G and G_i are the total gain of the system and the gain of each forward path, respectively. Δ is the determinant of the closed loops, and Δ_i is the cofactor for each path.

$$\Delta = 1 - t_1^2 x_1 - t_2^2 x_1 - k_1^2 k_2^2 x_1 x_2^2 + t_1^2 t_2^2 x_1^2 \tag{5-8.a}$$

$$\Delta_1 = 1 - T_2 - T_3 \tag{5-8.b}$$

$$= 1 - t_2^2 x_1 - k_1^2 k_2^2 x_1 x_2^2$$

$$\Delta_2 = 1 - T_1 = 1 - t_1^2 x_1 \tag{5-8.c}$$

The gain at the drop port is:

$$G = \frac{G_1 \Delta_1 + G_2 \Delta_2}{\Delta}$$

$$= \frac{-k_1^2 x_1^{\frac{1}{2}} + t_2^2 k_1^2 x_1^{\frac{3}{2}} + k_1^4 k_2^2 x_1^{\frac{3}{2}} x_2^2 - t_1^2 k_2^2 x_2^2 x_1^{\frac{1}{2}} + t_1^4 k_2^2 x_2^2 x_1^{3/2}}{1 - t_1^2 x_1 - t_2^2 x_1 - k_1^2 k_2^2 x_1 x_2^2 + t_1^2 t_2^2 x_1^2} \tag{5-9}$$

Equation (5-9) gives a closed form for the drop port response of the two rings in parallel based on the application of Mason's rule.

Considering the case of a single ring in order to validate this approach in the limiting case,

$$\mathrm{L_p} = 0, \quad k_2 = 0$$

$$\mathrm{G} = \frac{-{k_1}^2 {\mathrm{x}_1}^{1/2}}{1 - {\mathrm{t}_1}^2 \mathrm{x}_1}$$

This is the same as for single ring as presented in [104]. The rest of the model derivation for an arbitrary number of rings ($N > 2$) is presented in the appendix A.

The effect of different parameters on the through and drop port spectral responses of OADMs are studied as below:

1. An estimation of the separation distance ($\mathrm{L_p}$) effect is performed. A parallel double coupled OADM with rings of radii 5 μm (a typical value) is modelled analytically using (5-9). The drop port response is highly affected by the separation between the resonators. This comes from the phase accumulation between the dropped signals from the first and second resonators, which in turn results from the separation distance. The separation distance should be greater than the ring diameter to ensure that there is no coupling between rings. The optimum separation [152] is the distance over which the outputs of two rings are added in phase. Figure 5-4, shows the spectral response of the drop port for two different separation distances L_p. In this design the optimum separation is $\mathrm{L_p} = 0.50462 \times \mathrm{L_r}$.

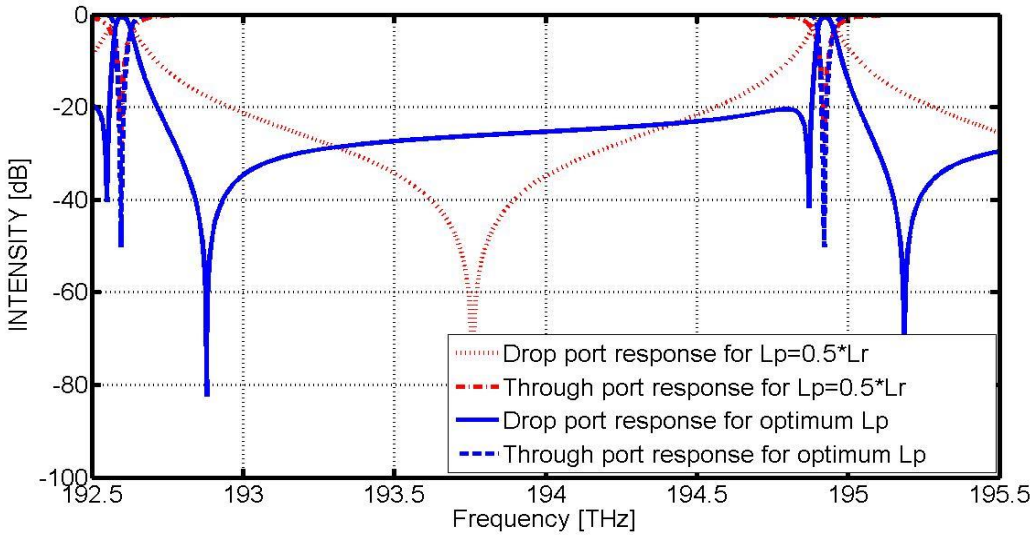

Figure 5-4. Analytically calculated spectral response for a 0.05 coupling.

2. For the optimum separation, the effect of changing coupling coefficients in both rings is simulated analytically and presented in Figure 5-5. Increasing coupling coefficients results in an increase in the filter bandwidth which can help to drop channels of high data rates with low level of crosstalk (intra-band crosstalk). However, the OBRR which represents the level of suppression to adjacent channels (inter-band crosstalk) will be low. The OBRR is highly affected by the coupling coefficients and for high coupling levels tends to be unacceptable for WDM filters [107].

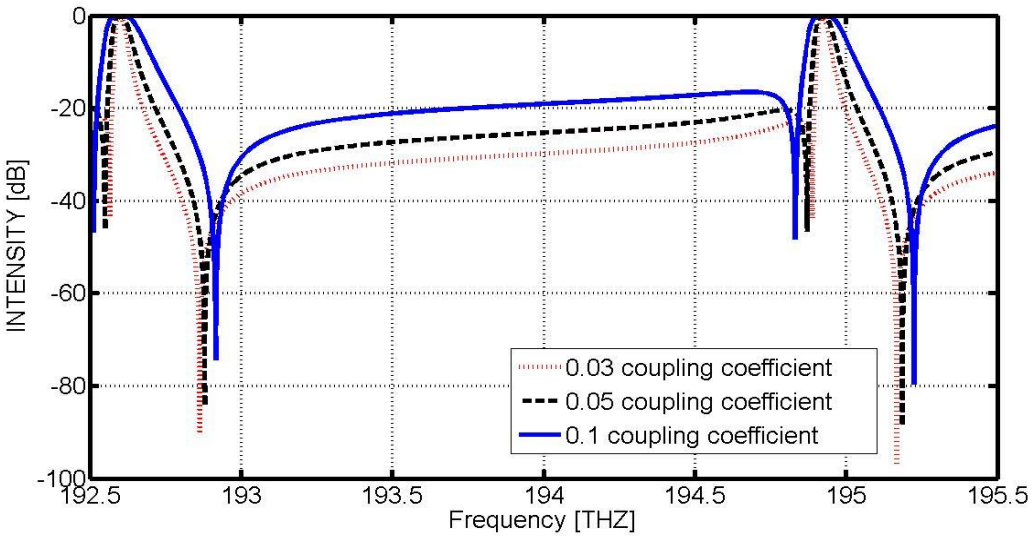

Figure 5-5. The model sensitivity for different coupling coefficients.

5.3. CST Simulation

A Silicon-On-Insulator ring resonator (Figure 5-1) is modelled using the following parameters (identical to those used with the SFG approach): ring radius equal to 5 μm, silicon waveguide with a core refractive index (n_{core}= 3.47), and silicon dioxide lower cladding with a refractive index (n_{clad}= 1.47). The upper clad refractive index was equal to 1 (air). The cross section of the silicon waveguide was chosen to ensure a single mode propagation (width = 460 nm and height = 220 nm) [18] and a 1 μm thick SiO_2 layer is assumed to ensure minimal substrate leakage losses [8, 9].

The time domain solver results using CST MWS for the parallel coupled ring resonator are shown in Figure 5-6. In this Figure, S_{21} and S_{31} represent through port and drop port

spectral responses respectively. The gap separation [g] was 100 nm. The accuracy of the CST model was first examined against the already modelled filter in [152]. This enables CST to be used as a reference to validate the analytical model presented in this chapter.

As shown in Figure 5-6, the OBRR is greater than 20 dB, which is similar to that obtained from the analytical model (Figure 5-5). There is also a comparison between the changes in the spectral responses with the separation distance in both models; good agreement was found for both optimum separation and separation equal to half resonator length. This allows the use of this model to study the effect of different parameters on the overall filter performance.

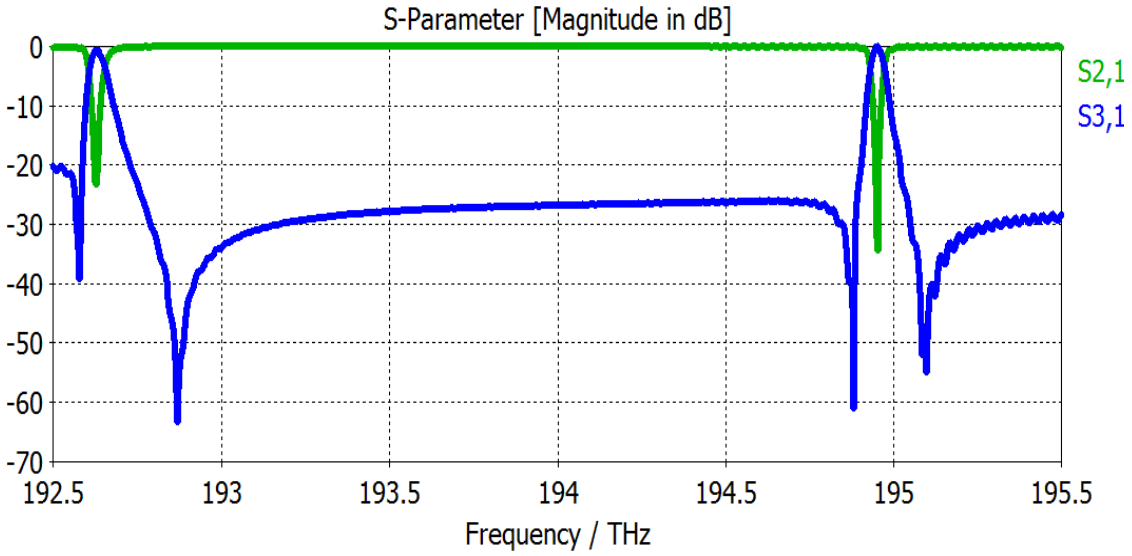

(a)

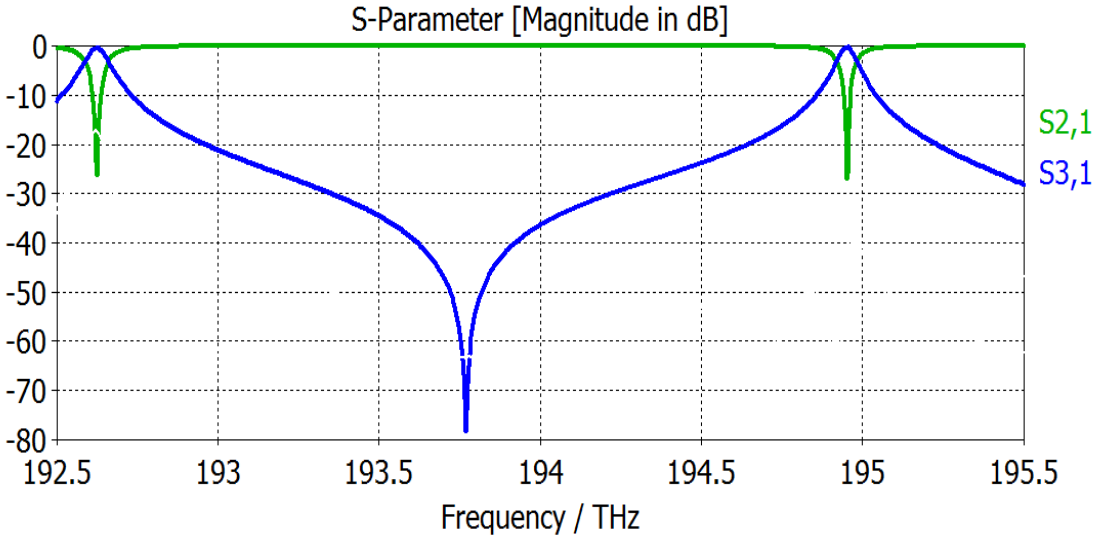

(b)

Figure 5-6. CST simulation of a symmetric parallel coupled ring resonator for optimum separation (a) and half resonator length (b).

5.4. Analytical and Simulation Results

In order to mitigate the crosstalk effect in parallel coupled OADMs, both types of crosstalk (inter and intra-band) should be considered. The proposed model, which has already been examined against CST MWS, can be used to suggest the optimum design parameters (separation distance, coupling coefficients, and loss coefficient) that reduce crosstalk and ensure improved signal integrity.

1. Inter-band crosstalk: Figure 5-5 shows the effect of changing coupling coefficients on the level of suppression (OBRR). However, that figure shows the change of OBRR for similar coupling coefficients in both rings. Examining the effect of different coupling coefficients to obtain optimized values is the aim of this section. The OBRR is calculated out of resonance to estimate the inter-band crosstalk suppression. Figure 5-7 shows that the coupling coefficient selection is limited by the OBRR. It is clear that for high coupling coefficients, the OBRR is less than $|20|$dB which is insufficient to suppress the WDM channels out of resonance.

2. Intra-band crosstalk: Figure 5-8 shows the effect of changing coupling coefficients in both rings on the level of crosstalk. Crosstalk suppression ratio is highly affected by coupling coefficients that control the level of drop and through port responses (as discussed in Chapter three).

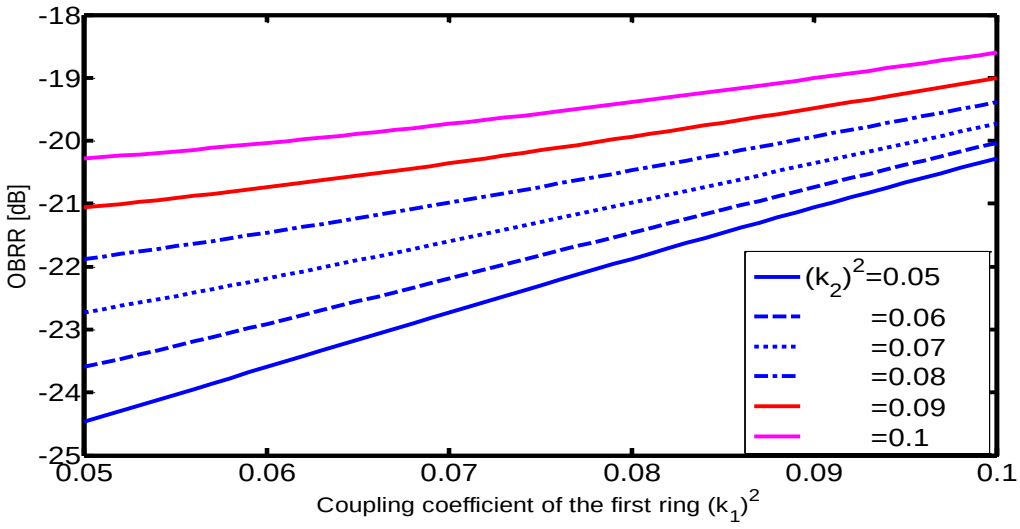

Figure 5-7. The OBRR sensitivity to the coupling coefficients.

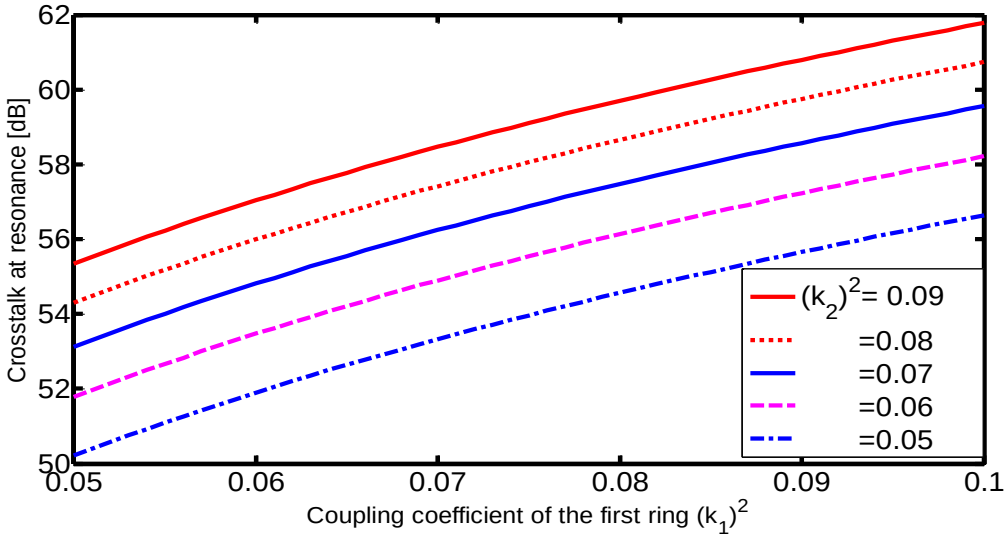

Figure 5-8. Coupling coefficient effects on the level of crosstalk suppression.

A high level of crosstalk suppression is obtained by increasing the coupling coefficients. However, for efficient design, both crosstalk suppression ratio and OBRR should be within an acceptable level (greater than $|20|$ dB). Based on Figure 5-7 and Figure 5-8 it can be seen that, to ensure acceptable levels for inter and intra-band crosstalk, a coupling coefficient of 0.05 for the second ring can be used with a wide range of coupling coefficients for the first ring.

For coupling coefficient of 0.05 in the second ring, the effect of losses on the level of crosstalk suppression was also simulated as shown in Figure 5-9. As expected from the analytical model, any increase in losses inside the rings will result in a reduction of crosstalk suppression due to the insertion loss.

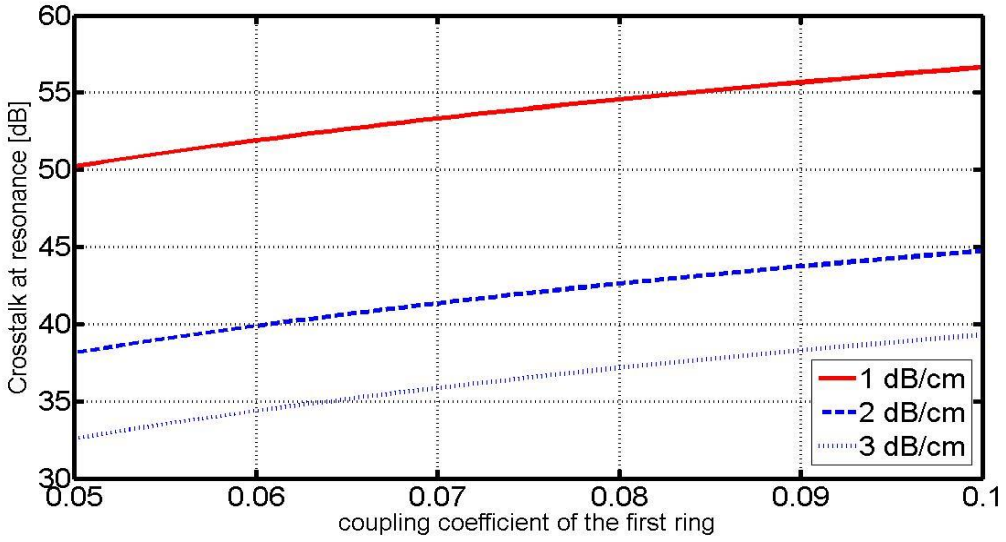

Figure 5-9. Crosstalk as a function of losses.

Using the analytical model presented in this chapter, estimations of crosstalk bandwidth are obtained as a function of coupling coefficients, as shown in Figure 5-10. For a 0.05 coupling coefficient for both rings, a bandwidth of about 14 GHz is obtained. Increasing the value of coupling coefficients leads to an increase in the bandwidth but decreases the OBRR.

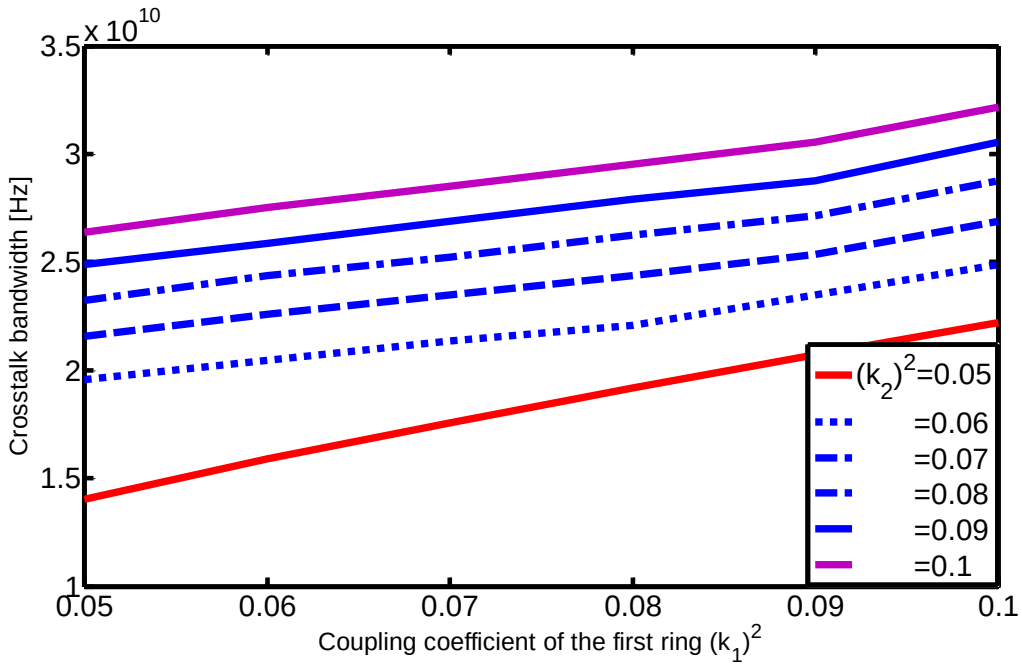

Figure 5-10. Crosstalk as a function of coupling coefficients calculated analytically.

To validate the bandwidth obtained using the SFG method, CST MWS was used to estimate the bandwidth. A time domain simulation for the filter using the optimized coupling values (calculated using SFG) was implemented and the result is shown in Figure 5-11.

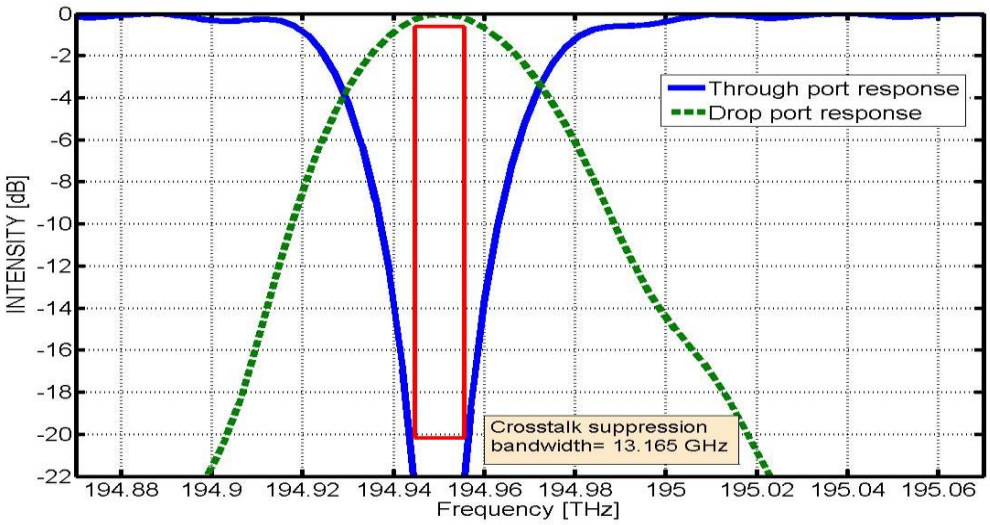

Figure 5-11. Crosstalk bandwidth for an optimal coupling coefficient of 0.05, calculated using CST MWS.

It is clear from Figure 5-11 that the crosstalk suppression bandwidth is 13.16 GHz, which agrees with that calculated using the SFG model (14 GHz as in Figure 5-10). Increasing the coupling of both rings to 0.06 will increase the bandwidth of crosstalk suppression to about 21GHz (Figure 5-10) and at the same time, maintain an acceptable level of OBRR (-23 dB, Figure 5-7). The new coupling coefficients were also modelled using CST, and the results are shown in Figure 5-12.

The simulation results show that a bandwidth of 20.2 GHz is obtained compared to 21 GHz from the analytical model. This difference between the calculated bandwidth (which can be related to meshing in CST) is small enough to allow to rely on the SFG model for crosstalk bandwidth estimation as a faster and easier approach, compared to the transfer matrix method [72].

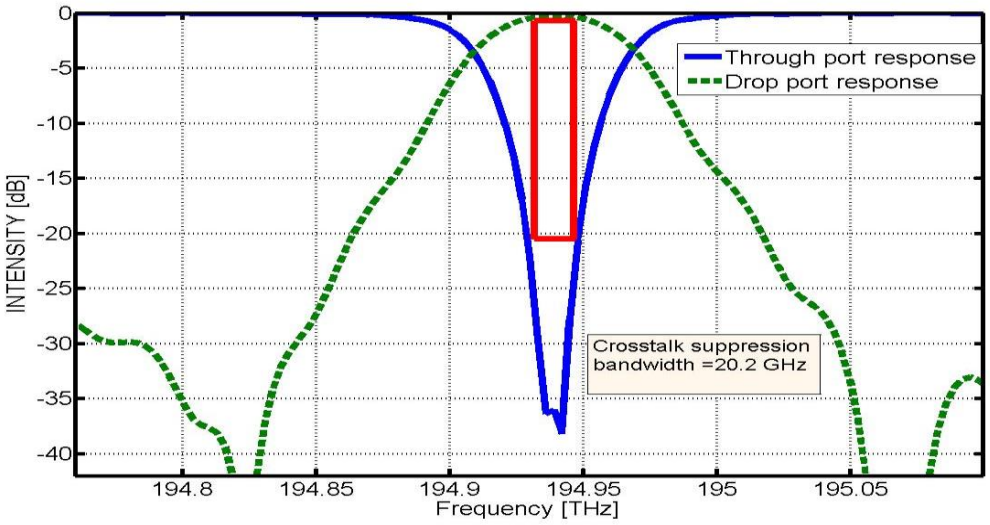

Figure 5-12. Crosstalk bandwidth for a 0.06 coupling coefficient calculated using CST MWS.

5.5. Conclusion

In this chapter, the crosstalk performance of a parallel coupled (double) ring resonator based OADM was studied and modelled. The spectral response was calculated analytically (using Mason's rule) and compared with CST MWS generated results for different separation distances. The SFG model derived in this chapter is sufficiently accurate and valid to be used for parallel coupled filter analysis. It was used to estimate the coupling coefficients, in both rings, to ensure an acceptable level of OBRR and increased crosstalk suppression bandwidth. The small difference between analytically calculated crosstalk suppression bandwidth (21 GHz) and that obtained numerically using CST MWS (20.2 GHz) provides further validation of the proposed (SFG) calculations. The SFG calculations

in parallel coupled OADMs shorten the crosstalk calculation time compared to full-wave electromagnetic simulation and reduces the computational complexity relative to the scattering matrix method.

CHAPTER SIX

VERTICALLY COUPLED RING RESONATOR OADM

This chapter proposes a design of small size (single ring) OADM that provides an increased crosstalk suppression bandwidth to drop 10 Gbps NRZ channels. A vertical coupled OADM is simulated and the effect of different design parameters on the crosstalk suppression bandwidth is numerically investigated. A simulation-driven design optimization procedure is used to determine the design parameters that produce 21 GHz crosstalk suppression bandwidth.

6.1. Introduction

Ring resonator based add/drop multiplexers (OADMs) and filters are used for adding and dropping channels entirely in the optical domain. The frequency response of an OADM depends on the coupling strength (as discussed in Chapter three) [50]. A high coupling strength will result in a deep notch in the through port response. However, it will reduce filter selectivity [18]. The coupling strength is highly dependent on the coupling scheme (lateral and vertical coupling) [103].

In order to design a small size OADM with improved signal integrity, a vertical coupled "single" ring resonator OADM is simulated and the effect of different design parameters on the crosstalk suppression bandwidth is numerically investigated. The proposed design guideline offers a large crosstalk suppression bandwidth with good opportunities for optimization and control. In a vertically coupled OADM, coupling efficiency between the evanescent tails of modes (in the bus and bent waveguides) is controlled by the vertical separation and lateral deviation between waveguides.

The aim of this chapter is to design a small-sized (single ring) vertically coupled OADM that provides improved crosstalk suppression bandwidth.

This chapter is organized as follows:

1. Vertical coupling in a ring resonator based OADM is introduced and the coupling coefficient definition in term of ring parameters is presented.

2. Ring parameters effects on the crosstalk suppression ratio are studied and numerically modelled. Vertical separation and lateral deviation between bus and bent waveguides are examined to suggest an initial range of parameters for optimization.

3. A simulation-driven design optimization procedure is used to determine the design parameters that increase the crosstalk suppression bandwidth. The optimization in this chapter was performed in collaboration with Reykjavik University.

This chapter concludes with a design of a vertically coupled OADM that allows for 21 GHz crosstalk suppression bandwidth. More discussion of this design is presented in the following sections.

6.2. Crosstalk Suppression: Analytical and Simulation Model

In a vertically coupled OADM, bus waveguides are buried in silicon dioxide material which will result in a low scattering loss [23]. Moreover, the fabrication process depends on the well-controlled deposition instead of etching to control the coupling separation [88, 153], which represents another advantage over the lateral coupling. Coupling coefficients in vertically coupled structures can be controlled to a fine degree using a number of parameters such as: vertical separation, lateral deviation and waveguides height. These are all considered in this chapter.

6.2.1. Analytical Model

The transfer function of the vertically coupled OADM shown in Figure 6-1 is calculated based on the Coupled Mode Theory (in space domain). A similar approach to that of the laterally coupled ring resonator used in chapter four is applied [154].

The drop port response is given by:

$$\mathrm{DR} = \frac{k_1{}^2 k_2{}^2 \mathrm{e}^{-\alpha l}}{1 + \mathrm{t}_1{}^2 \mathrm{t}_2{}^2 \mathrm{e}^{-2\alpha l} - 2\mathrm{t}_1 \mathrm{t}_2 \mathrm{e}^{-\alpha \mathrm{L}} \cos \beta l} \tag{6-1}$$

whereas the through port intensity response can be calculated as:

$$\mathrm{IR} = \frac{\mathrm{t}_1{}^2 + \mathrm{t}_2{}^2 \mathrm{e}^{-2\alpha l} - 2\mathrm{t}_1 \mathrm{t}_2 \mathrm{e}^{-\alpha l} \cos \beta l}{1 + \mathrm{t}_1{}^2 \mathrm{t}_2{}^2 \mathrm{e}^{-2\alpha l} - 2\mathrm{t}_1 \mathrm{t}_2 \mathrm{e}^{-\alpha l} \cos \beta l} \tag{6-2}$$

Here, l is the resonator perimeter, α is the field loss coefficient (the round trip amplitude reduction $\exp(-\alpha l)$), and $\beta = 2\pi \mathrm{n}_{\mathrm{eff}}/\lambda$.

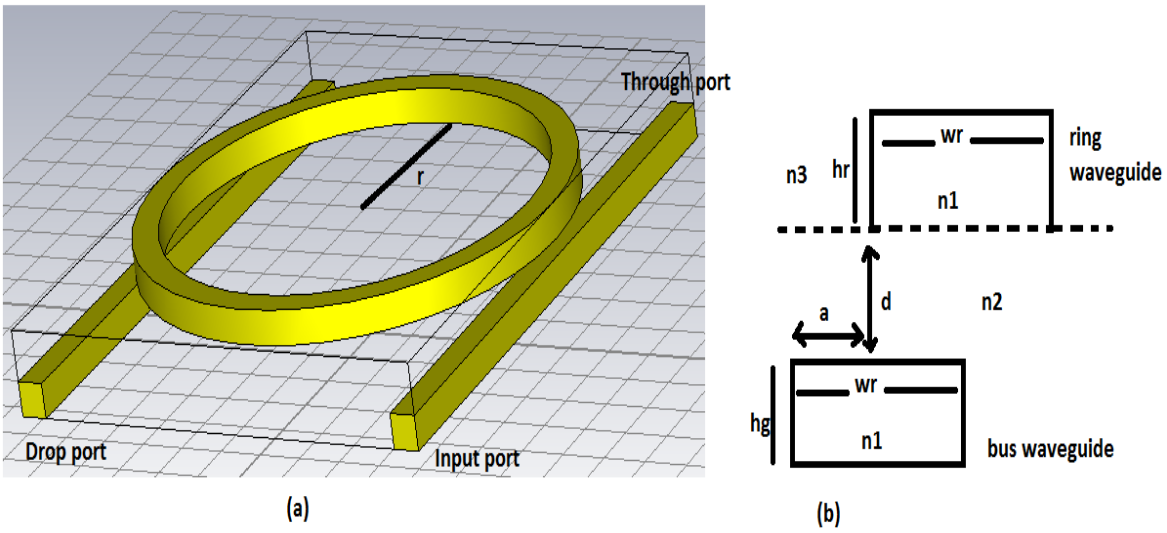

Figure 6-1 (a) Vertical coupled ring resonator. (b) Cross section of the bent and bus waveguides.

Based on the coupled mode calculations, the power coupling coefficient k^2 is related to structure dimensions as [155-157]:

$$k^2 = \left[\sin\left[\left(\frac{(2\mathrm{r} + w_r)^2}{4w_r}\right)\mathrm{K}_0 \int_{-\theta_\mathrm{o}}^{\theta_\mathrm{o}} (\cos\theta - \cos\theta_\mathrm{o})\cos^2\theta \mathrm{d}\theta\right]\right]^2 \tag{6-3}$$

Where,

$$\theta_0 = \cos^{-1}\frac{2\mathrm{r} - w_r + 2\mathrm{a}}{2\mathrm{r} + w_r}$$

$$\mathrm{K}_0 = \frac{\omega\epsilon_0}{4}\cdot(\mathrm{n_1}^2 - \mathrm{n_2}^2)\iint \mathrm{f_1}^*(\mathrm{x},\mathrm{y})\cdot \mathrm{f_2}(\mathrm{x},\mathrm{y})\,\mathrm{dx.dy}$$

$\mathrm{f_1}^*(\mathrm{x},\mathrm{y})$, and $\mathrm{f_2}(\mathrm{x},\mathrm{y})$ are the field profile of bus and bent waveguides, respectively [158]. ω is the angular frequency of light, w_r is a waveguide width, r is the radius, a is the lateral deviation and ϵ_0 is the free space permittivity.

The crosstalk suppression ratio (XT) is measured as the difference between drop and through port responses.

$$\mathrm{XT} = 10\cdot\log\mathrm{DR} - 10\cdot\log\mathrm{IR} \tag{6-4}$$

$$\mathrm{XT} = 10\log\frac{k^4\mathrm{e}^{-\alpha l}}{1+\mathrm{t}^4\mathrm{e}^{-2\alpha l}-2\mathrm{t}^2\mathrm{e}^{-\alpha l}\cos\beta l} - 10\log\frac{\mathrm{t}^2+\mathrm{t}^2\mathrm{e}^{-2\alpha l}-2\mathrm{t}^2\mathrm{e}^{-\alpha l}\cos\beta l}{1+\mathrm{t}^4\mathrm{e}^{-2\alpha l}-2\mathrm{t}^2\mathrm{e}^{-\alpha l}\cos\beta l} \tag{6-5}$$

Since the calculation of crosstalk suppression in (6-5) depends mainly on the coupling coefficients, which are difficult to calculate from (6-3) without an estimation of the field profile, a full-wave electromagnetic (EM) simulation is necessary to reliably model the resonator, and numerically calculate the spectral responses of different ports. The coupling

coefficient values are mainly affected by the vertical separation (*d*), lateral deviation (*a*), waveguides height (h_g, and h_r) and the intermediate layer (n_2) refractive index.

6.2.2. CST Simulation

The CST MWS [139] model for an SOI ring resonator is shown in Figure 6-2. Bus waveguides are modelled using silicon (Si) with refractive index of 3.47, buried in a silicon dioxide (SiO_2) layer with refractive index of 1.47. The ring waveguide is modelled using Si on the top of SiO_2 layer. The cross section of silicon waveguide is (0.34 µm × 0.34 µm). The ring radius is chosen to be 5 µm (typical value).

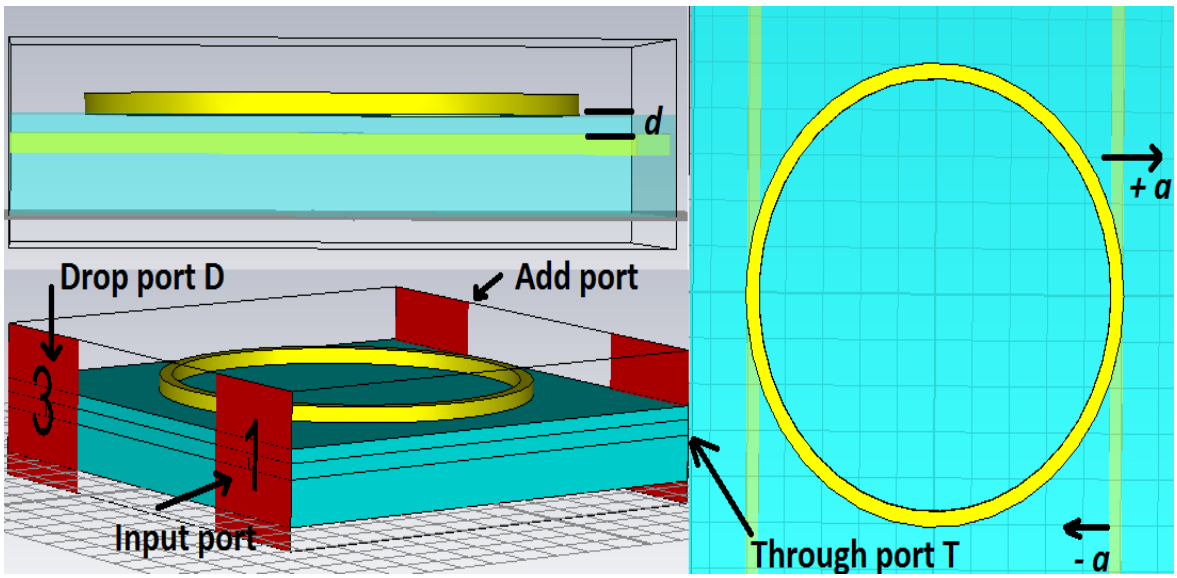

Figure 6-2. CST model of a vertically coupled ring resonator OADM.

To determine the optimum crosstalk suppression ratio, the time domain solver in CST MWS is used to perform the numerical calculations for different values of coupling coefficient (by changing *d* and *a*). Lateral deviation is considered as (–*a*) if the bus waveguides are moving towards each other. The value of (*a*) is set initially equal to 0, and then different values of (*d*) are simulated. Figure 6-3 shows the through and drop port responses, and demonstrates the spectral features of the OADM. Insertion loss is calculated from the drop port response (S_{31}) at resonance, while the OBRR represents the minimum value of (S_{31}) out of resonance. The crosstalk suppression is calculated as ($XT = S_{31} - S_{21}$).

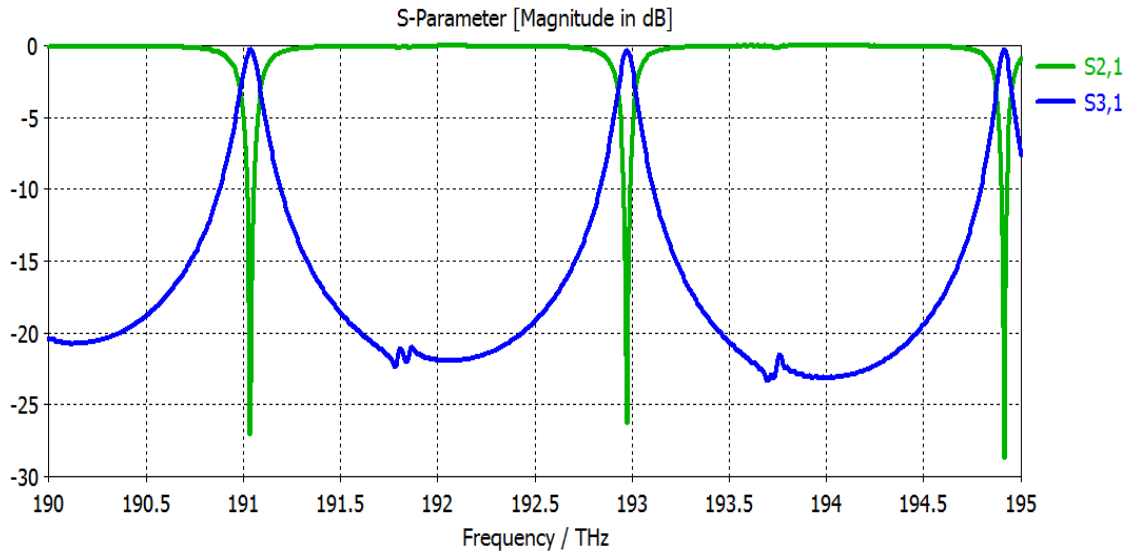

Figure 6-3. The spectral response of CST simulated ring resonator OADM.

The results of XT calculations are shown in Figure 6-4, where the value of d that results in optimum crosstalk suppression and acceptable OBRR is found as 0.3 μm. For $d = 0.3$ μm and $a = 0$, the crosstalk suppression is found to be 20 dB. However, by keeping (d) and changing the value of (a), the crosstalk suppression increases to 23 dB with −25 dB Out-of-Band Rejection Ratio. The design parameters [a d] for optimal XT are [−0.001 0.3].

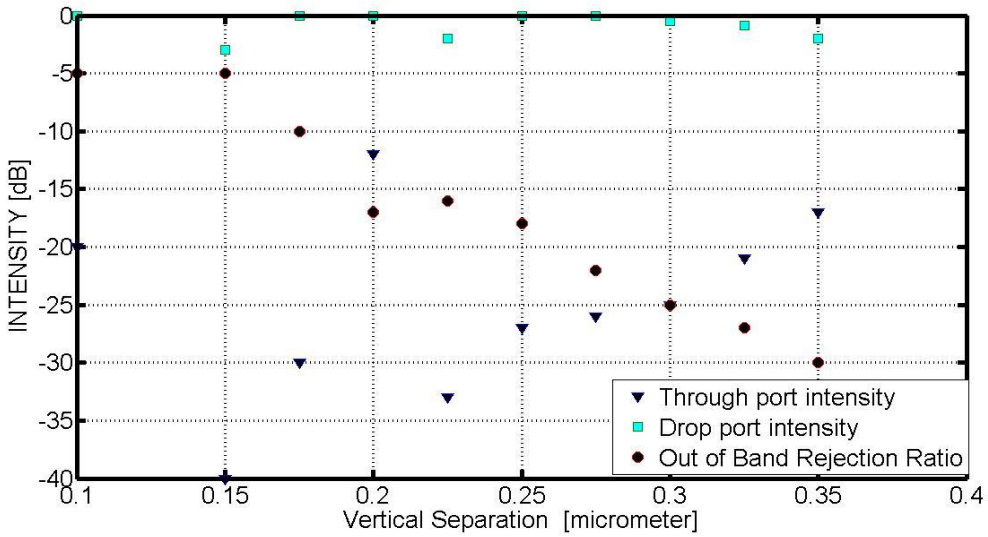

Figure 6-4. Through port, Drop port, and out of band rejection ratio (OBRR) of the ring resonator as a function of vertical separation for optimized offset (a).

6.3. Crosstalk Suppression Bandwidth

Based on the crosstalk suppression bandwidth calculations in [154], the bandwidth over which a $|20|$ dB XT is maintained can be written as:

$$\Delta f = \frac{c}{\pi n_{eff} l}\left[2\pi N + \cos^{-1}\frac{t^2 + t^2 e^{-2\alpha l} - 0.01k^4 e^{-\alpha l}}{2t^2 e^{-\alpha l}}\right] \quad (6\text{-}6)$$

Where, N is the mode index of the resonator, and c speed of light in free space.

It is clear from (6-6) that the crosstalk suppression bandwidth depends on coupling coefficients and the effective refractive index. Analytically, Figure 6-5 shows the effect of changing power coupling coefficient on the useful bandwidth. Based on Figure 6-5, it is clear that to drop a 10 Gbps NRZ signal (20 GHz crosstalk suppression bandwidth is required) the required coupling coefficient is 0.625. For a laterally coupled single ring resonator this value refers to a strong coupling which means a narrow gap between the bus and bent waveguides (as discussed in Chapter four).

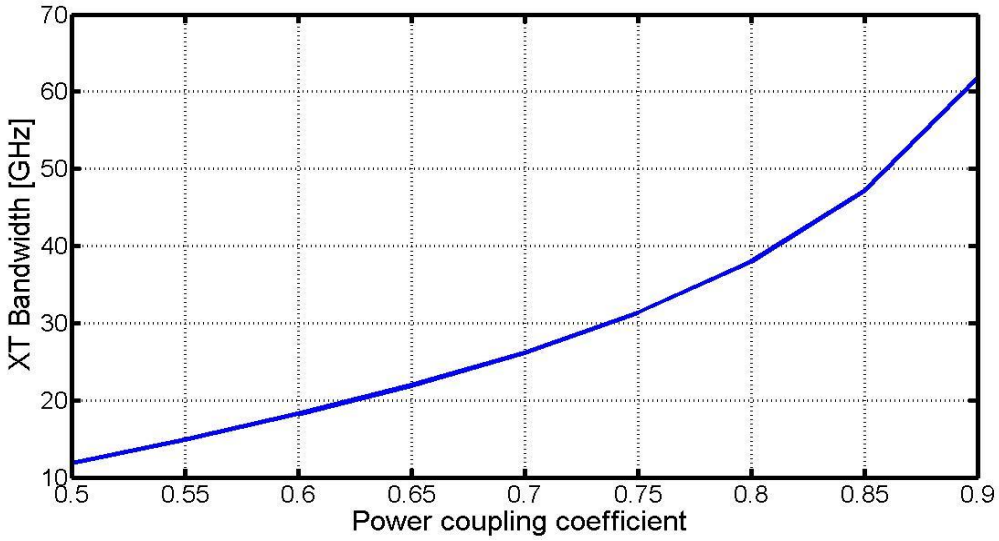

Figure 6-5. Analytically calculated crosstalk suppression bandwidth as a function of coupling coefficient.

6.4. Optimization Method

In this chapter, the crosstalk suppression bandwidth is maximized using an EM-simulation-driven design optimization [141]. Two design scenarios, with (i) two, and (ii) four design parameters, are considered. The design variable vectors for these two scenarios are as follows:

- $x = [a\ d]^T$
- $x = [a\ d\ h_g\ h_r]^T$

For the first scenario, the parameters h_g and h_r are fixed to 0.34 μm. Design variable ranges are as follows: –0.0025 μm ≤ a ≤ 0.0025 μm, 0.1 μm ≤ d ≤ 0.35 μm, 0.1 μm ≤ h_g ≤ 0.4 μm, 0.1 μm ≤ h_r ≤ 0.4 μm.

The optimization process design specifications are concerning S_{21} and S_{31} as follows:

- Maximize the bandwidth (here, denoted as B); the minimum required B is 20 GHz;
- Ensure high OBRR, specifically, $|S_{31}| \leq -20$ dB.

The above design problem is formulated as a nonlinear minimization task of the form

$$\boldsymbol{x}^* = \arg\min_{\boldsymbol{x}} H(\boldsymbol{R}(\boldsymbol{x})) \tag{6-7}$$

Where **R(x)** is a response vector of the EM-simulated ring model, H is an objective function that encodes the specification requirements, whereas $\boldsymbol{x}^*$ is an optimal design to be found. The first of the aforementioned design goals is treated as the primary objective. The second goal is handled using a suitably defined penalty function. Thus, the objective function takes the form:

$$\mathrm{H}\big(\mathbf{R}(x)\big) = -\mathrm{B}(x) + \beta \cdot \left[\frac{max\{min|S_{31}| + 20,0\}}{20}\right]^2 \tag{6-8}$$

Where β is a penalty factor (here, $\beta = 10$). Formulation (6-8) maximizes the bandwidth while penalizing the designs for which the second goal is not satisfied (i.e., $|S_{31}| > -20$ dB at its minimum).

To solve (6-7), a pattern search algorithm [159] is used. Pattern search is a derivative-free stencil-based optimization technique where the search is constrained to a grid (here, rectangular), which is iteratively refined as necessary (i.e., when the search on a current grid fails to improve the design). A specific version of the method is utilized here, a grid-constrained line search and a few other modifications [160] to reduce the computational cost of the optimization process. The use of pattern search technique is motivated by the fact that the EM-simulation model is rather noisy. For this kind of problems the use of gradient-based methods is generally not recommended [141].

The initial design is $x_{init} = [0\ 0.275\ 0.34\ 0.34]^T$. The bandwidth for this design is around 9 GHz. Upon optimization, it turns out that the constraint $|S_{31}| \leq -20$ dB is too strict, and 20 GHz bandwidth cannot be achieved for either design scenario (two- and four-variable case). For the two-variable case, the maximum obtained bandwidth (while keeping $|S_{31}| \leq -20$ dB) is 11.9 GHz, and the optimal parameters are $[-0.002\ 0.2577]^T$. For the four-variable case, the obtained bandwidth is wider (13.7 GHz) but still below the requested threshold of 20 GHz.

As the intra-band crosstalk results in a higher system performance degradation compared to inter-band crosstalk (which is easier to remove in the optical receiver) [67, 73], the intention is to increase the bandwidth of the intra-band crosstalk suppression. Another, somehow relaxed OBRR constraint ($|S_{31}| \leq -15$dB) is applied in the optimization; the obtained results show an improvement in the bandwidth calculations. For two-variable optimization, the obtained bandwidth is 19.8 GHz (see Figure 6-6) with the corresponding

parameter setup $x_{opt.1} = [-0.0025\ 0.2145\ 0.34\ 0.34]^T$. For four-variable case, the optimization process yields the design $x_{opt.2} = [-0.0023\ 0.2152\ 0.34\ 0.345]^T$ and the corresponding bandwidth is 21 GHz (see Figure 6-7). The design cost for the two- and four-variable case is 36 and 80 EM analyses of the structure, respectively. The optimization results are summarized in Table 6-1.

Table 6-1. Optimization results

Lateral deviation (a) [μm]	Vertical separation (d) [μm]	Bus WG height (h_g) [μm]	Bent WG height (h_r) [μm]	OBRR Constraint [dB]	XT bandwidth [GHz]
– 0.002	0.2577	0.34	0.34	≤ – 20	11.9
– 0.0015	0.2471	0.3406	0.3456	≤ – 20	13.7
– 0.0025	0.2145	0.34	0.34	≤ – 15	19.8
– 0.0023	0.2152	0.34	0.345	≤ – 15	21.0

The design setup $X_{opt.2}$ presented in Table 6.1 results in a 21 GHz crosstalk suppression bandwidth. However, the dimensions of *a* and *d* seem to be difficult to realise in the practical implementation. Therefore, examining of different sets of *a* and *d* is performed in order to reduce the fabrication sensitivity resulted from using very small dimensions. A new parameter setup is obtained where the dimensions are more realistic and at the same time result in a 20GHz (which is sufficient to drop 10 Gbps modulated channel). The new parameter setup is $X= [-0.002\ 0.21\ 034\ 0.345\ ]$ which results in a 20.1 GHz XT bandwidth.

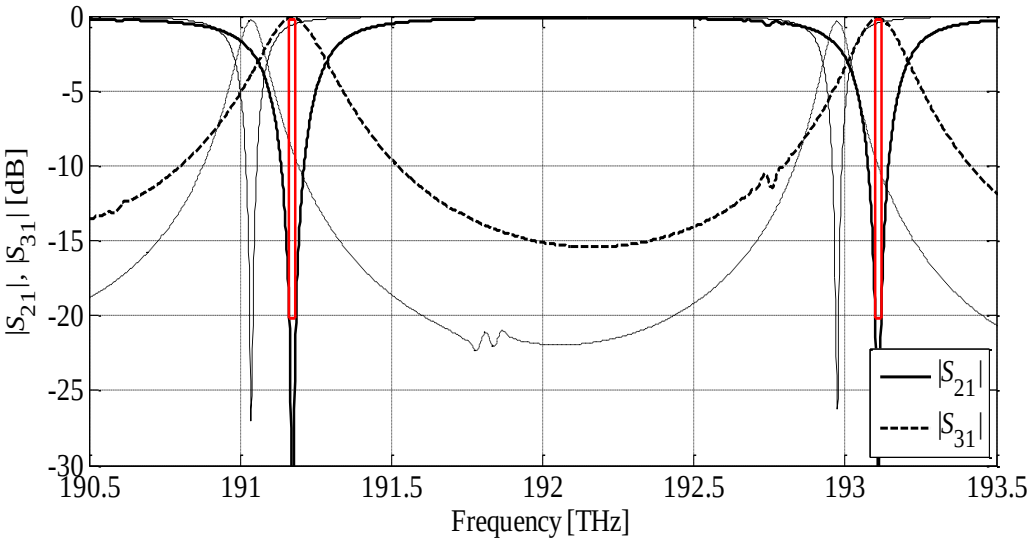

(a)

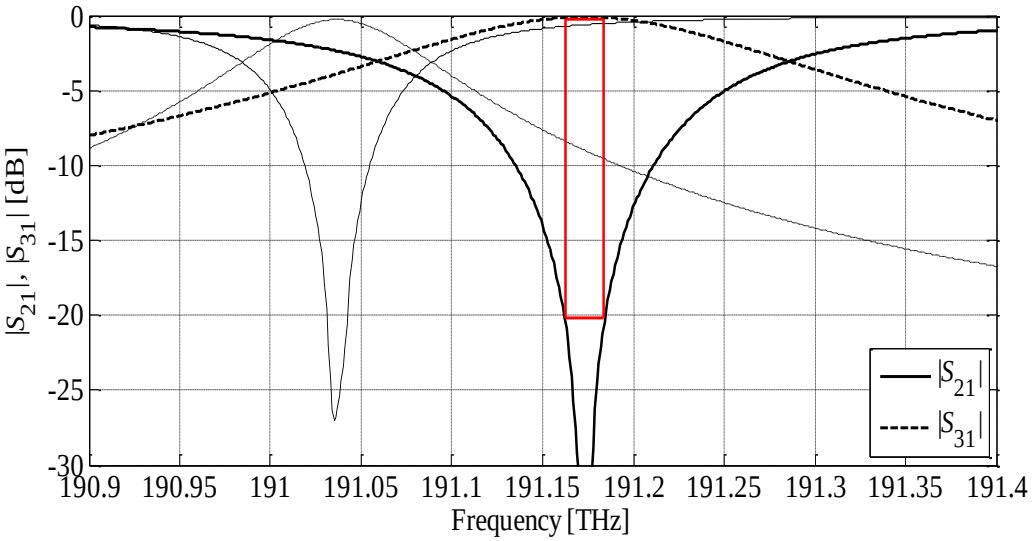

(b)

Figure 6-6. Initial (thin lines) and optimized (thick lines) responses for design case (i) (two design variables): (a) |S21| and |S31| for 190.5 to 193.5 THz range, (b) magnification around 191 THz. Optimized 20dB-bandwidth is 19.8 GHz.

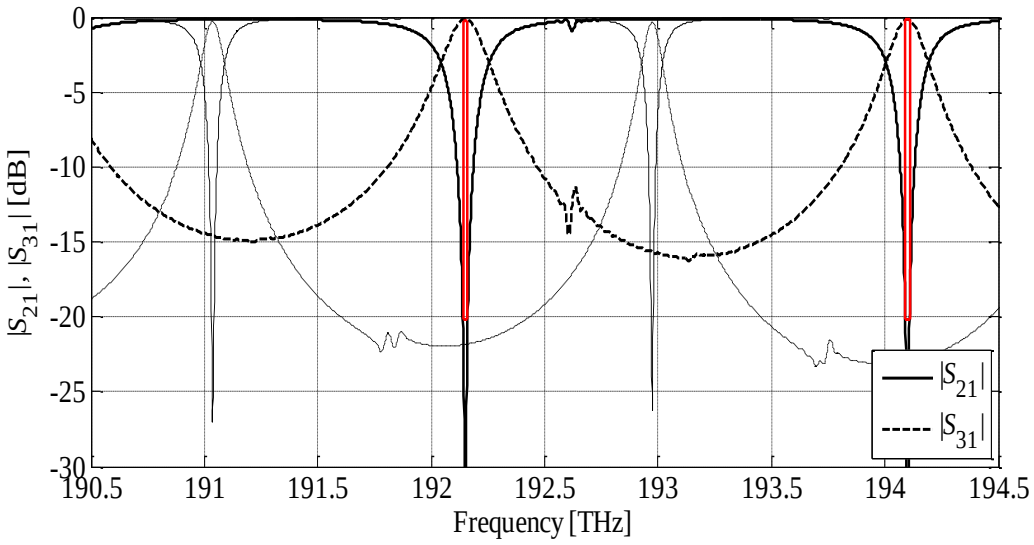

(a)

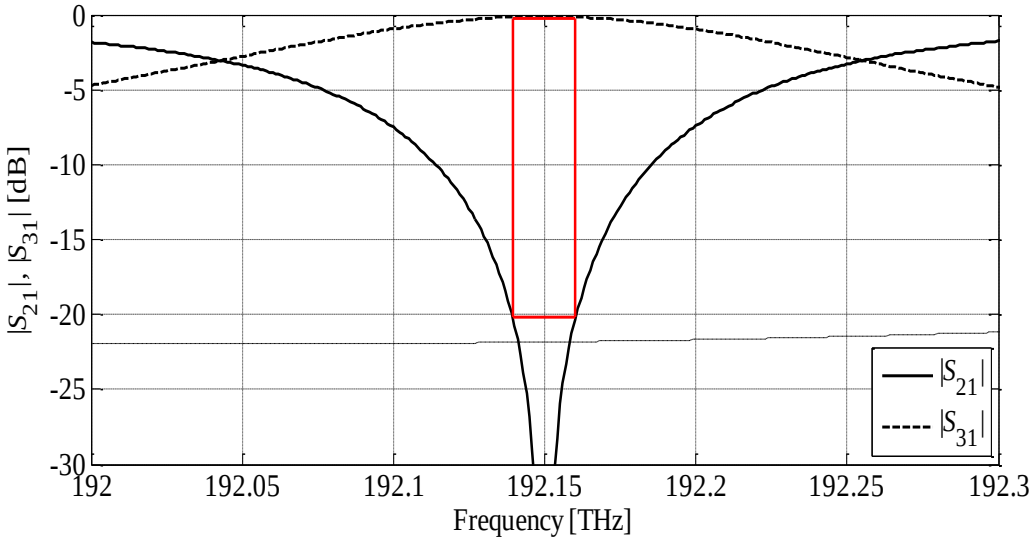

(b)

Figure 6-7. Initial (thin lines) and optimized (thick lines) responses for design case (ii) (four design variables): (a) |S21| and |S31| for 190.5 to 193.5 THz range, (b) magnification around 192THz. Optimized 20dB-bandwidth is 21 GHz.

6.5. Conclusion

The crosstalk suppression in a vertically coupled ring resonator OADM was investigated and numerically simulated. This chapter was started by proposing design parameters that increase the crosstalk suppression ratio. Vertical separation and lateral deviation between bus and bent waveguides were used to maximize the through port notch of the filter. Then, a pattern search optimization algorithm was used to maximize the crosstalk suppression bandwidth in a single ring based OADM. This approach allows using an electromagnetic simulation to perform the optimization and provides the coupling region dimensions (vertical separation and lateral deviation). Design parameters that produce a 21 GHz crosstalk suppression bandwidth were proposed.

CHAPTER SEVEN

GRATING-ASSISTED RING RESONATOR OADM

In this chapter, resonance splitting induced by sidewall roughness in silicon waveguides is exploited to increase the crosstalk suppression bandwidth over the value that would be expected from a smooth-walled resonator. A general form for the spectral response of a rough-walled ring resonator is derived analytically using the space and time domain Coupled Mode Theory. Verification against results generated from numerical modelling of a randomized rough-walled ring resonator is performed. A design which is more controllable during manufacture than a purely randomized variation is proposed. This chapter concludes with the design of a grating-assisted single ring resonator that provides 28 GHz crosstalk suppression bandwidth.

7.1. Introduction

Optical add/drop multiplexer analyses exhibit a high dependency of the spectral response upon the characteristics of coupling regions (gap separation and the length of coupling regions) [50]. Theoretical analysis shows a symmetric spectral response at different resonant wavelengths. However, experimental results of ring resonators reveal a high difference in the through and drop port responses at consecutive resonances [161].

The frequency response discrepancy results from the sidewall roughness induced back reflection inside the ring [116]. Sidewall roughness leads to a splitting of response at resonance due to the mutual coupling between the forward and backward propagated modes [18].

Estimation of mutual coupling and reflection coefficients depends mainly on the nature of the sidewall roughness. In most cases sidewall roughness was considered as a random perturbation. Therefore, the resulting back reflection is treated as a stochastic average [114]. However, it was shown in [71] that sidewall roughness can be treated similarly to a structure comprising gratings with rectangular shapes. The corrugation can consist of a group of ridges with a similar length and period. A semi-periodic arrangement of $30-50\ nm$ ridges was formed using the electron beam lithography, and the backscattering level was calculated as a deterministic function of wavelength [71].

The possibility of predefining backscattering levels by controlling the shape of quasi-grating in the fabrication process allows for new applications of grating-assisted ring resonators [71, 161, 162]. Using Fibre Bragg Grating calculations [70], back reflection effect can be controlled by changing gratings dimensions (grating length, period, and number of ridges).The dual-mode filter model that is used in microwave engineering field [163] has been exploited in the field of optical photonics to improve filter performance by exploiting the controllable reflectivity [118, 164].

This chapter aims to:

1. Propose a general model for rough-walled ring resonators.
2. Use the controllable reflectivity resulting from a periodic variation of the sidewall roughness to increase the crosstalk suppression bandwidth.

This chapter is organized as follows:

1. A mathematical model based on the time domain Coupled Mode Theory (CMT) is presented. This model allows for a complete characterization of all parameters of the ring including back reflection.
2. An equivalent structure of the rough-walled ring is proposed and the space domain CMT calculations are used to model different ports spectral responses.
3. The accuracy of the time and space domain CMT calculations is examined against existing experimental results. A rough-walled ring resonator is modelled using CST MWS to simulate the spectral response of different ports.
4. Controllable reflectivity resulting from semi-periodic gratings is modelled and validated using the ASPIC design simulator [165] to examine its accuracy. A general model of a grating-assisted ring resonator is derived.
5. An optimization approach based on the goal maximization algorithm (in Excel) is performed to calculate all parameters that maximize the crosstalk suppression bandwidth.

This chapter proposes a general solution for rough-walled ring resonators modelling, as well as a particular solution to maximize the crosstalk suppression bandwidth. It concludes

with a design that provides a 28 GHz crosstalk bandwidth. This bandwidth can be used to drop 10 Gbps NRZ channels with a low level of crosstalk.

7.2. Coupled Mode Analysis

In this section, the analysis of mutual coupling between the forward mode (deliberately excited by the bus waveguide) and back reflected mode (induced by sidewall roughness) is presented and analytically modelled using CMT.

7.2.1. Time Domain Analysis

Referring to Figure 7-1, if the incident wave at the input port is S_i and considering that there is no added signal, the amplitude of forward mode inside the resonator is $a(t)$ and the sidewall roughness induced backward mode is $b(t)$. The mutual coupling between $a(t)$ and $b(t)$ depends mainly on the reflection coefficient R.

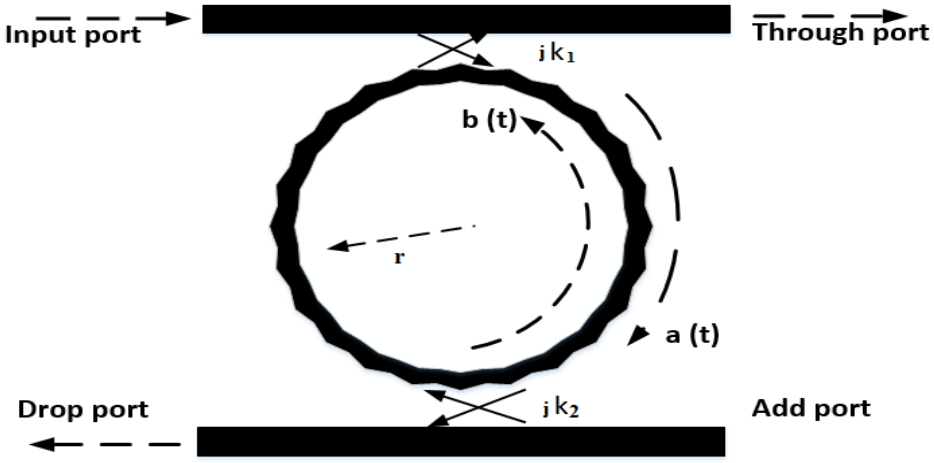

Figure 7-1. Forward and backward modes in a rough-walled ring resonator add/drop filter.

Starting with the time domain CMT analysis presented in [93, 116], the change rate equation of the energy stored in the ring (forward mode) is modified to include $b(t)$ as below:

$$\frac{\mathrm{da(t)}}{\mathrm{dt}} = \left(\mathrm{j}\omega_0 - \frac{1}{\tau}\right)\mathrm{a(t)} - \mathrm{j}k_1\mathrm{S_i} - \mathrm{jub(t)} \tag{7-1}$$

where, $\mathrm{u} = \sqrt{\mathrm{R}} \cdot \frac{V_g}{l}$ is the mutual coupling, V_g is the group velocity, l is the perimeter of the resonator, and $\frac{1}{\tau}$ is the decay rate of energy inside the resonator (determined by coupling coefficient and losses in the ring).

Similarly, the change rate equation of back reflection mode energy is modified as:

$$\frac{\mathrm{db(t)}}{\mathrm{dt}} = \left(\mathrm{j}\omega_0 - \frac{1}{\tau}\right)\mathrm{b(t)} - \mathrm{jua(t)} \tag{7-2}$$

The power transfer characteristics are calculated at a steady state by considering the input signal with time dependency $e^{j\omega t}$. From (7-1) and (7-2), $a(t)$ and $b(t)$ are:

$$a(t) = \frac{-jk_1 S_i - jub(t)}{A} \tag{7-3}$$

$$A = j(\omega - \omega_o) + \frac{1}{\tau} \tag{7-4}$$

$$b(t) = \frac{-jua(t)}{A} \tag{7-5}$$

And from (7-3) and (7-5), (7-6) is obtained:

$$a(t) = \frac{-jk_1 A}{A^2 + u^2} \cdot S_i \tag{7-6}$$

Assuming the propagation constant in the bus waveguide of length l is β, different port responses can be expressed as below:

i. Through port spectral response

$$S_t = e^{j\beta l}\left(S_i - jk_1 a(t)\right) \tag{7-7}$$

$$\left|\frac{S_t}{S_i}\right|^2 = \left|1 - \frac{{k_1}^2 A}{A^2 + u^2}\right|^2 \tag{7-8}$$

ii. Drop port spectral response

$$S_d = -jk_2 a(t) \tag{7-9}$$

$$\left|\frac{S_d}{S_i}\right|^2 = \left|\frac{k_1 k_2 A}{A^2 + u^2}\right|^2 \tag{7-10}$$

iii. Back reflection at the add port

$$S_a = -jk_2 b(t) \tag{7-11}$$

$$S_a = \frac{-k_1 k_2 u}{A} a(t) \tag{7-12}$$

$$\left|\frac{S_a}{S_i}\right|^2 = \left|\frac{k_1 k_2 u}{A^2 + u^2}\right|^2 \tag{7-13}$$

At resonance, the three ports transmission spectra are as below:

$$\left|\frac{S_t}{S_i}\right|^2 = \frac{\left[u^2 + \frac{1}{\tau^2} - \frac{k_1^2}{\tau}\right]^2}{\left[u^2 + \frac{1}{\tau^2}\right]^2} \tag{7-14}$$

$$\left|\frac{S_d}{S_i}\right|^2 = \frac{\frac{k_1^2 k_2^2}{\tau^2}}{\left[u^2 + \frac{1}{\tau^2}\right]^2} \tag{7-15}$$

And

$$\left|\frac{S_a}{S_i}\right|^2 = \frac{k_1^2 k_2^2 u^2}{\left[u^2 + \frac{1}{\tau^2}\right]^2} \tag{7-16}$$

Different port responses at resonance can be written as below:

$Th_o = \left|\frac{S_t}{S_i}\right|^2$, $Dr_o = \left|\frac{S_d}{S_i}\right|^2$, and $Re_o = \left|\frac{S_a}{S_i}\right|^2$

Where, $\mathrm{Th_o}$, $\mathrm{Dr_o}$ and $\mathrm{Re_o}$ are the through, drop and back reflection levels at resonance, respectively.

From (7-15) and (7-16):

$$\frac{\mathrm{Dr_o}}{\mathrm{Re_o}} = \frac{1}{\tau^2 \mathrm{u}^2} \tag{7-17}$$

Then

$$\mathrm{u}^2 = \frac{1}{\tau^2} \cdot \frac{\mathrm{Re_o}}{\mathrm{Dr_o}} \tag{7-18}$$

To calculate τ, the ratio of drop (7-10) and back reflection (7-13) responses is taken at the frequency of $\mathrm{Re} = \frac{1}{2}\mathrm{Re_o}$, which is denoted as $\mathrm{f_1}$. After some rearrangements:

$$\tau = \frac{1}{\Delta\omega}\sqrt{\frac{2\mathrm{Dr}}{\mathrm{Dr_o}} - 1} \tag{7-19}$$

Dr is the value of the drop response at $\mathrm{f_1}$ and $\Delta\omega$ is the frequency difference between $\mathrm{f_1}$ and the resonance frequency.

By calculating τ, the value of reflection coefficient is easily calculated from (7-18) as:

$$R = \frac{(\Delta\omega)^2 l^2}{{v_g}^2} \cdot \frac{\mathrm{Dr_o Re_o}}{\sqrt{2\mathrm{Dr} - \mathrm{Dr_o}}} \tag{7-20}$$

while the values of coupling coefficients can be calculated from (7-14) and (7-15) as below:

$${k_1}^2 = \frac{l}{v_g \tau} \cdot \frac{(\mathrm{Re_o} + \mathrm{Dr_o})}{D_{eo}} \cdot \left[1 - \sqrt{Th_o}\right] \tag{7-21}$$

$$k_2{}^2 = \frac{l}{v_g \tau} \cdot \frac{(\mathrm{Re_o} + \mathrm{Dr_o})}{\left[1 - \sqrt{Th_o}\right]} \tag{7-22}$$

And the power loss coefficient $k_p{}^2$ can be calculated based on the calculation of [166] as:

$$k_p{}^2 = [\frac{2l}{v_g \tau}] - k_1{}^2 - k_2{}^2 \tag{7-23}$$

Then the loss factor α can be calculated as:

$$\alpha = \frac{1}{l}[-10\log(1 - k_p{}^2)] \tag{7-24}$$

7.2.2. Space Domain Analysis

Although the reflection is distributed along the ring, it can be considered as a lumped scattering point without loss of generality [113]. The lumped scattering point is defined by the reflection coefficient ($K_r{}^2$) and transmission coefficient ($t_r{}^2$). Figure 7-2 (**a**) shows the rough-walled single ring model. An equivalent structure is proposed, shown in Figure 7-2 (**b**), in which the reflection is considered to be coming from a virtual mirror image of the ring. This illustrates the generation of the counter-directional mode inside the ring as a result of sidewall roughness.

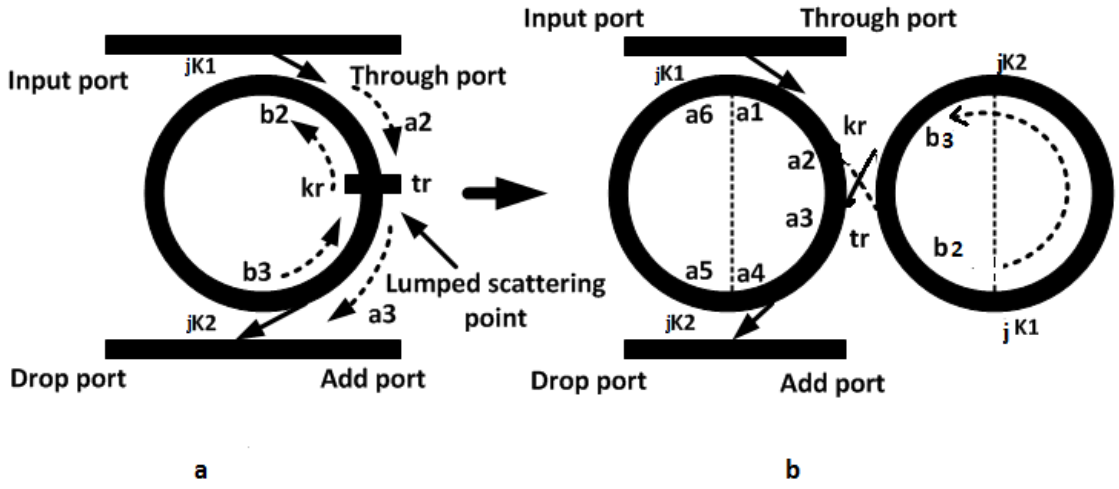

Figure 7-2. a. The schematic diagram of a rough-walled ring resonator, b. Its equivalent structure.

The drop port (S_d), through port (S_t) and back-reflection (S_{back}) responses of the single ring resonator add/drop filter are calculated by writing loop equations at different nodes inside the ring as follows:

$$S_t = -jk_1 a_6 + t_1 S_i$$

$$\mathrm{S_d} = -\mathrm{j}k_2 \mathrm{a_4} \tag{7-25}$$

$$\mathrm{S_{back}} = -\mathrm{j}k_2 \mathrm{t_2} b_2 \mathrm{x}^{3/2}$$

$$a_6 = a_5 x^{1/2} \tag{7-26}$$

where, $x = e^{-\alpha l - j\beta l}$ and,

$$a_5 = t_2 a_4 = t_2 a_3 x^{1/2} e^{-j\theta} \tag{7-27}$$

with θ the phase position of the lumped scattering point.

$$a_3 = -jk_r b_3 + t_r a_2 \tag{7-28}$$

$$b_3 = b_2 t_1 t_2 x \tag{7-29}$$

$$b_2 = -jk_r a_2 + t_r b_3 \tag{7-30}$$

$$a_2 = a_1 e^{-j\theta} = (t_1 a_6 - jk_1 S_i) e^{-j\theta} \tag{7-31}$$

The drop port response in the presence of sidewall roughness is derived using the above equations as:

$$S_d = \frac{-k_1 k_2 \left[t_r - t_1 t_2 e^{-j\emptyset}\right] e^{-j\emptyset/2}}{1 - 2t_1 t_2 t_r e^{-j\emptyset} + {t_1}^2 {t_2}^2 e^{-2j\emptyset}} \tag{7-32}$$

Where, $\emptyset = \alpha l + j\beta l$ is the propagation constant around the ring, α and β are the loss and phase coefficients respectively. k_1 and k_2 are the coupling coefficient between bus and ring waveguides, l is the perimeter of the ring and $t_r = \sqrt{1 - {k_r}^2}$.

The through port response is calculated as:

$$S_t = \frac{t_1 - t_r {t_1}^2 t_2 e^{-j\emptyset} - t_r t_2 e^{-j\emptyset} + t_1 {t_2}^2 e^{-2j\emptyset}}{1 - 2t_1 t_2 t_r e^{-j\emptyset} + {t_1}^2 {t_2}^2 e^{-2j\emptyset}} \tag{7-33}$$

And finally, the reflected signal at the add port as a result of the backward propagated mode induced by the sidewall roughness is given by:

$$S_{back} = \frac{jk_r k_1 k_2 t_1 e^{-j3\emptyset/2}}{1 - 2t_1 t_2 t_r e^{-j\emptyset} + {t_1}^2 {t_2}^2 e^{-2j\emptyset}} \quad (7\text{-}34)$$

The above equations provide the spectral features of a rough-walled ring resonator and can be used to obtain the spectral responses of different ports based on the parameters calculated from the time domain model. This allows for a general modelling of a rough-walled ring resonator and reproducing the experimental results without the need for curve fitting.

These models (time and space domain) are validated first against the experimental results presented in [111].

1. The analytical model (time domain) represented by equations (7-20) to (7-23) is used to extract the coupling coefficients from the experimentally calculated spectral response presented in [111] and shown in Figure 7-3 (**b)**. The calculated parameters are: ${k_1}^2 = 4.8\%$, ${k_2}^2 = 1.76\%$, $t_r = 0.9991$ and the round trip loss $= 0.9639$.

2. The space domain model is used to plot the spectral response and reproduce the experimental results using coupling coefficients (${k_1}^2, {k_2}^2, t_r$, and loss coefficient) calculated in step 1, as shown in Figure 7-3 a.

A comparison between Figure 7-3 (**a**) and (**b**) shows a good agreement between the proposed models and experimental results, and allows for the use of these models for filter performance optimization in terms of crosstalk and signal integrity. For further validation, a rough-walled ring resonator is modelled using CST MWS and the proposed models are

used to extract different resonator parameters from the simulation result, as will be shown in the next section.

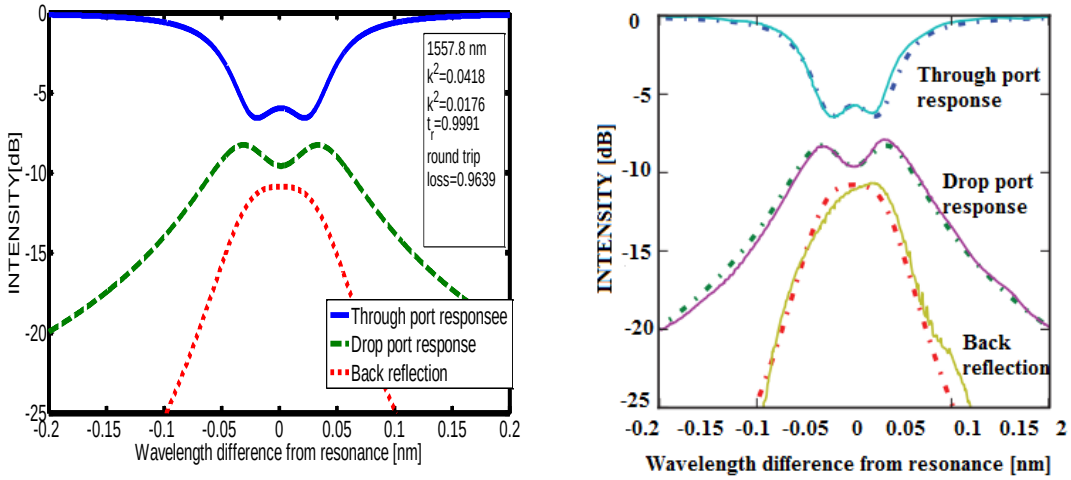

A b

Figure 7-3. a. Ring resonator response analytically modelled using time and space models. b. Experimental (line) and analytical (dot) results presented in [111].

7.3. CST Validation

CST MWS [139] is used to model a ring resonator with random sidewall roughness. The rough-walled ring is first created as a solid model programmatically using Ruby code [167]. The ring was assembled from cuboids. There were two types of cuboid: those that were narrow, which just had side and top/bottom faces, and those which were wide, which also had partial front and back faces where they joined the narrow cuboids. The narrow cuboids were assembled into the bulk of the ring, and the wide cuboids were used to create the ridged parts of the ring. The cuboids subtended about 1 degree at the centre of the ring for the smooth parts. These cuboids were collections of 8 points, 12 in the case of the wide

cuboids, with an associated list declaring how they were to be wired into faces so that the normals would face outwards, i.e. the points were listed clockwise around the normal vector. This was done with triangular meshing for portability. These were joined together to create one .obj file using Ruby code, and then imported into CST as an object file. The Ruby code is presented in appendix B. The CST MWS model of the ring resonator based add/drop filter is shown in Figure 7-4.

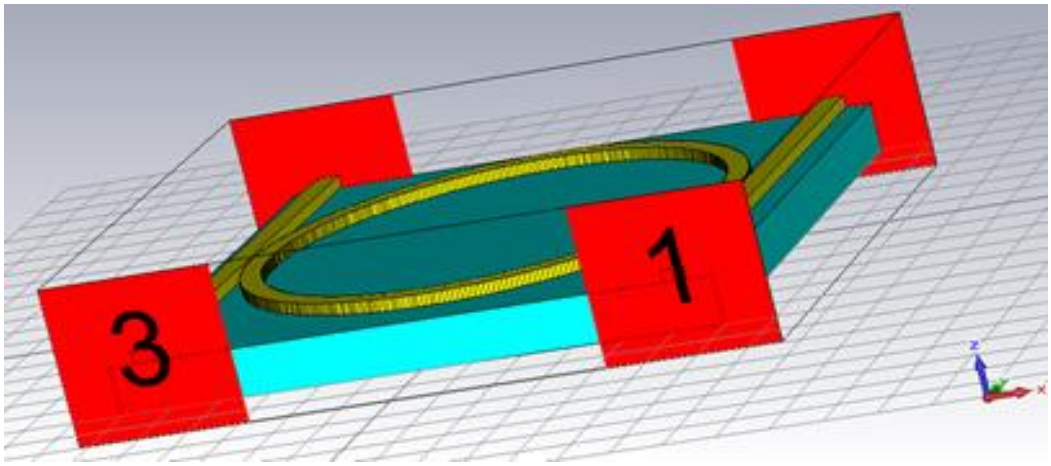

Figure 7-4. CST model of sidewall roughness in a single ring resonator add /drop filter.

In the electromagnetic model, the refractive index of the silicon waveguide is 3.47, and that of the 1 μm silicon dioxide substrate is 1.47 [146]. The upper cladding is air. The ring radius is 8μm. The cross-section dimensions of the input-output silicon waveguides are (0.5 μm width × $0.22\mu m$ height) to ensure a single mode propagation in the bus waveguides [18]. Coupling coefficients are determined by the separation between the ring and bus waveguides, which are taken as 60 *nm* and 160 *nm* for the input and output waveguides, respectively. These values are chosen to ensure the resonance splitting.

Figure 7-5 shows the spectral responses for different ports of a rough-walled ring resonator. S_{21}, S_{31}, and S_{41} represent the through, drop and back-reflection responses, respectively.

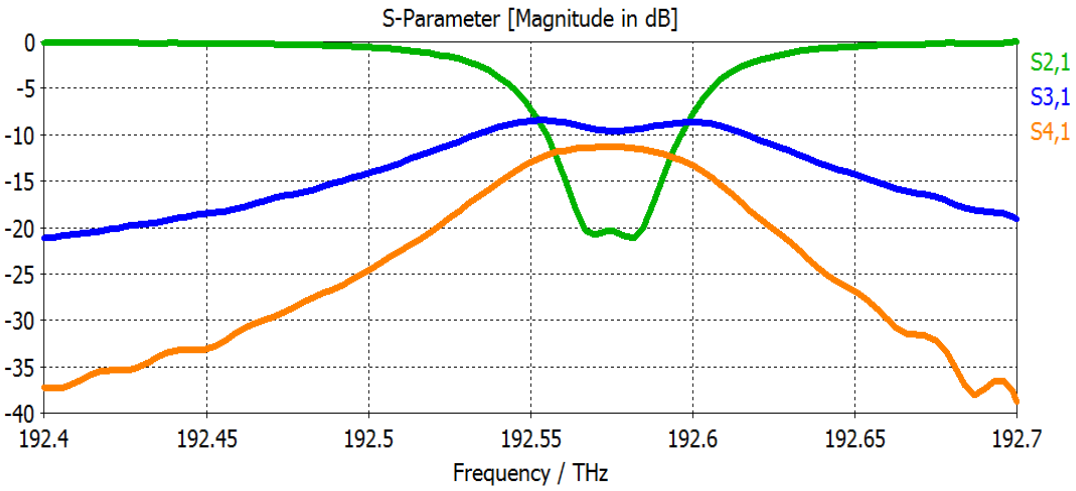

Figure 7-5. CST frequency response of a rough-walled Ring Resonator.

The analytical model (time domain) is used, first, to extract the modelled rough-walled ring parameters (coupling, reflection, and loss coefficients) from the simulation result. By using equations (7-20) to (7-23), the ring parameters are calculated as below:

$$k_1{}^2 = 10.774\%$$

$$k_2{}^2 = 1.422\%$$

$$t_r = 0.998$$

And

$$e^{-\alpha l} = 0.986$$

The second step for validation is to put the above obtained values in (7-32) and (7-34) to

obtain the spectral responses. Analytically calculated spectral responses of the through, drop and back-reflection ports are plotted in Figure 7-6 using Matlab code in combination with CST simulation results to show the validity of the time and space domain calculations. This provides an extra validation for the proposed analytical models, and allows for using it to examine the effect of back reflection on the crosstalk suppression and crosstalk suppression bandwidth.

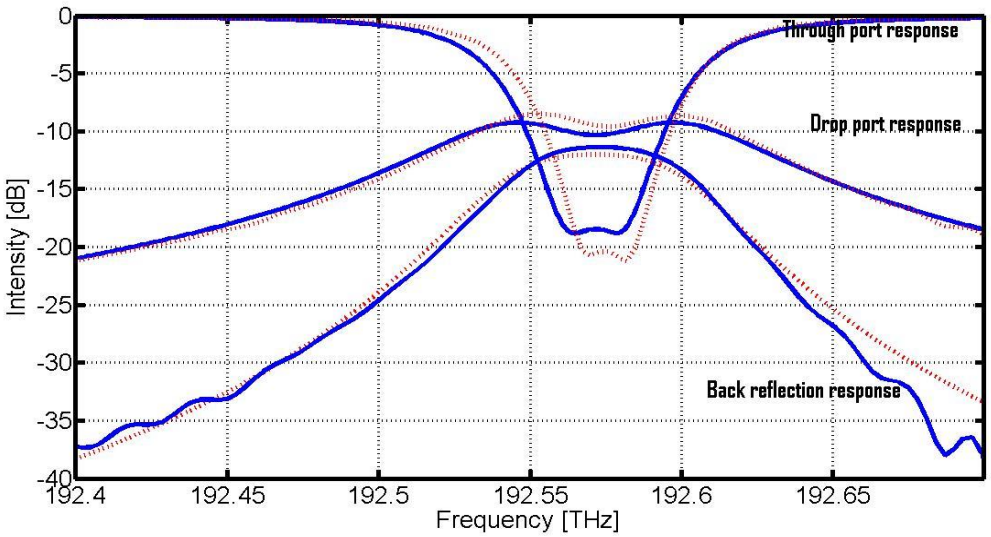

Figure 7-6. CST (solid) and analytically (dotted) modelled spectral response for a rough-walled ring resonator.

The effect of back reflection on the crosstalk suppression can be estimated by changing the reflection coefficient (t_r) and calculating the difference between drop and through port responses at resonance. Figure 7-7 shows clearly that, increasing back reflection coefficient (reduction of t_r) will result in a strong splitting of the response. In a single ring resonator, a double minimum and single maximum will appear in the through port response as a result of back reflection as shown in Figure 7-7, and at the same time a double maximum and

single minimum will appear in the drop port response. Crosstalk suppression is the difference between the single minimum of the drop port and the single maximum of the through port responses. Keeping the crosstalk suppression higher than the required level of adequate filter performance ($\geq |20|$ dB [23]), for as wide a bandwidth as possible, means improved crosstalk suppression bandwidth. This can be achieved by controlling the reflectivity of sidewall roughness in order to propose a filter design which allows for dropping channels with a low level of crosstalk.

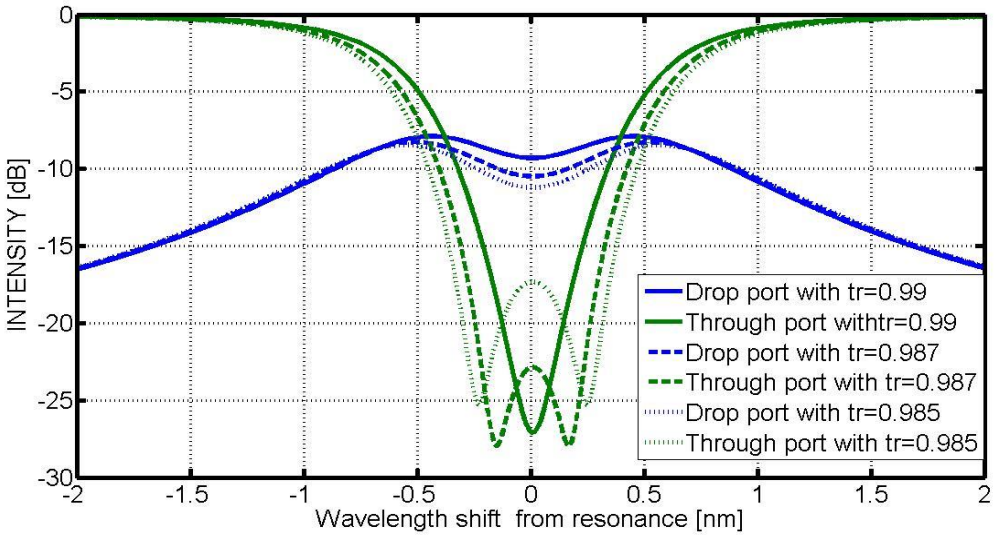

Figure 7-7. The effect of back-reflection coefficient on the through and drop port response.

7.4. Controllable Reflectivity

Based on Bragg grating reflectivity calculations [70], a perturbation of the refractive index due to the variation of waveguide width will result in a generation of backward propagated mode inside the waveguide. The mutual coupling between forward and backward modes will lead to the occurrence of resonance splitting due to power transfer between modes. Figure 7-8 shows single and double gratings.

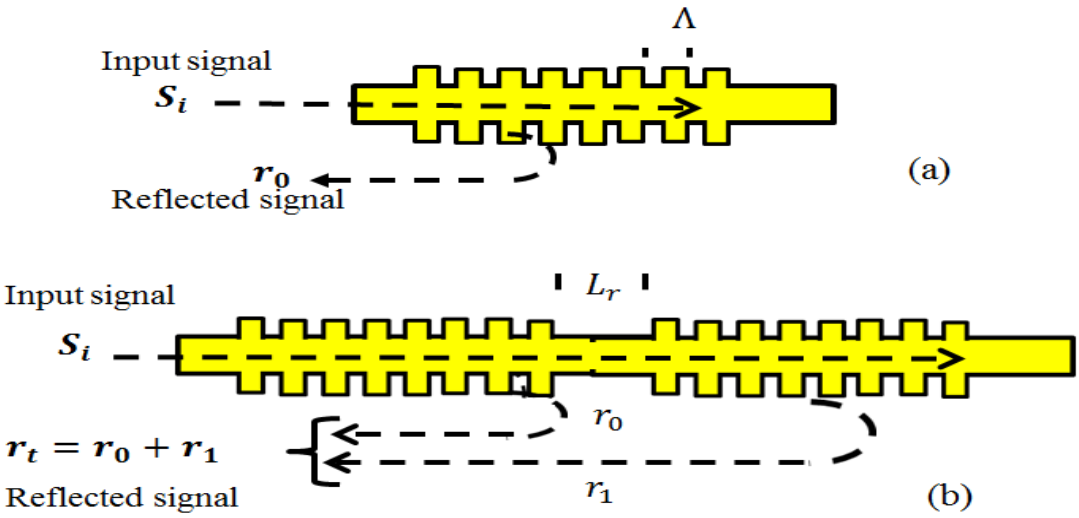

Figure 7-8. (a) Single and (b) double gratings.

The power reflection coefficient R of a single grating can be expressed as [168]:

$$R = |r_0|^2 = \frac{K^2 sinh^2(SL)}{\delta^2 sinh^2(SL) + S^2 cosh^2(SL)} \quad (7\text{-}35)$$

where r_0 is the field reflection coefficient and K is the coupling coefficient of the forward and backward modes which is expressed as:

$$K = \frac{\pi \Delta n_{eff}}{\lambda} \tag{7-36}$$

δ is the detuned propagation constant ($\delta = \frac{2\pi n_{eff}}{\lambda} - \frac{\pi}{\Lambda}$), Λ is the grating period, L is the grating length and $S = \sqrt{K^2 - \delta^2}$. Based on (7-35), the reflectivity is dependent on the change of the effective refractive index, grating length, and grating period. The calculations in this section aim to increase the reflectivity by examining different parameters. The effective refractive index of the SOI waveguide is 2.55 and a uniform change of the effective refractive index over the grating is considered with $\Delta n_{eff} = 0.5$ [18].

The effects of different parameter are examined as follows:

1. The grating length effect: Figure 7-9 shows that increasing the length of grating will result only in increasing the changing rate of the reflectivity over the wavelength range (around 1550 nm). In this case the range of wavelengths is 1540-1560 nm and the best grating length (as shown in Figure 7-9) is 6500 nm since it gives relatively high reflectivity over the wavelength range. A grating period of 100 nm and duty cycle of 50% (duty cycle is the ratio of ridge width to the grating period) are used.

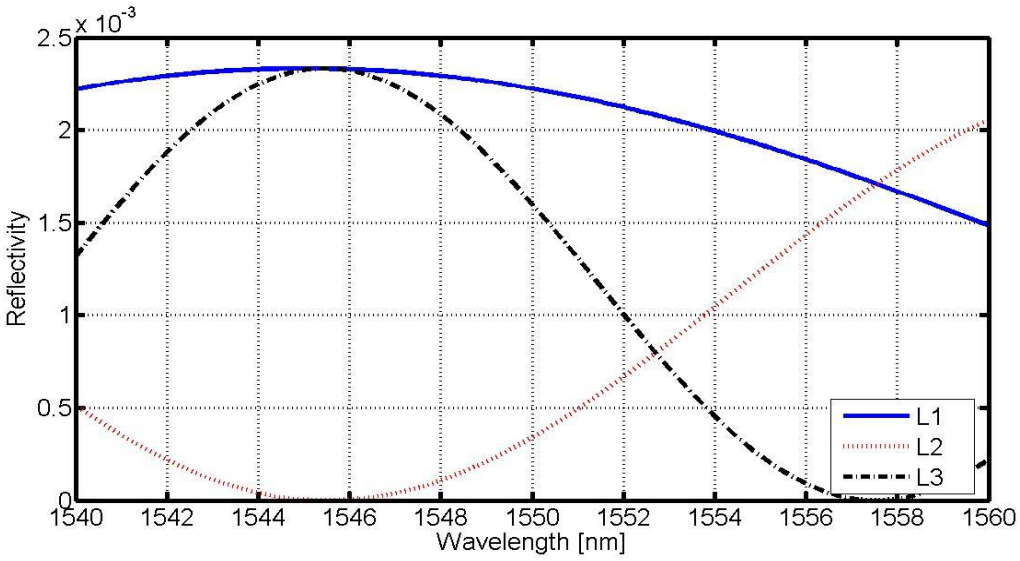

Figure 7-9. Grating length effect on the reflectivity for L1=6500 nm, L2= 13000 nm and L3= 19500 nm.

2. The grating period effect: for a grating length of 6.5 μm and the same duty cycle, Figure 7-10 shows an increase in the reflectivity with an increasing grating period. Based on the diffraction theory, the Bragg wavelength is ($\lambda_{Bragg} = 2 \cdot n_{eff} \cdot \Lambda$) [71]. Therefore, increasing the grating period will increase λ_{Bragg} and makes it close to the wavelength range of interest.

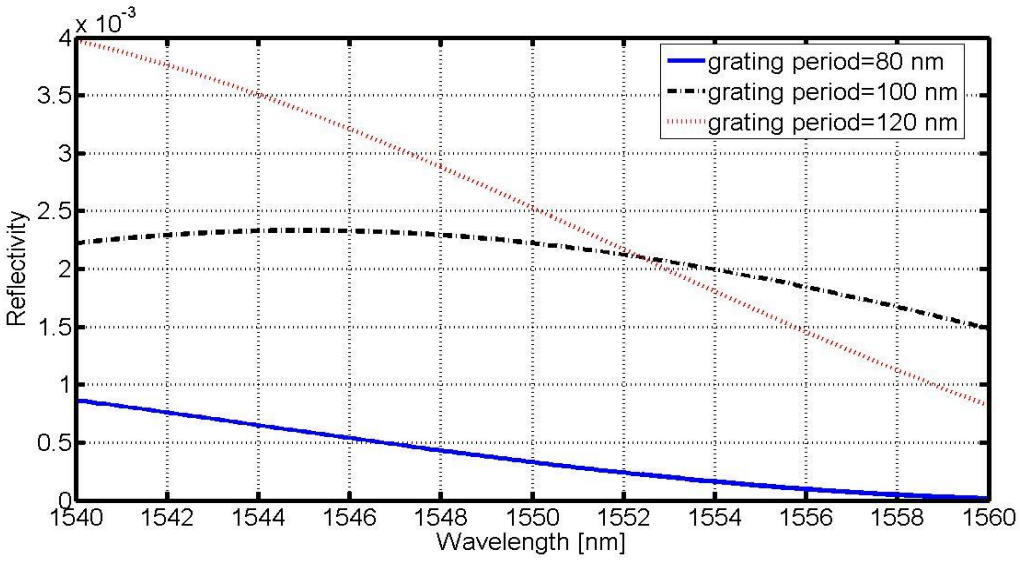

Figure 7-10. The grating period effect on the reflectivity.

3. Number of reflectors effect: to increase the level of reflectivity two or more gratings can be used separated by a distance Lr which should be chosen to ensure a proper phase change between reflected modes from each reflector. If double gratings are used, as shown in Figure 7-8 b, the overall reflectivity will be a combination of the contributions of each reflector. However, when adding the two reflectivities, r_0 and r_1, a closed loop will be formed between the two reflectors. Using the Signal Flow Graph method [149] the overall reflectivity of two gratings:

$$r_0 + r_1 = \frac{r_0 + r_1 e^{-j2\beta L_r}}{1 + r_0 r_1 e^{-j\beta L_r}} \tag{7-37}$$

However, if the number of gratings is increased to be three, for example, the total reflectivity will be more due to the number of reflectors. The total reflectivity of three gratings is:

$$r_0 + r_1 + r_2 = \frac{r_0 + r_1 e^{-j2\beta L_{r1}} + r_2 e^{-l2\beta(L_{r1}+L_{r2})} + r_0 r_1 r_2 e^{-j2\beta L_{r2}}}{1 + r_0 r_1 e^{-j2\beta L_{r1}} + r_1 r_2 e^{-j2\beta L_{r2}} + r_0 r_2 e^{-l2\beta(L_{r1}+L_{r2})}} \quad (7\text{-}38)$$

where L_{r1} and L_{r2} are the separations between gratings. Figure 7-11 shows the overall reflectivity of a single, double and three gratings.

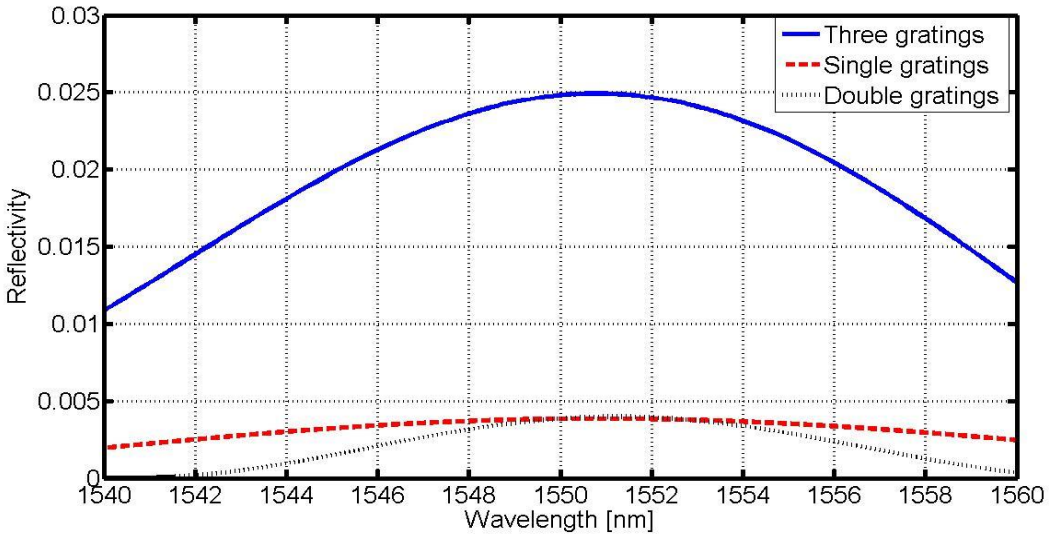

Figure 7-11. Changing the reflectivity with increasing the number of gratings.

These results are validated first using ASPIC design software [165]. ASPIC is a frequency domain simulator, it calculates the results by assembling the scattering matrix of each component in a single large matrix (based on the circuit topology) then uses it to find the optical field in each node of the OADM [169, 170]. ASPIC is a model based simulation

software and approaches simulation differently to the physically based CST MWS simulation software. Having verified its performance, the validation allows the use the model for OADM performance optimization. Figure 7-12, shows the effect of using single, double and three grating. It is shown in Figure 7-12 (**b**) that, increasing the number of gratings will result in an increase of back reflection as in [71].

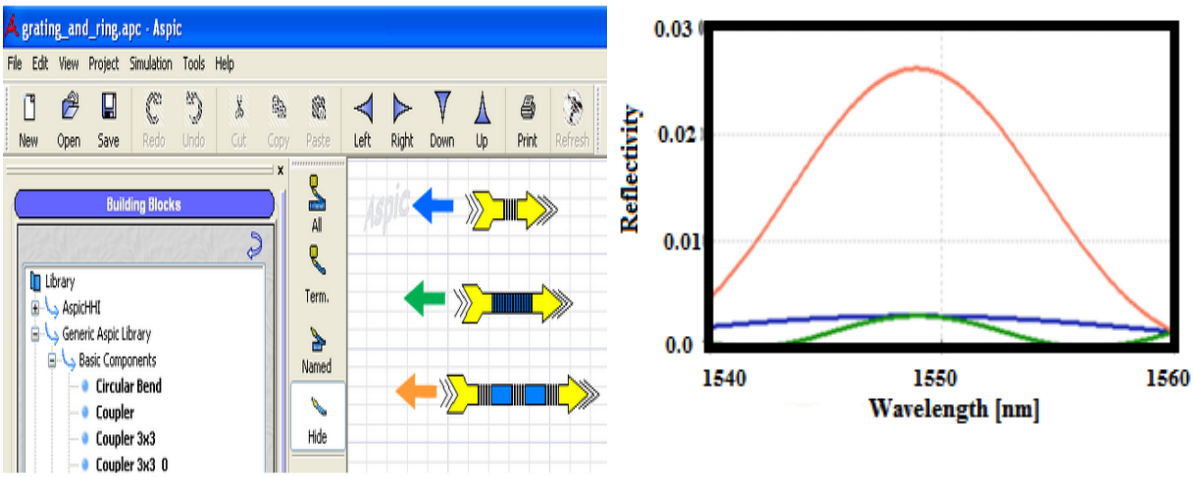

a **b**

Figure 7-12. ASPIC model for three gratings (a), and the reflectivity as a function of wavelength (b) for single grating (blue), double gratings (green) and three gratings (red).

4. The effect of changing the separation between gratings can be seen in Figure 7-13. To ensure high reflectivity, the space between the gratings should correspond to a π phase shift. The total reflectivity is hence strongly related by the length of the waveguides between the gratings. Therefore, when the gratings are added to the ring, the ring radius should be optimized in order to ensure a proper separation to maximize the reflection.

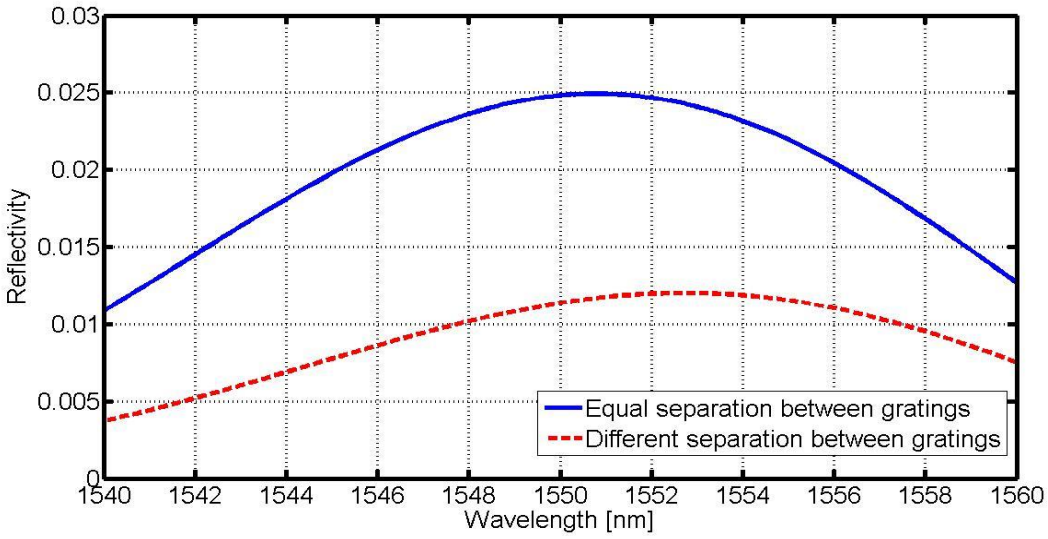

Figure 7-13. The effect of separation between gratings for three gratings.

7.5. Grating-Assisted Single Ring

In this section, a design of grating-assisted ring resonator OADM that provides wider crosstalk suppression bandwidth is presented as follows:

Step 1: Based on the calculations of crosstalk suppression bandwidth [154], the coupling and back reflection coefficients that that maximize the crosstalk suppression bandwidth can be calculated using (7-32) and (7-33). The optimization process starts by calculating the difference between drop and through port responses (crosstalk suppression), over the range of frequencies of one resonance. Different sets of coupling and reflection coefficients are used. For each set of the coefficients, the bandwidth over which the crosstalk suppression ratio ($S_{31}-S_{21}$) exceeds $|20|$ dB threshold is calculated. The goal maximization algorithm

in Excel is used to optimize the values of the coupling and reflection coefficients that produce a maximum crosstalk suppression bandwidth.

Step 2: In addition to the coupling coefficient optimization, the ring radius needed to be selected to match the resonance wavelength with the required value of reflectivity. The separation between the three gratings (as discussed in 7.4 step 4) is calculated as ($L_r = ((l - 3 \times L))/3$), where l is the ring perimeter. To maximize the reflectivity, the separation between the gratings should be optimized (through the proper choice of ring radius). A general model that combines all the parameters (coupling coefficients, grating length, number of gratings, grating period and ring radius) is used. The optimization approach is performed for two values of grating period (100 and 120 mm) since these two values provide increased reflectivity as shown in Figure 7-10.

For an asymmetric coupled ring resonator, the optimized ring parameters for crosstalk bandwidth maximization are obtained as follows: The power coupling coefficients ${k_1}^2 = 0.2258$, ${k_2}^2 = 0.0329$, and the reflection coefficient $t_r = 0.9914$. Figure 7-14 shows the spectral response for different ports using the optimized parameters. The maximum crosstalk bandwidth obtained is 28 GHz, which is sufficient to drop a channel of 10 Gbps NRZ transmission with low level of crosstalk. Based on step 2 above, the back-reflection coefficient obtained above is used with the grating model [71] to produce the length of the quasi-gratings inside the ring.

The dimensions for the grating-assisted ring resonator that produces 28 GHz crosstalk suppression bandwidth are found analytically as follows:

1. Three gratings along the ring of $9.64\ \mu m$ to be used, the length of each grating is $6.5\mu m$.
2. The period of ridges in each grating is $0.1\mu m$.

Based on the above results, a single ring resonator of $9.64\mu m$ radius, comprising of three gratings of total length $19.5\ \mu m$, each grating has 65 ridges, is shown analytically to provide a crosstalk bandwidth of 28 GHz. To achieve a similar crosstalk suppression bandwidth using a smooth-walled ring resonator, the coupling coefficient would need to exceed 0.625 [154], which would reduce the selectivity of the filter and increase the crosstalk resulting from the adjacent channels. A similar bandwidth requires the use of a double ring resonator [154], which means increasing the filter size and reducing the integration density. To this extent it is shown analytically that a grating-assisted single ring resonator can be used to drop higher data-rate signals compared to a smooth-walled resonator. The ASPIC simulator results for a single ring resonator with three gratings are shown in Figure 7-15, which shows a good agreement with that of [164] where the resonance splitting is clear and $|20|$ dB crosstalk suppression is maintained for a wide crosstalk suppression bandwidth.

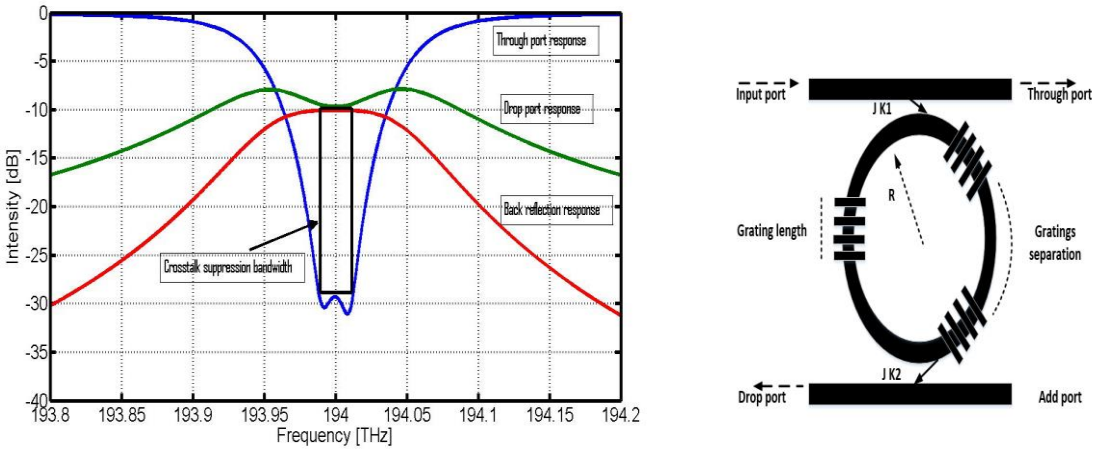

a **b**

Figure 7-14. a. The spectral response of a single ring resonator (using optimized parameters that maximize crosstalk bandwidth), b. Schematic of a grating-assisted OADM.

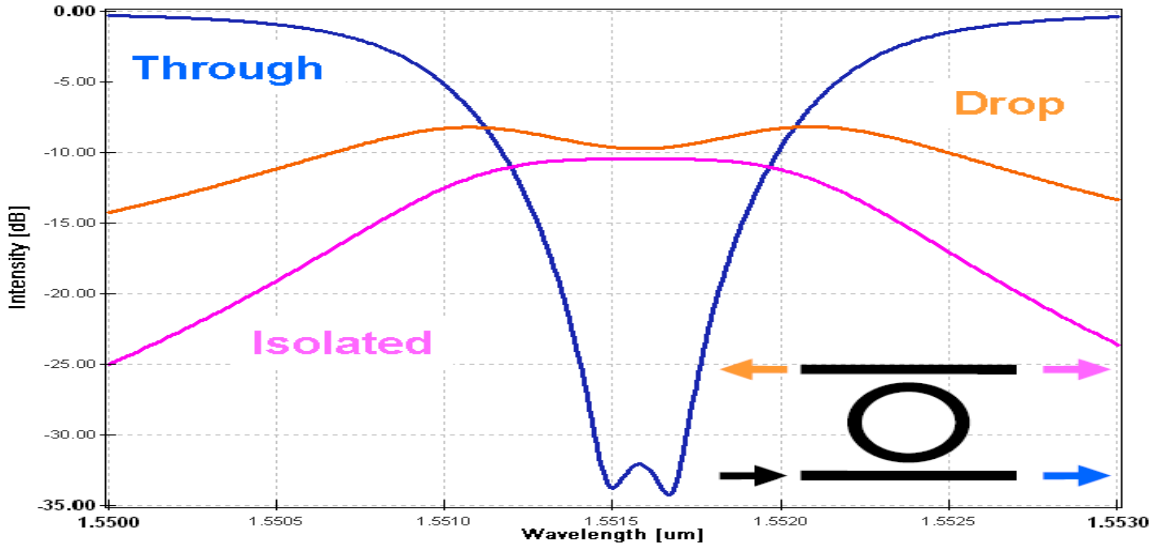

Figure 7-15. The three port response for a grating assisted ring resonator (ASPIC simulated results).

7.6. Conclusion

Resonance splitting induced by sidewall roughness in a single ring resonator was studied and exploited to increase the crosstalk suppression bandwidth. An equivalent structure of the rough-walled ring resonator was proposed. The spectral responses of different ports were defined mathematically and validated against experimental results. These models provide a simple and direct approach to calculate all ring parameters based on the simulated spectral response without the need for curve fitting. A method of optimizing the number of grating groups and the length of individual gratings for a given required performance is proposed. A design of grating-assisted ring resonator was proposed based on semi-periodic sidewall roughness. This chapter showed that a single ring with three gratings, each grating measuring 6.5 μm in length, is capable of providing 28 GHz crosstalk suppression bandwidth.

CHAPTER EIGHT

CONCLUSIONS AND FUTURE WORK

In this chapter, a summary of the thesis is presented, results are discussed and recommendations for further work are proposed. The conclusions are provided in Section8.1, while the suggestions for future works are listed in Section 8.2.

8.1. Conclusions

In this thesis, the topic of "Optical" EMC was approached by studying the crosstalk in all-optical networks; in the particular case of optical ring resonator based add/drop multiplexers (OADMs) and filters. Optical EMC was of relevance because OADMs are used in all-optical networks to introduce and drop channels in WDM nodes. Crosstalk in ring resonator based OADMs results from the adjacent channels (inter-band crosstalk) and the residual of new added channel (intra-band crosstalk). Crosstalk was mitigated either by increasing the number of rings (to improving filter response) or increasing the through port notch depth (increasing the crosstalk suppression ratio). Increasing the crosstalk suppression ratio leads to high crosstalk suppression in a narrow frequency band around the resonance frequency, while increasing the number of rings results in an increase in the filter size conflicting with the goal of greater device density. The integrated solutions to meet

WDM network requirements require the use of small-size filers that provide adding/dropping of the modulated channels with low level of crosstalk and improved signal integrity.

In this thesis,

- Defining "optical" EMC in small-sized OADMs for WDM networks was the main motivation for this research.
- The key research question in this thesis was: how to improve signal integrity and mitigate the crosstalk effect in a small-sized OADMs in order to enhance the optical EMC in all-optical networks and contribute to the increase in integration scalability?

It was answered by:

1. Using SOI ring resonator based OADMs in order to contribute to the increase in integration scalability (compared to the AWG and FBG based OADMs).
2. Increasing the crosstalk suppression bandwidth rather than the crosstalk suppression ratio. Crosstalk suppression bandwidth was defined as the bandwidth over which the level of crosstalk suppression $\geq |20|$ dB. The bandwidth of modulated channels is mainly affected by the data rate and the transmission technique. For example, 10 Gbps of NRZ transmission requires 20 GHz bandwidth. Therefore, the crosstalk suppression bandwidth needs to be more than 20 GHz to ensure adding/ dropping of this channel with a reduced level of crosstalk.

- The objectives were:
    1. To exploit the resonance splitting that occurs due to inter-ring coupling coefficients in a series coupled OADM.
    2. To enhance the crosstalk suppression bandwidth by optimizing ring parameters in a parallel coupled OADM.
    3. To optimize coupling coefficients in a vertically coupled ring resonator OADM to increase the crosstalk suppression bandwidth in a small-sized OADM.
    4. To exploit the resonance splitting induced by sidewall roughness in rough-walled ring resonator OADMs.

- A comparison of the research findings with the already existing results are listed and summarized as below:

1. **Series coupled ring resonator OADM**:

i. Based on [24, 25], the critical values for inter-ring coupling coefficients that result in a deep notch of the through port response of the filter were calculated. Above the critical values, the response will show a resonance splitting.

ii. In CHAPTER Four, exploiting resonance splitting, and keeping the crosstalk suppression over a sufficient level ($|20|dB$) yielded a design of an OADM with a crosstalk suppression bandwidth sufficient to drop 10 Gbps (RZ and NRZ) with a mitigated level of crosstalk. The over-coupling condition between rings to produce wider crosstalk suppression was proposed.

iii. A comparison between the over-coupled design suggested in this thesis with the critical coupled series ring resonator [24] showed an increase of about 40% in crosstalk suppression bandwidth for similar outer coupling coefficients (similar gap width).

2. Parallel coupled ring resonator OADM:

i. Based on [81, 102], long and sophisticated analytical forms of the transfer function (using scattering method) were proposed. These forms are hard to use for crosstalk calculations.

ii. In CHAPTER Five, the transfer function was derived analytically using the Signal Flow Graph method (based on Mason's rule), for the first time. A closed form of the spectral response was presented. It provides a simple and direct method to calculate the transfer function of the parallel coupled OADM.

iii. The derived transfer function was used to calculate the crosstalk suppression bandwidth. This model provides the possibility of examining different parameters that affect the crosstalk and OBRR levels.

3. Vertically coupled single ring OADM:

i. Based on [23, 77], vertical coupled ring resonator OADMs were used to improve crosstalk performance by increasing the crosstalk suppression ratio.

ii. In CHAPTER Six, an electromagnetic simulation-driven design optimization method procedure was used to optimize the ring parameters (vertical separation, lateral deviation, and waveguide's height) in order to increase the crosstalk suppression bandwidth.

iii. The pattern search algorithm was used and a 21 GHz crosstalk suppression bandwidth was shown to be achievable by arranging the height of the waveguide as well as the vertical and lateral separation. This bandwidth is sufficient to drop a 10 Gbps NRZ transmission using a small size OADM.

4. Grating-assisted ring resonator OADM:

i. Based on [118, 162], controllable reflectivity resulting from a semi-periodic grating was used in all-pass filters to improve the spectral response.

ii. In CHAPTER Seven, the resonance splitting induced by sidewall roughness was exploited. The time and space domain CMT were used to derive the analytical models that calculate the rough-walled ring parameters from experimental and numerical results, without the need for curve fitting calculations. An optimization technique based on the goal maximization algorithm (in Excel) was used to calculate the back reflection coefficient that results in a wide bandwidth (over 20 GHz).

iii. A design of single ring OADM, with three gratings, that provides a 28 GHz crosstalk suppression bandwidth was proposed.

- ***As a conclusion***, a number of methods that can be applied to the existing OADM designs, to improve the optical EMC, were proposed and validated. Several small-size OADM designs, with a crosstalk suppression bandwidth $> 20\,GHz$, were presented and optimized. These designs provide efficient dropping for 10 Gbps modulated channels in WDM networks. Improving signal integrity in small size filters has the advantage of

enhancing the overall optical EMC in the PLCs and allows for increasing integration density. The proposed designs can be used as a basis for higher order OADMs to improve the response shape, and moreover, to support higher data rate transmissions (40 Gbps, 100 Gbps and 400 Gbps).

- ***In summary***, issues of crosstalk have long been research topics in the Photonic community. However, the term "Optical EMC" is becoming more widespread as the reduction in wavelengths and the increase in scale of integration results in these phenomena being increasingly barriers to successful operation. This thesis has approached the topic of 'Photonics' crosstalk with EMC approach. It is anticipated that this thesis will be a starting point for future research rather than the last word on crosstalk in OADMs.

8.2. Suggestions for Future Work

EMC issues in optical systems are worthy of consideration. Therefore, several further investigations would be beneficial for a fuller understanding of optical EMC. This thesis addressed the crosstalk in small-sized ring resonator based OADMs. However, in order to have further improvement in optical EMC in WDM networks, a number of directions can be suggested for future work as listed below:

1. The influence of parasitic factors like unbounded (substrate) radiation, which could be important in the optical EMC context, need to be considered. Generic foundry models [169] and the related S-parameter models can be enhanced to simulate the unintended coupling to adjacent components and stray light propagating modes in the design stage.

2. Two stage OADMs need to be analysed and optimised in terms of crosstalk suppression bandwidth. Although a single stage module for all the operations is desirable, usually in order to minimize the crosstalk effects a single stage is used to realize the drop function and another single stage is used for the add function. Thus, the optimization of multi-stage filters (e.g. high drop port rejection ratio, box-shaped response, etc.) is desirable.

3. The proposed structure in Chapter seven consists of a single ring resonator with partial reflectors embedded in the ring. Further study of the counter-directional coupling by using FBG on the coupling region would be beneficial to propose OADMs with improved crosstalk performance.

4. Concentric rings based OADMs also deserves study. An increase in the through port notch depth has been reported by placing another ring inside the resonator in all-pass filter structure. Therefore, applying this for an OADM structure would increase the crosstalk suppression bandwidth.

REFERENCES

[1] G. Kramer and G. Pesavento, "Ethernet passive optical network (EPON): building a next-generation optical access network," *Communications Magazine, IEEE,* vol. 40, pp. 66-73, 2002.

[2] IEEE Standard for Information Technology, "Telecommunications and information exchange between systems--Local and metropolitan area networks," *IEEE Std 802. 3-2005 (Revision of IEEE Std 802. 3-2002 Including all Approved Amendments),* vol. Section2, pp. 1-810, 2005.

[3] G. Kramer, B. Mukherjee and G. Pesavento, "IPACT a dynamic protocol for an Ethernet PON (EPON)," *Communications Magazine, IEEE,* vol. 40, pp. 74-80, 2002.

[4] M. Hajduczenia, H. J. da Silva and P. P. Monteiro, "Development of 10 Gb/s EPON in IEEE 802.3 av," *Communications Magazine, IEEE,* vol. 46, pp. 40-47, 2008.

[5] P. Winzer, "Beyond 100G ethernet," *Communications Magazine, IEEE,* vol. 48, pp. 26-30, 2010.

[6] J. L. Pleumeekers, P. W. Evans, W. Chen, R. P. Schneider Jr and R. Nagarajan, "A new era in optical integration," *Opt. Photonics News,* vol. 20, pp. 20-25, 2009.

[7] W. Bogaerts, M. Fiers and P. Dumon, "Design challenges in silicon photonics," *Selected Topics in Quantum Electronics, IEEE Journal Of,* vol. 20, pp. 1-8, 2014.

[8] W. Bogaerts, R. Baets, P. Dumon, V. Wiaux, S. Beckx, D. Taillaert, B. Luyssaert, J. Van Campenhout, P. Bienstman and D. Van Thourhout, "Nanophotonic waveguides in silicon-on-insulator fabricated with CMOS technology," *Lightwave Technology, Journal Of,* vol. 23, pp. 401-412, 2005.

[9] S. K. Selvaraja, P. Jaenen, W. Bogaerts, D. Van Thourhout, P. Dumon and R. Baets, "Fabrication of photonic wire and crystal circuits in silicon-on-insulator using 193-nm optical lithography," *Lightwave Technology, Journal Of,* vol. 27, pp. 4076-4083, 2009.

[10] A. Parini, G. Bellanca, A. Annoni, F. Morichetti, A. Melloni, M. Strain, M. Sorel, M. Gay, C. Pareige and L. Bramerie, "BER Evaluation of a Passive SOI WDM Router," *IEEE Photonics Technology Letters,* vol. 25, pp. 2285-2288, 2013.

[11] T. Williams, *EMC for Product Designers: Meeting the European EMC Directive.* Newnes, 2014.

[12] P. Dong, S. F. Preble and M. Lipson, "All-optical compact silicon comb switch," *Optics Express,* vol. 15, pp. 9600-9605, 2007.

[13] J. Lee, S. Park and G. Kim, "Multichannel silicon WDM ring filters fabricated with DUV lithography," *Opt. Commun.,* vol. 281, pp. 4302-4306, 2008.

[14] Y. A. Vlasov, "Silicon CMOS-integrated nano-photonics for computer and data communications beyond 100G," *Communications Magazine, IEEE,* vol. 50, pp. s67-s72, 2012.

[15] G. F. Lipscomb and M. Stiller, "Planar optical integration- Progress and promise," *Photonics Spectra,* vol. 36, pp. 82-84, 2002.

[16] A. Vorckel, M. Monster, W. Henschel, P. H. Bolivar and H. Kurz, "Asymmetrically coupled silicon-on-insulator microring resonators for compact add-drop multiplexers," *Photonics Technology Letters, IEEE,* vol. 15, pp. 921-923, 2003.

[17] S. Chu, B. E. Little, Wugen Pan, T. Kaneko and Y. Kokubun, "Cascaded microring resonators for crosstalk reduction and spectrum cleanup in add-drop filters," *Photonics Technology Letters, IEEE,* vol. 11, pp. 1423-1425, 1999.

[18] W. Bogaerts, P. De Heyn, T. Van Vaerenbergh, K. De Vos, S. Kumar Selvaraja, T. Claes, P. Dumon, P. Bienstman, D. Van Thourhout and R. Baets, "Silicon microring resonators," *Laser & Photonics Reviews,* vol. 6, pp. 47-73, 2012.

[19] R. D. Mansoor, H. Sasse and A. P. Duffy, "Analysis of optical ring resonator add/drop filters," in *The 62nd IWCS*, USA, 2013, pp. 471-475.

[20] O. Schwelb, "Microring resonator based photonic circuits: Analysis and design," in *Telecommunications in Modern Satellite, Cable and Broadcasting Services,* 2007, pp. 187-194.

[21] S. Park, K. Kim, I. Kim and G. Kim, "Si micro-ring MUX/DeMUX WDM filters," *Optics Express,* vol. 19, pp. 13531-13539, 2011.

[22] ITU Recommendation, "Spectral grids for WDM applications: DWDM frequency grid," vol. G.694, 2006.

[23] O. Schwelb, "Crosstalk and bandwidth of lossy microring add/drop multiplexers," *Opt. Commun.,* vol. 265, pp. 175-179, 2006.

[24] H. Simos, C. Mesaritakis, D. Alexandropoulos and D. Syvridis, "Dynamic analysis of crosstalk performance in microring-based add/drop filters," *J. Lightwave Technol.,* vol. 27, pp. 2027-2034, 2009.

[25] H. Simos, C. Mesaritakis, D. Alexandropoulos and D. Syvridis, "Intraband crosstalk properties of add–drop filters based on active microring resonators," *Photonics Technology Letters, IEEE,* vol. 19, pp. 1649-1651, 2007.

[26] T. Kato and Y. Kokubun, "Optimum coupling coefficients in second-order series-coupled ring resonator for nonblocking wavelength channel switch," *J. Lightwave Technol.,* vol. 24, pp. 991, 2006.

[27] S. V. Kartalopoulos, *DWDM: Networks, Devices and Technology*. Wiley-Interscience, John Wiley & Sons: Chichester, 2003.

[28] J. Zhang, J. Yu, N. Chi, Z. Dong and X. Li, "Nonlinear compensation and crosstalk suppression for 4× 160.8 Gb/s WDM PDM-QPSK signal with heterodyne detection," *Optics Express,* vol. 21, pp. 9230-9237, 2013.

[29] A. A. Saleh and J. M. Simmons, "All-optical networking—Evolution, benefits, challenges, and future vision," *Proc IEEE,* vol. 100, pp. 1105-1117, 2012.

[30] G. P. Agrawal, *Fiber-Optic Communication Systems.* New York, NY: John Wiley & Sons, 1997.

[31] R. S. Tucker and K. Hinton, "Energy consumption and energy density in optical and electronic signal processing," *Photonics Journal, IEEE,* vol. 3, pp. 821-833, 2011.

[32] A. AM Saleh, "Defining all-optical networking and assessing its benefits in metro, regional and backbone networks," in *Optical Fiber Communication Conference,* 2003, pp. WQ1.

[33] B. Mukherjee, "WDM optical communication networks: progress and challenges," *Selected Areas in Communications, IEEE Journal On,* vol. 18, pp. 1810-1824, 2000.

[34] G. I. Papadimitriou, C. Papazoglou and A. S. Pomportsis, "Optical switching: switch fabrics, techniques, and architectures," *Lightwave Technology, Journal Of,* vol. 21, pp. 384-405, 2003.

[35] R. Ramaswami, K. Sivarajan and G. Sasaki, *Optical Networks: A Practical Perspective.* San Francisco: Morgan Kaufmann Publisher Inc., 2009.

[36] T. Gyselings, G. Morthier and R. Baets, "Crosstalk analysis of multiwavelength optical cross connects," *J. Lightwave Technol.,* vol. 17, pp. 1273, 1999.

[37] K. Rottwitt and A. J. Stentz, "Raman amplification in lightwave communication systems," *Optical Fiber Telecom,* vol. 4, pp. 213-257, 2002.

[38] M. Herzog, M. Maier and M. Reisslein, "Metropolitan area packet-switched WDM networks: a survey on ring systems," *Communications Surveys & Tutorials, IEEE,* vol. 6, pp. 2-20, 2004.

[39] J. M. Simmons, *Optical Network Design and Planning.* New York: Springer, 2014.

[40] J. M. Elmirghani and H. T. Mouftah, "Technologies and architectures for scalable dynamic dense WDM networks," *Communications Magazine, IEEE,* vol. 38, pp. 58-66, 2000.

[41] F. Tong, "Multiwavelength receivers for WDM systems," *IEEE Communications Magazine,* vol. 36, pp. 42-49, 1998.

[42] T. L. Koch and U. Koren, "Semiconductor photonic integrated circuits," *Quantum Electronics, IEEE Journal Of,* vol. 27, pp. 641-653, 1991.

[43] Y. A. Akulova, G. A. Fish, P. Koh, C. L. Schow, P. Kozodoy, A. P. Dahl, S. Nakagawa, M. C. Larson, M. P. Mack and T. A. Strand, "Widely tunable

electroabsorption-modulated sampled-grating DBR laser transmitter," *Selected Topics in Quantum Electronics, IEEE Journal Of,* vol. 8, pp. 1349-1357, 2002.

[44] A. J. Ward, D. J. Robbins, G. Busico, E. Barton, L. Ponnampalam, J. P. Duck, N. D. Whitbread, P. J. Williams, D. C. Reid and A. C. Carter, "Widely tunable DS-DBR laser with monolithically integrated SOA: design and performance," *Selected Topics in Quantum Electronics, IEEE Journal Of,* vol. 11, pp. 149-156, 2005.

[45] G. Roelkens, D. Van Thourhout and R. Baets, "Silicon-on-insulator ultra-compact duplexer based on a diffractive grating structure," *Optics Express,* vol. 15, pp. 10091-10096, 2007.

[46] B. G. Lee, B. A. Small and K. Bergman, "Signal integrity of RZ data in micron-scale silicon ring resonators," in *Lasers and Electro-Optics Society, 2006. LEOS 2006. 19th Annual Meeting of the IEEE,* 2006, pp. 627-628.

[47] S. D. Dods, J. P. R. Lacey and R. S. Tucker, "Performance of WDM ring and bus networks in the presence of homodyne crosstalk," *Lightwave Technology, Journal Of,* vol. 17, pp. 388-396, 1999.

[48] H. A. Pereira, D. A. Chaves, C. J. Bastos-Filho and J. F. Martins-Filho, "OSNR model to consider physical layer impairments in transparent optical networks," *Photon. Network Commun.,* vol. 18, pp. 137-149, 2009.

[49] Y. Pointurier and M. Brandt-Pearce, "Analytical study of crosstalk propagation in all-optical networks using perturbation theory," *Lightwave Technology, Journal Of,* vol. 23, pp. 4074-4083, 2005.

[50] B. E. Little, S. T. Chu, H. A. Haus, J. Foresi and J. -. Laine, "Microring resonator channel dropping filters," *Lightwave Technology, Journal Of,* vol. 15, pp. 998-1005, 1997.

[51] G. P. Agrawal, *Nonlinear Fiber Optics.* Burlington, MA: Elsevier Inc., 2007.

[52] E. Ciaramella and F. Curti, "Impairments due to the interplay between node crosstalk and nonlinear propagation in all optical transport networks," *Photonics Technology Letters, IEEE,* vol. 11, pp. 563-565, 1999.

[53] L. Velasco, A. Jirattigalachote, M. Ruiz, P. Monti, L. Wosinska and G. Junyent, "Statistical approach for fast impairment-aware provisioning in dynamic all-optical networks," *Optical Communications and Networking, IEEE/OSA Journal Of,* vol. 4, pp. 130-141, 2012.

[54] S. D. Dods and R. S. Tucker, "A comparison of the homodyne crosstalk characteristics of optical add-drop multiplexers," *Lightwave Technology, Journal Of,* vol. 19, pp. 1829-1838, 2001.

[55] X. Wu, C. Lu, Z. Ghassemlooy and Y. Wang, "Evaluation of intraband crosstalk in an FBG-OC-based optical cross connect," *Photonics Technology Letters, IEEE,* vol. 14, pp. 212-214, 2002.

[56] Y. Shen, K. Lu and W. Gu, "Coherent and incoherent crosstalk in WDM optical networks," *Lightwave Technology, Journal Of,* vol. 17, pp. 759-764, 1999.

[57] M. R. Jimenez, R. Passy, M. A. Grivet and J. P. von der Weid, "Computation of power penalties due to intraband crosstalk in optical systems," *Photonics Technology Letters, IEEE,* vol. 15, pp. 156-158, 2003.

[58] E. Tangdiongga, "Crosstalk mitigation techniques in multi-wavelength networks comprising photonic integrated circuits," *PhD Thesis,* Eindhoven : Technische Universiteit, Netherlands, 2001.

[59] H. J. S. Dorren, H. de Waardt and I. T. Monroy, "Statistical analysis of crosstalk accumulation in WDM networks," *Lightwave Technology, Journal Of,* vol. 17, pp. 2425-2430, 1999.

[60] A. Chraplyvy, "Optical power limits in multi-channel wavelength-division-multiplexed systems due to stimulated Raman scattering," *Electron. Lett.,* vol. 20, pp. 58-59, 1984.

[61] T. Okoshi, *Coherent Optical Fiber Communications.* Boston, MA: Kluwer, 1988.

[62] T. Chikama, H. onaka and S. Kuroyanagi,, "Photonic networking using optical add drop multiplexers and optical cross-connects," *Fujitsu Sci Tech J,* vol. 35, pp. 46-55, 1999.

[63] E. J. Klein, D. H. Geuzebroek, H. Kelderman, G. Sengo, N. Baker and A. Driessen, "Reconfigurable optical add-drop multiplexer using microring resonators," *Photonics Technology Letters, IEEE,* vol. 17, pp. 2358-2360, 2005.

[64] M. P. McGarry, M. Maier and M. Reisslein, "Ethernet PONs: a survey of dynamic bandwidth allocation (DBA) algorithms," *Communications Magazine, IEEE,* vol. 42, pp. S8-15, 2004.

[65] X. J. Leijtens, B. Kuhlow and M. K. Smit, "Arrayed waveguide gratings," in *Wavelength Filters in Fibre Optics*, Springer Verlag, Ed. Germany: 2006, pp. 125-187.

[66] S. M. Gemelos, D. Wonglumsom and L. G. Kazovsky, "Impact of crosstalk in an arrayed-waveguide router on an optical add-drop multiplexer," *Photonics Technology Letters, IEEE,* vol. 11, pp. 349-351, 1999.

[67] H. Takahashi, K. Oda and H. Toba, "Impact of crosstalk in an arrayed-waveguide multiplexer on NxN optical interconnection," *Lightwave Technology, Journal Of,* vol. 14, pp. 1097-1105, 1996.

[68] M. Gustavsson, L. Gillner and C. P. Larsen, "Statistical analysis of interferometric crosstalk: theory and optical network examples," *Lightwave Technology, Journal Of,* vol. 15, pp. 2006-2019, 1997.

[69] C. Giles, "Lightwave applications of fiber Bragg gratings," *J. Lightwave Technol.,* vol. 15, pp. 1391-1404, 1997.

[70] K. O. Hill and G. Meltz, "Fiber Bragg grating technology fundamentals and overview," *J. Lightwave Technol.,* vol. 15, pp. 1263-1276, 1997.

[71] T. Wang, Z. Zhang, F. Liu, Y. Tong, J. Wang, Y. Tian, M. Qiu and Y. Su, "Modeling of quasi-grating sidewall corrugation in SOI microring add-drop filters," *Opt. Commun.,* vol. 282, pp. 3464-3467, 2009.

[72] K. Hattori, M. Abe, J. Albert, F. Bilodeau, K. Hill, Y. Hibino, T. Kitagawa and K. Oguchi, "Coherent crosstalk of an optical add/drop filter with Bragg gratings in a PLC Mach-Zehnder interferometer for optical LAN," *Photonics Technology Letters, IEEE,* vol. 11, pp. 272-274, 1999.

[73] P. André, J. Pinto, A. N. Pinto and T. Almeida, "Performance degradations due to crosstalk in multiwavelength optical networks using optical add drop multiplexers based on fibre Bragg gratings," *Electrónica E Telecomunicações,* vol. 3, pp. 85-89, 2012.

[74] D. G. Rabus, "Realization of optical filters using ring resonators with integrated semiconductor optical amplifiers in GaInAsP/InP," 2002.

[75] D. G. Rabus, "Ring Resonators: Theory and Modeling," *Integrated Ring Resonators: The Compendium*, pp. 3-40, 2007.

[76] A. Canciamilla, M. Torregiani, C. Ferrari, F. Morichetti, R. De La Rue, A. Samarelli, M. Sorel and A. Melloni, "Silicon coupled-ring resonator structures for slow light applications: potential, impairments and ultimate limits," *Journal of Optics*, vol. 12, pp. 104008, 2010.

[77] Y. Yanagase, S. Suzuki, Y. Kokubun and S. T. Chu, "Box-like filter response and expansion of FSR by a vertically triple coupled microring resonator filter," *Lightwave Technology, Journal Of*, vol. 20, pp. 1525-1529, 2002.

[78] J. Zhou, M. J. O'Mahony and S. D. Walker, "Analysis of optical crosstalk effects in multi-wavelength switched networks," *Photonics Technology Letters, IEEE*, vol. 6, pp. 302-305, 1994.

[79] H. W. Ott and H. W. Ott, *Noise Reduction Techniques in Electronic Systems*. Wiley, New York, 1988.

[80] Y. Goebuchi, T. Kato and Y. Kokubun, "Optimum arrangement of high-order series-coupled microring resonator for crosstalk reduction," *Japanese Journal of Applied Physics*, vol. 45, pp. 5769, 2006.

[81] C. J. Kaalund, "Critically coupled ring resonators for add-drop filtering," *Opt. Commun.*, vol. 237, pp. 357-362, 2004.

[82] S. T. Chu, B. E. Little, W. Pan, T. Kaneko and Y. Kokubun, "Second-order filter response from parallel coupled glass microring resonators," *Photonics Technology Letters, IEEE*, vol. 11, pp. 1426-1428, 1999.

[83] N. Rouger, L. Chrostowski and R. Vafaei, "Temperature Effects on Silicon-on-Insulator (SOI) Racetrack Resonators: A Coupled Analytic and 2-D Finite Difference Approach," *Lightwave Technology, Journal Of*, vol. 28, pp. 1380-1391, 2010.

[84] T. Barwicz, H. Byun, F. Gan, C. Holzwarth, M. Popovic, P. Rakich, M. Watts, E. Ippen, F. Kärtner and H. Smith, "Silicon photonics for compact, energy-efficient interconnects [Invited]," *Journal of Optical Networking*, vol. 6, pp. 63-73, 2007.

[85] S. Xiao, M. H. Khan, H. Shen and M. Qi, "Silicon-on-insulator microring add-drop filters with free spectral ranges over 30 nm," *J. Lightwave Technol.*, vol. 26, pp. 228-236, 2008.

[86] F. Xia, L. Sekaric and Y. A. Vlasov, "Mode conversion losses in silicon-on-insulator photonic wire based racetrack resonators," *Optics Express*, vol. 14, pp. 3872-3886, 2006.

[87] D. G. Rabus, M. Hamacher, U. Troppenz and H. Heidrich, "High-Q channel-dropping filters using ring resonators with integrated SOAs," *Photonics Technology Letters, IEEE*, vol. 14, pp. 1442-1444, 2002.

[88] B. Little, S. Chu, P. Absil, J. Hryniewicz, F. Johnson, F. Seiferth, D. Gill, V. Van, O. King and M. Trakalo, "Very high-order microring resonator filters for WDM applications," *Photonics Technology Letters, IEEE*, vol. 16, pp. 2263-2265, 2004.

[89] A. Densmore, D. Xu, P. Waldron, S. Janz, P. Cheben, J. Lapointe, A. Delâge, B. Lamontagne, J. Schmid and E. Post, "A silicon-on-insulator photonic wire based evanescent field sensor," *Photonics Technology Letters, IEEE*, vol. 18, pp. 2520-2522, 2006.

[90] E. Marcatili, "Bends in optical dielectric guides," *Bell System Technical Journal*, vol. 48, pp. 2103-2132, 1969.

[91] C. Madsen and G. Lenz, "Optical all-pass filters for phase response design with applications for dispersion compensation," *Photonics Technology Letters, IEEE,* vol. 10, pp. 994-996, 1998.

[92] E. J. Klein, *Densely Integrated Microrooring-Resonator Based Components for Fiber-to-the-Home Applications.* University of Twente, 2007, http://purl.utwente.nl/publications/60711.

[93] C. Manolatou, M. Khan, S. Fan, P. R. Villeneuve, H. Haus and J. Joannopoulos, "Coupling of modes analysis of resonant channel add-drop filters," *Quantum Electronics, IEEE Journal Of,* vol. 35, pp. 1322-1331, 1999.

[94] A. Yariv, "Coupled-mode theory for guided-wave optics," *Quantum Electronics, IEEE Journal Of,* vol. 9, pp. 919-933, 1973.

[95] R. Orta, P. Savi, R. Tascone and D. Trinchero, "Synthesis of multiple-ring-resonator filters for optical systems," *Photonics Technology Letters, IEEE,* vol. 7, pp. 1447-1449, 1995.

[96] A. Melloni and M. Martinelli, "Synthesis of direct-coupled-resonators bandpass filters for WDM systems," *Lightwave Technology, Journal Of,* vol. 20, pp. 296-303, 2002.

[97] S. Xiao, M. H. Khan, H. Shen and M. Qi, "Multiple-channel silicon micro-resonator based filters for WDM applications," *Optics Express,* vol. 15, pp. 7489-7498, 2007.

[98] H. Yan, X. Feng, D. Zhang and Y. Huang, "Integrated optical add-drop multiplexer based on a compact parent-sub microring-resonator structure," *Opt. Commun.,* vol. 289, pp. 53-59, 2012.

[99] M. S. Dahlem, C. W. Holzwarth, A. Khilo, F. X. Kärtner, H. I. Smith and E. P. Ippen, "Eleven-channel second-order silicon microring-resonator filterbank with tunable channel spacing," in *Conference on Lasers and Electro-Optics,* 2010, pp. CMS5.

[100] M. A. Popovic, T. Barwicz, M. S. Dahlem, F. Gan, C. W. Holzwarth, P. T. Rakich, H. I. Smith, E. P. Ippen and F. X. Krtner, "Tunable, fourth-order silicon microring-resonator add-drop filters," in *33rd ECOC,* Germany, 2007, .

[101] F. Xia, M. Rooks, L. Sekaric, and Y. Vlasov, "Ultra-compact high order ring resonator filters using submicron silicon photonic wires for on chip optical interconnections." *Optical Communications and Networking, IEEE/OSA Journal Of,* vol. 15, 2007.

[102] A. Melloni, "Synthesis of a parallel-coupled ring-resonator filter," *Opt. Lett.*, vol. 26, pp. 917-919, 2001.

[103] A. Taflove, and S. C. Hagness, *Computational Electrodynamics: The Finite-Difference Time-Domain Method.* London: Artech House Inc., 3rd ed., 2005.

[104] C. Chaichuay, P. P. Yupapin and P. Saeung, "The serially coupled multiple ring resonator filters and Vernier effect," *Optica Applicata*, vol. 39, pp. 175-194, 2009.

[105] P. Urquhart, "Compound optical-fiber-based resonators," *JOSA A,* vol. 5, pp. 803-812, 1988.

[106] K. Oda, N. Takato and H. Toba, "A wide-FSR waveguide double-ring resonator for optical FDM transmission systems," *Lightwave Technology, Journal Of,* vol. 9, pp. 728-736, 1991.

[107] O. Schwelb, "The nature of spurious mode suppression in extended FSR microring multiplexers," *Opt. Commun.*, vol. 271, pp. 424-429, 2007.

[108] T. Barwicz, M. A. Popović, M. R. Watts, P. T. Rakich, E. P. Ippen and H. I. Smith, "Fabrication of add-drop filters based on frequency-matched microring resonators," *J. Lightwave Technol.*, vol. 24, pp. 2207, 2006.

[109] B. E. Little, J. Foresi, G. Steinmeyer, E. Thoen, S. Chu, H. Haus, E. Ippen, L. Kimerling and W. Greene, "Ultra-compact Si-SiO_2 microring resonator optical channel dropping filters," *Photonics Technology Letters, IEEE,* vol. 10, pp. 549-551, 1998.

[110] A. Bianco, D. Cuda, M. Garrich, G. G. Castillo, V. Martina and F. Neri, "Crosstalk minimization in microring-based wavelength routing matrices," in *Global Telecommunications Conference (GLOBECOM), IEEE,* 2011, pp. 1-5.

[111] G. Ballesteros, J. Matres, J. Martí and C. Oton, "Characterizing and modeling backscattering in silicon microring resonators," *Optics Express*, vol. 19, pp. 24980-24985, 2011.

[112] C. Sui, Q. Wang, S. Xiao and P. Li, "Analysis of microdisk/microring's surface roughness effect by orthogonal decomposition," *Optics and Photonics Journal,* vol. 3, pp. 288, 2013.

[113] B. E. Little, J. Laine and S. T. Chu, "Surface-roughness-induced contradirectional coupling in ring and disk resonators," *Opt. Lett.*, vol. 22, pp. 4-6, 1997.

[114] F. Morichetti, A. Canciamilla and A. Melloni, "Statistics of backscattering in optical waveguides," *Opt. Lett.*, vol. 35, pp. 1777-1779, 2010.

[115] F. Morichetti, A. Canciamilla, M. Martinelli, A. Samarelli, R. De La Rue, M. Sorel and A. Melloni, "Coherent backscattering in optical microring resonators," *Appl. Phys. Lett.*, vol. 96, pp. 081112-081112-3, 2010.

[116] Z. Zhang, M. Dainese, L. Wosinski and M. Qiu, "Resonance-splitting and enhanced notch depth in SOI ring resonators with mutual mode coupling," *Optics Express,* vol. 16, pp. 4621-4630, 2008.

[117] G. T. Paloczi, J. Scheuer and A. Yariv, "Compact microring-based wavelength-selective inline optical reflector," *IEEE Photonics Technology Letters,* vol. 17, pp. 390-392, 2005.

[118] C. Alonso-Ramos, F. Morichetti, A. Ortega-Monux, I. Molina-Fernandez, M. J. Strain and A. Melloni, "Dual-mode coupled-resonator integrated optical filters," *IEEE Photonics Technology Letters,* vol. 26, pp. 929-932, 2014.

[119] P. Dumon, W. Bogaerts, V. Wiaux, J. Wouters, S. Beckx, J. Van Campenhout, D. Taillaert, B. Luyssaert, P. Bienstman and D. Van Thourhout, "Low-loss SOI photonic wires and ring resonators fabricated with deep UV lithography," *IEEE Photonics Technology Letters,* vol. 16, pp. 1328-1330, 2004.

[120] J. Niehusmann, A. Vörckel, P. H. Bolivar, T. Wahlbrink, W. Henschel and H. Kurz, "Ultrahigh-quality-factor silicon-on-insulator microring resonator," *Opt. Lett.,* vol. 29, pp. 2861-2863, 2004.

[121] T. Baehr-Jones, M. Hochberg, C. Walker and A. Scherer, "High-Q ring resonators in thin silicon-on-insulator," *Appl. Phys. Lett.,* vol. 85, pp. 3346-3347, 2004.

[122] X. Zhang and X. Li, "Design, fabrication and characterization of optical microring sensors on metal substrates," *J Micromech Microengineering,* vol. 18, pp. 015025, 2008.

[123] R. Grover, T. Ibrahim, T. Ding, Y. Leng, L. Kuo, S. Kanakaraju, K. Amarnath, L. Calhoun and P. Ho, "Laterally coupled InP-based single-mode microracetrack notch filter," *Photonics Technology Letters, IEEE,* vol. 15, pp. 1082-1084, 2003.

[124] R. Boeck, N. A. Jaeger, N. Rouger and L. Chrostowski, "Series-coupled silicon racetrack resonators and the Vernier effect: theory and measurement," *Optics Express,* vol. 18, pp. 25151-25157, 2010.

[125] H. Haus, W. Huang, S. Kawakami and N. Whitaker, "Coupled-mode theory of optical waveguides," *Lightwave Technology, Journal Of,* vol. 5, pp. 16-23, 1987.

[126] M. Rothschild, T. M. Bloomstein, T. H. Fedynyshyn, R. R. Kunz, V. Liberman, M. Switkes, N. N. Efremow, S. T. Palmacci, J. H. Sedlacek and D. E. Hardy, "Recent trends in optical lithography," *Lincoln Laboratory Journal,* vol. 14, pp. 221-236, 2003.

[127] K. Ronse, "Optical lithography-a historical perspective," *Comptes Rendus Physique,* vol. 7, pp. 844-857, 2006.

[128] H. Li, "Refractive index of silicon and germanium and its wavelength and temperature derivatives," *Journal of Physical and Chemical Reference Data,* vol. 9, pp. 561-658, 1980.

[129] D. G. Rabus, *Integrated Ring Resonator: The Compendium.* New York: Springer, 1st ed., 2007.

[130] K. Okamoto, *Fundamentals of Optical Waveguides.* Burlington, MA: Elsevier, 2010.

[131] A. Yariv and P. Yeh, *Photonics: Optical Electronics in Modern Communications (the Oxford Series in Electrical and Computer Engineering).* Oxford University Press, Inc., 2006.

[132] E. Kapon, J. Katz and A. Yariv, "Supermode analysis of phase-locked arrays of semiconductor lasers," *Opt. Lett.,* vol. 9, pp. 125-127, 1984.

[133] A. B. Fallahkhair, K. S. Li and T. E. Murphy, "Vector finite difference mode solver for anisotropic dielectric waveguides," *J. Lightwave Technol.,* vol. 26, pp. 1423-1431, 2008.

[134] (2014). *Photonics Research Lab at the University of Maryland;*. Available: http://www.photonics.umd.edu/software/wgmodes/.

[135] R. Scarmozzino, A. Gopinath, R. Pregla and S. Helfert, "Numerical techniques for modeling guided-wave photonic devices," *Selected Topics in Quantum Electronics, IEEE Journal Of,* vol. 6, pp. 150-162, 2000.

[136] D. Gallagher, "Photonic CAD matures," *IEEE LEOS NewsLetter,* pp. 8-14, Feb. 2008.

[137] Y. Chung and N. Dagli, "Explicit finite difference beam propagation method: application to semiconductor rib waveguide Y-junction analysis," *Electron. Lett.,* vol. 26, pp. 711-713, 1990.

[138] G. Sztefka and H. Nolting, "Bidirectional eigenmode propagation for large refractive index steps," *Photonics Technology Letters, IEEE,* vol. 5, pp. 554-557, 1993.

[139] (2013). *3D Electromagnetic Simulation software*. Available: www.cst.com.

[140] J. J. Moré and D. C. Sorensen, "Computing a trust region step," *SIAM Journal on Scientific and Statistical Computing,* vol. 4, pp. 553-572, 1983.

[141] S. Koziel and S. Ogurtsov, "Simulation-driven optimization approach for fast design of integrated photonic components," in *30th Annual Review of Progress in Applied Computational Electromagnetic,* Jacksonville, FL, 2014, pp. 679-684.

[142] K. J. Vahala, "Optical microcavities," *Nature,* vol. 424, pp. 839-846, 2003.

[143] R. Mansoor, S. Koziel, H. Sasse and A. Duffy, "Crosstalk suppression bandwidth optimisation of a vertically coupled ring resonator add/drop filter," *IET Optoelectronics*, vol. 9, pp. 30-36, 2015.

[144] W. McKinnon, D. Xu, C. Storey, E. Post, A. Densmore, A. Delâge, P. Waldron, J. Schmid and S. Janz, "Extracting coupling and loss coefficients from a ring resonator," *Optics Express*, vol. 17, pp. 18971-18982, 2009.

[145] O. S. Ahmed, M. A. Swillam, M. H. Bakr and Xun Li, "Efficient design optimization of ring resonator-based optical filters," *Lightwave Technology, Journal Of*, vol. 29, pp. 2812-2817, 2011.

[146] O. Schwelb, "Transmission, group delay, and dispersion in single-ring optical resonators and add/drop filters-a tutorial overview," *Lightwave Technology, Journal Of*, vol. 22, pp. 1380-1394, 2004.

[147] Y. Kokubun and T. Kato, "Series-coupled and parallel-coupled add/drop filters and FSR extension," in *Photonic Microresonator Research and Applications*Anonymous Springer, 2010, pp. 87-113.

[148] O. Schwelb, "Generalized analysis for a class of linear interferometric networks. I. Analysis," *Microwave Theory and Techniques, IEEE Transactions On*, vol. 46, pp. 1399-1408, 1998.

[149] S. J. Mason, *Feedback Theory: Further Properties of Signal Flow Graphs.* Research Laboratory of Electronics, Massachusetts Institute of Technology, 1956.

[150] I. S. Hidayat, Y. Toyota, O. Torigoe, O. Wada and R. Koga, "Application of transfer matrix method with signal flow-chart to analyze optical multi-path ring-resonator," *Mem.Fac.Eng.Okayama Univ*, vol. 36, pp. 73-82, 2002.

[151] P. Yupapin, P. Saeung and C. Li, "Characteristics of complementary ring-resonator add/drop filters modeling by using graphical approach," *Opt. Commun.*, vol. 272, pp. 81-86, 2007.

[152] Schwelb, O., and Frigyes,I., "A design for a high finesse parallel-coupled microring resonator filter," *Microwave and Optical Technology Letters*, vol. 38, pp. 125-129, 2003.

[153] W. Ye, K. Goshu and A. Tam, "Vertically coupled si-based ring resonators for sensing applications," in *Group IV Photonics (GFP), 7th IEEE International Conference*, 2010, pp. 66-68.

[154] R. D. Mansoor, H. Sasse, M. A. Asadi, S. J. Ison and A. Duffy, "Over coupled ring resonator-based add/drop filters," *Quantum Electronics, IEEE Journal Of*, vol. 50, pp. 598-604, 2014.

[155] X. Yan, C. Ma, Y. Xu, X. Wang, H. Li and D. Zhang, "Characteristics of vertical bent coupling between straight and curved rectangular optical waveguides," *Optik-International Journal for Light and Electron Optics*, vol. 116, pp. 397-403, 2005.

[156] W. Yuhai, Q. Zhengkun, W. Chunxu and W. Lizhong, "Analysis of characteristics of vertical coupling microring resonator," *Journal of Semiconductors*, vol. 34, pp. 074012, 2013.

[157] X. Cai, D. Huang and X. Zhang, "Numerical analysis of polarization splitter based on vertically coupled microring resonator," *Optics Express*, vol. 14, pp. 11304-11311, 2006.

[158] E. A. Marcatili, "Dielectric rectangular waveguide and directional coupler for integrated optics," *Bell System Technical Journal*, vol. 48, pp. 2071-2102, 1969.

[159] T. G. Kolda, R. M. Lewis and V. Torczon, "Optimization by direct search: New perspectives on some classical and modern methods," *SIAM Rev,* vol. 45, pp. 385-482, 2003.

[160] S. Koziel, "Multi-fidelity multi-grid design optimization of planar microwave structures with Sonnet," *International Review of Progress in Applied Computational Electromagnetics*, pp. 26-29, 2010.

[161] W. Shi, X. Wang, W. Zhang, H. Yun, C. Lin, L. Chrostowski and N. Jaeger, "Grating-coupled silicon microring resonators," *Appl. Phys. Lett.*, vol. 100, pp. 121118-121118-4, 2012.

[162] Y. M. Kang, A. Arbabi and L. L. Goddard, "Engineering the spectral reflectance of microring resonators with integrated reflective elements," *Optics Express*, vol. 18, pp. 16813-16825, 2010.

[163] A. E. Atia and A. E. Williams, "Narrow-bandpass waveguide filters," *Microwave Theory and Techniques, IEEE Transactions On*, vol. 20, pp. 258-265, 1972.

[164] R. Mansoor, H. Sasse, S. Ison and A. Duffy, "Crosstalk bandwidth of grating-assisted ring resonator add/drop filter," *Opt. Quant. Electron.*, vol. 47, pp. 1127-1137, 2015.

[165] (2014). *ASPIC design software*. Available: www.aspicdesign.com.

[166] S. Xiao, M. H. Khan, H. Shen and M. Qi, "Modeling and measurement of losses in silicon-on-insulator resonators and bends," *Optics Express*, vol. 15, pp. 10553-10561, 2007.

[167] (2014). *Ruby Programming language*. Available: https//:www.ruby-lang.org.

[168] S. P. Ugale and V. Mishra, "Modeling and characterization of fiber Bragg grating for maximum reflectivity," *Optik-International Journal for Light and Electron Optics,* vol. 122, pp. 1990-1993, 2011.

[169] A. Melloni, A. Canciamilla, G. Morea, F. Morichetti, A. Samarelli and M. Sorel, "Design kits and circuit simulation in integrated optics," in *Integrated Photonics Research, Silicon and Nanophotonics,* Monterey, CA, 2010, pp. Paper JTuB24.

[170] M. Smit, X. Leijtens, H. Ambrosius, E. Bente, J. van der Tol, B. Smalbrugge, T. de Vries, E. Geluk, J. Bolk and R. van Veldhoven, "An introduction to InP-based generic integration technology," *Semiconductor Science and Technology,* vol. 29, pp. 083001, 2014.

APPENDICES

Appendix A: SFG METHOD FOR PARALLEL COUPLED OADMS

Filter characteristics such as higher selectivity and better Out-of-Band Rejection Ratio (OBRR) can be obtained by increasing the order of the filter ($N > 2$). Mason's rule is applicable to any value of N. For N rings in parallel, the number of forward paths is equal to N, while the number of closed loops is $\sum_{i=1}^{N} i$. The general form of the transfer function is:

$$G = \frac{B(X)}{A(X)} \tag{A -1}$$

Where,

$$A(X) = 1 + x_1 \sum_{m=0}^{N} [a_m] {x_2}^{2\times m} + {x_1}^2 \sum_{m2=0}^{N-1} [a_{m2}] {x_2}^{2\times m2} + \cdots + {x_1}^n . \sum_{mn=0}^{N-n} [a_{mn}] \cdot {x_2}^{2\times mn} \tag{A-2}$$

$n = 3, \ldots, N$

$$B(X) = {x_1}^{1/2} \sum_{m=1}^{N} b_{1m} . {x_2}^{m-1} + {x_1}^{3/2} \sum_{m=1}^{N} b_{2m} {x_2}^{m-1} + \cdots + {x_1}^{\frac{N+1}{2}} \sum_{m=1}^{N} b_{nm} {x_2}^{m-1} \tag{A-3}$$

After finding the general form, consider the case of two ring resonators, N=2.

$$G = \frac{b_{11}{x_1}^{1/2} + b_{12}{x_1}^{1/2}{x_2}^2 + b_{21}{x_1}^{3/2} + b_{22}{x_1}^{3/2}{x_2}^2}{1 + a_{11}x_1 + a_{12}x_1{x_2}^2 + a_2{x_1}^2} \quad \text{(A.4)}$$

$b_{11} = -{k_1}^2$

$b_{12} = -{t_1}^2\,{k_2}^2$

$b_{21} = {t_2}^2{k_1}^2$

$b_{22} = {k_1}^4{k_2}^2 + {t_1}^4{k_2}^2$

$a_{11} = -({t_1}^2 + {t_2}^2)$

$a_{12} = -{k_1}^2{k_2}^2$

$a_{22} = {t_1}^2{t_2}^2$

The intensity response is obtained by multiplying G by G^*, and the result is shown in (A.5)

$$|G|^2 = \frac{M}{D} \quad \text{(A.5)}$$

$M = B + B_3\,cos\beta L_r + B_4\,cos2\beta L_c + B_5\;cos(\beta L_r + 2\beta L_c) + B_6\,cos(\beta L_r - 2\beta L_c)$

$D = A_1 + A_2\,cos\beta L_r + A_3\,cos2\beta L_r + A_4\,cos2\beta L_c + A_5\;cos(\beta L_r + 2\beta L_c\,) +$

$A_6\,cos(\beta L_r - 2\beta L_c)$

Where,

$B = \left({b_{11}}^2 + {b_{12}}^2\right)e^{-\alpha L_r} + ({b_{21}}^2 + {b_{22}}^2)e^{-3\alpha L_r}$

$B_3 = (2b_{11}b_{21} + 2b_{12}b_{22})\;e^{-2\alpha L_r}$

$$B_4 = (2b_{11}b_{21}e^{-\alpha L_r} + 2b_{12}b_{22}e^{-3\alpha L_r})$$

$$B_5 = 2b_{11}b_{21}e^{-2\alpha L_r}$$

$$B_6 = 2b_{12}b_{22}e^{-2\alpha L_r}$$

And,

$$A_1 = 1 + {a_{12}}^2 e^{-2\alpha L_r} + {a_{11}}^2 e^{-2\alpha L_r} + {a_2}^2 e^{-4\alpha L_r}$$

$$A_2 = 2a_{11}e^{-\alpha L_r} + 2a_{11}a_2 e^{-3\alpha L_r}$$

$$A_3 = 2a_2 e^{-2\alpha L_r}$$

$$A_4 = 2a_{11}a_{12}e^{-2\alpha L_r}$$

$$A_5 = 2a_{12}e^{-\alpha L_r}$$

$$A_6 = 2a_{12}a_2 e^{-3\alpha L_r}$$

The phase constant is $\beta = 2\pi n_{eff}$, and the condition that the phase constants for the bus and bent waveguide sections are the same is considered. However, there is a small difference between the effective refractive indices of straight and curved waveguides since the field in the bent waveguide tends to propagate near the outer wall (rather than the centre as in the bus waveguide) which means a lower velocity and higher effective refractive index than in the bent waveguide; this is a relatively small difference [130].

Appendix B: RUBY CODE FOR SIDEWALL ROUGHNESS GENERATION

```
#!/usr/local/bin/ruby -w
#
# Program to generate a collection of roughness voxels to add
# to a ring resonator.  It should produce a .OBJ file for import
# into CST.

# 2 dimensional point
class BiPoint

  attr_accessor :x, :y

  include Comparable

  def <=>(other)
    [self.x, self.y] <=> [other.x, other.y]
  end

  def initialize(x,y)
    @x, @y = x,y
  end

  # city block (Manhattan) distance function
  def manhattan(other)
    distance = (other.x - @x).abs + (other.y - @y).abs
    return distance
  end

  # Check points are the same (x,y)
  def ==(other)
    return ((other.x == @x) and (other.y == @y))
  end


  # Vector addition
  def +(other)
    return BiPoint.new(@x + other.x, @y + other.y)
  end

  # reduce vector by scale factor. Raises
  # ZeroDivisionError if k is zero.
  def /(k)
    raise ZeroDivisionError if k.zero?
    return BiPoint.new(@x / k, @y / k)
  end

end

# 3 dimensional point
class TriPoint

  attr_accessor :x, :y, :z
```

```
  include Comparable

  def <=>(other)
    [self.x, self.y, self.z] <=> [other.x, other.y, other.z]
  end

  def initialize(x,y,z)
    @x, @y, @z = x,y,z
  end

  # City Block distance but in 3-space.
  # Cheaper to compute than Euclidean, but of
  # sufficient utility.
  def manhattan(other)
    distance = (other.x - @x).abs + (other.y - @y).abs + (other.z -
@z).abs
    return distance
  end

  # Map distance.  There doesn't seem to be a good
  # single word for horizontal distance in English.
  # (Can't think of one in Esperanto either.)
  # Can't really call it map_manhatten because ruby
  # uses map as in {map, filter, reduce}.
  def horizontal_manhattan(other)
    distance = (other.x - @x).abs + (other.y - @y).abs
    return distance
  end

  # vertical distance.
  def vertical_manhattan(other)
    distance = (other.z - @z).abs
    return distance
  end

  # Check if they are the same point.
  # Note, if they are floats the value of this may be
  # almost nil.
  def ==(other)
    return ((other.x == @x) and (other.y == @y) and (other.z = @z))
  end

  # Add two vectors together
  def +(other)
    return TriPoint.new(@x + other.x, @y + other.y, @z + other.z)
  end

  # Reduce vector by a scale factor.
  def /(k)
    raise ZeroDivisionError if k.zero?
    return TriPoint.new(@x / k, @y / k, @z / k)
  end
```

```
  def to_vertex
     "v #{@x.to_f} #{@y.to_f} #{@z.to_f}"
  end

end



class Grid

  VERBOSITY = 5 # controls diagnostic output ...
  @@verbose = :verbose

  def Grid.verbose(value)
    @@verbose = value
  end

  def Grid.verbose?
    @@verbose == :verbose
  end

  def verbose?
    Grid.verbose?
  end

  # convert from the real space to grid co-ordinates.
  # which are integers.
  #
  def scale_to_grid(x,y)
    c = (((x - @xmin)/@step) + 0.5).to_i
    r = (((y - @ymin)/@step) + 0.5).to_i
    return r, c
  end

  # Set up a grid between (minx,miny) and (maxx,maxy)
  # spaced (equally in both directions) by step
  def initialize(minx, miny, maxx, maxy, step)
    # The grid is actually a collection of
    # TriPoints.
    @xmin = minx
    @ymin = miny
    @xmax = maxx
    @ymax = maxy
    @step = step

    @grid = []
    Logger.logwrite "@step = #{@step}" if self.verbose?

    y = @ymin
    @rows = 0
    while (y <= @ymax)
      Logger.logwrite "initialize: y=#{y}" if self.verbose?
      @rows += 1
      @columns = 0
```

```
      x = @xmin
      while (x <= @xmax)
        if @@verbose == :verbose
          if VERBOSITY == 10
            Logger.logwrite "initialize: (xmin,ymin) <= (x, y) <=
(xmax,ymax)"
            Logger.logwrite "..... (#{@xmin},#{@ymin} <= (#{x},
#{y}) <= (#{@xmax},#{@ymax})"
            Logger.logwrite "@step = #{@step}"
          end
        end
        @columns += 1
        @grid << TriPoint.new(x,y,0)
        x += @step
      end
      y += @step
    end

  end


  # Populate the grid at k with v.  If there is already
  # data there it is added to unless op is :replace, or
  # something else.  Something else should use method missing.
  # Probably on TriPoint.
  def populate(k,v, op=:add)
     Logger.logwrite "populate: k: #{k.inspect} => #{v}" if self.verbose?
     r,c = scale_to_grid(k.x, k.y)
     Logger.logwrite "(c,r) is (#{c},#{r})" if self.verbose?
     irc = index(r,c)
     Logger.logwrite "@grid[#{irc}] = #{@grid[irc]}" if self.verbose?
     p0 = BiPoint.new(@grid[irc].x,
                      @grid[irc].y)
     # Check we are looking at the right place
     if (p0.manhattan(k) < (2 * @step))
       case op
       when :add
         #Just move the point up.
         @grid[irc] += TriPoint.new(0,0,v)
       when :replace
         @grid[irc] = TriPoint.new(k.x,k.y,v)
       else
         @grid[irc].send(:op, k, v)
       end
     else
       # Not looking in the right place
       if @@verbose == :vebose
         Logger.logwrite "KLAXON!!!"
         Logger.logwrite "r = #{r}, c = #{c}, p0 = #{p0.inspect},"
         Logger.logwrite "@grid[index(r,c)] =
#{@grid[index(r,c)].inspect}"
       end
     end
  end
```

```
  # Given a row and column, find the entry in Grid, which
  # is a normal array, not 2D
  def index(r,c)
    (r * @columns) + c
  end

  # In .OBJ format, vertices are numbered from 1, not zero.
  def vertex_index(r,c)
    index(r,c) + 1
  end

  # Make a Coarser grid, so that spikiness in the grid
  # is smoothed out.
  def subsample(k)
    Grid.verbose(@@verbose)
    subgrid = Grid.new(@xmin, @ymin, @xmax, @ymax, @step * k)
    0.step(@rows,k) do |r|
      0.step(@columns,k) do |c|
         sum = 0
         (0...k).each do |i|
           (0...k).each do |j|
             idx = index(r+i, c+j)
             sum += @grid[idx].z if @grid[idx]
           end
         end
         p =  @grid[index(r,c)]
         subgrid.populate(p, sum)
      end
    end
    return subgrid
  end

  # Outputs the grid in .OBJ format.
  def display_grid(outfile)
    if @@verbose == :verbose
      Logger.logwrite "@columns = #{@columns}"
      Logger.logwrite "@rows = #{@rows}"
      Logger.logwrite "product @rows * @columns = #{@rows * @columns}"
      Logger.logwrite "\nEND OF CALCULATIONS\n"
    end
    open(outfile, "w") do |outf|
      @grid.each do |p|
        vertex = p.to_vertex
        Logger.logwrite vertex if @@verbose == :verbose
        outf.puts vertex
      end

      r = 0
      while (r < (@rows-1))
        c = 0
        while (c < (@columns-1))
          face =  "f #{vertex_index(r,c)} #{vertex_index(r,c+1)}
#{vertex_index(r+1,c+1)} #{vertex_index(r+1,c)}"
```

```
          Logger.logwrite face if @@verbose == :verbose
          outf.puts face
          c += 1
        end
        r += 1
      end

    end # close file
  end

end

# define a rough surface over a hollow cylinder.
class Roughness

  # Points list for a cuboid.
  # The front face is 1,2,3,4, the back face is
  # 5,6,7,8. We want this in triangles for best(?)
  # meshing -- programs like Anim8or, and other .OBJ
  # loaders seem to require it.
  #    7--6
  #    |\ |
  #    | \|
  # 7--3--2--6--7
  # |\ |\ |\ |\ |
  # | \| \| \| \|
  # 8--4--1--5--8
  #    |\ |
  #    | \|
  #    8--5
  #
  CUBENET=[[1,2,3],
           [1,3,4],
           [2,6,7],
           [2,7,3],
           [4,3,7],
           [4,7,8],
           [5,6,2],
           [5,2,1],
           [8,7,6],
           [8,6,5],
           [5,1,4],
           [5,4,8]]
  #
  # Setup parameters for the the surface.
  # r0 = internal diamere of the cylinder.
  # r1 = external diameter of the cylinder.
  # h  = height of the cylinder
  # dr = max depth of the roughness to penetrate
  #      the surface of the cylinder.
  def initialize(r0, r1, h1, h2, dr)
    @r0 = r0
    @r1 = r1
    @h1 = h1
```

```
  @h2 = h2
  @dr = dr
  @vertex_list = []
  @face_list = []
  @cube_count = 0
end

# Convert polar to rectangular co-ordinates, return as array.
# We don't need the height for this purpose as we are assuming the
# ring is horizontal.
def rectangular(r, theta)
  return r*Math.cos(theta), r*Math.sin(theta)
end

# setup probability of a suface voxel being roughened, and
# the number of samples per degree.
def set_roughness_params(density = 0.25,
                         angular_granularity = Math::PI/180.0,
                         vertical_granularity = 1.0 * (@h2 - @h1))
  @density = density
  @angular_granularity = angular_granularity
  @vertical_granularity = vertical_granularity
end


# Create a list of voxels by iterating around and over the
# inner and outer vertical surfaces of the ring.
# For now we don't bother with the top and bottom walls of
# the guide.
def create_list_of_voxels
  theta = 0
  toggle = 0
  while theta < 2.0 * Math::PI
    h = @h1
    while h < @h2
      # p = Kernel.rand()
      # if p < @density
      if toggle == 1
        create_inside_voxel(h,theta)
        @cube_count += 1
      end

      # p = Kernel.rand()
      # if p < @density
      if toggle == 1
        create_outside_voxel(h,theta)
        @cube_count += 1
      end
      h += @vertical_granularity
    end

    toggle = (toggle + 1) % 2
    theta += @angular_granularity
  end
```

```
  end

  # Create a voxel on the inside surface of the ring
  def create_inside_voxel(h, theta)
    p = Array.new(8)
    x,y = rectangular(@r0,theta)
    p[0] = TriPoint.new(x,y,h)
    x,y = rectangular(@r0,theta + @angular_granularity)
    p[1] = TriPoint.new(x,y,h)
    x,y = rectangular(@r0,theta + @angular_granularity)
    p[2] = TriPoint.new(x,y,h+@vertical_granularity)
    x,y = rectangular(@r0,theta)
    p[3] = TriPoint.new(x,y,h+@vertical_granularity)
    x,y = rectangular(@r0+@dr,theta)
    p[4] = TriPoint.new(x,y,h)
    x,y = rectangular(@r0+@dr,theta + @angular_granularity)
    p[5] = TriPoint.new(x,y,h)
    x,y = rectangular(@r0+@dr,theta + @angular_granularity)
    p[6] = TriPoint.new(x,y,h+@vertical_granularity)
    x,y = rectangular(@r0+@dr,theta)
    p[7] = TriPoint.new(x,y,h+@vertical_granularity)

    p.each do |point|
      @vertex_list.push(point.to_vertex)
    end

    CUBENET.each do |row|
      @face_list.push("f " + row.map{|x| x + (8 * @cube_count)}.join("
"))
    end

  end

  # Create a voxel on the outside surface of the ring
  def create_outside_voxel(h, theta)
    p = Array.new(8)
    x,y = rectangular(@r1,theta)
    p[0] = TriPoint.new(x,y,h)
    x,y = rectangular(@r1,theta + @angular_granularity)
    p[1] = TriPoint.new(x,y,h)
    x,y = rectangular(@r1,theta + @angular_granularity)
    p[2] = TriPoint.new(x,y,h+@vertical_granularity)
    x,y = rectangular(@r1,theta)
    p[3] = TriPoint.new(x,y,h+@vertical_granularity)
    x,y = rectangular(@r1-@dr,theta)
    p[4] = TriPoint.new(x,y,h)
    x,y = rectangular(@r1-@dr,theta + @angular_granularity)
    p[5] = TriPoint.new(x,y,h)
    x,y = rectangular(@r1-@dr,theta + @angular_granularity)
    p[6] = TriPoint.new(x,y,h+@vertical_granularity)
    x,y = rectangular(@r1-@dr,theta)
    p[7] = TriPoint.new(x,y,h+@vertical_granularity)

    p.each do |point|
```

```
      @vertex_list.push(point.to_vertex)
    end

    CUBENET.each do |row|
      @face_list.push("f " + row.map{|x| x + (8 * @cube_count)}.join("
"))
    end

  end

  def create_alias_wavefront_file(filename)
    File.open(filename,"w") do |fp|
      @vertex_list.each do |vertex|
        fp.puts vertex
      end
      @face_list.each do |face|
        fp.puts face
      end
    end
  end

end

class Roughness2 < Roughness
  # Points list for a cuboid with no ends -- part of a cylinder.
  # The missing front face is 1,2,3,4, the missing back face is
  # 5,6,7,8. We want this in triangles for best(?)
  # meshing -- programs like Anim8or, and other .OBJ
  # loaders seem to require it.
  #    7--6
  #    |\ |
  #    | \|
  # 7--3--2--6..7
  # |\ |  |\ |  .
  # | \|  | \|  .
  # 8--4--1--5..8
  #    |\ |
  #    | \|
  #    8--5
  #
  MESHNET=[[2,6,7],
           [2,7,3],
           [4,3,7],
           [4,7,8],
           [5,6,2],
           [5,2,1],
           [5,1,4],
           [5,4,8]]


  # For wiring up the last points
  #    6--7
  #    |\ |
  #    | \|
```

```
  # 6--3--2--7..6
  # |\ |  |\ |  .
  # | \|  | \|  .
  # 5--4--1--8..5
  #    |\ |
  #    | \|
  #    5--8
  #
  CROSSWIRE=[[2,7,6],
             [2,6,3],
             [4,3,6],
             [4,6,5],
             [8,7,2],
             [8,2,1],
             [8,1,4],
             [8,4,5]]

  def initialize(r0, r1, h1, h2, dr)
    super(r0, r1, h1, h2, dr)
  end

  def set_roughness_params(density = 0.25,
                           angular_granularity = Math::PI/180.0,
                           vertical_granularity = 0.1 * (@h2 - @h1))
    @density = density
    @angular_granularity = angular_granularity
  end

  def create_list_of_voxels
    theta = 0
    fcount = 0
    while theta < (2.0 * Math::PI - @angular_granularity)
      x1,y1 = rectangular(@r0 + @dr * Kernel.rand(), theta)
      x2,y2 = rectangular(@r1 - @dr * Kernel.rand(), theta)
      @vertex_list.push(TriPoint.new(x1,y1,@h1).to_vertex)
      @vertex_list.push(TriPoint.new(x1,y1,@h2).to_vertex)
      @vertex_list.push(TriPoint.new(x2,y2,@h2).to_vertex)
      @vertex_list.push(TriPoint.new(x2,y2,@h1).to_vertex)
      fcount += 1
      if fcount >= 2
        @cube_count += 1
      end
      theta += @angular_granularity
    end

    @cube_count.times do |count|
      MESHNET.each do |row|
        @face_list.push("f " + row.map{|x| x + (4 * count)} .join(" "))
      end
    end
    #join front and back faces.  Hope this works
   # MESHNET.each do |row|
   #   @face_list.push("f " + row.map{|x| (x + (4 * @cube_count)) % (4*
(@cube_count+1)) + 1}.join(" "))
```

```
    # end

     # Close off front face
     @face_list.push("f 1 2 3")
     @face_list.push("f 1 3 4")
     # close off back face
      s = "f "
     [0,-1,-2].each do |count|
       v = @vertex_list.size + count
       s = s + v.to_s + " "
     end
     @face_list.push(s)
     [0,-3,-2].each do |count|
       v = @vertex_list.size + count
       s = s + v.to_s + " "
     end
     @face_list.push(s)

     puts "@face_list size is #{@face_list.size}"
     puts "@vertex_list size is #{@vertex_list.size}"
     puts "@cube_count is #{@cube_count}"
     puts "4 * (@cube_count+1) is #{4 * (@cube_count+1)}"
   end

end


class Roughness3 < Roughness
   # Points list for a cuboid with no ends -- part of a cylinder.
   # The missing front face is 1,2,3,4, the missing back face is
   # 5,6,7,8. We want this in triangles for best(?)
   # meshing -- programs like Anim8or, and other .OBJ
   # loaders seem to require it.
   #    7--6
   #    |\ |
   #    | \|
   # 7--3--2--6..7
   # |\ |  |\ |  .
   # | \|  | \|  .
   # 8--4--1--5..8
   #    |\ |
   #    | \|
   #    8--5
   #
   MESHNET=[[2,6,7],
            [2,7,3],
            [4,3,7],
            [4,7,8],
            [5,6,2],
            [5,2,1],
            [5,1,4],
            [5,4,8]]
```

```
# For wiring up the last points
#    6--7
#    |\ |
#    | \|
# 6--3--2--7..6
# |\ |  |\ |  .
# | \|  | \|  .
# 5--4--1--8..5
#    |\ |
#    | \|
#    5--8
#
CROSSWIRE=[[2,7,6],
          [2,6,3],
          [4,3,6],
          [4,6,5],
          [8,7,2],
          [8,2,1],
          [8,1,4],
          [8,4,5]]

def initialize(r0, r1, h1, h2, dr)
  super(r0, r1, h1, h2, dr)
end

def set_roughness_params(density = 0.25,
                         angular_granularity = Math::PI/180.0,
                         vertical_granularity = (@h2 - @h1))
  @density = density
  @angular_granularity = angular_granularity
end

def create_list_of_voxels
  theta = 0
  fcount = 0
  toggle = 0
  while theta < (2.0 * Math::PI - @angular_granularity)
    x1,y1 = rectangular(@r0 + (@dr * (toggle >> 1)), theta)
    x2,y2 = rectangular(@r1 - (@dr * (toggle >> 1)), theta)
    @vertex_list.push(TriPoint.new(x1,y1,@h1).to_vertex)
    @vertex_list.push(TriPoint.new(x1,y1,@h2).to_vertex)
    @vertex_list.push(TriPoint.new(x2,y2,@h2).to_vertex)
    @vertex_list.push(TriPoint.new(x2,y2,@h1).to_vertex)
    fcount += 1
    if fcount >= 2
      @cube_count += 1
    end
    theta += @angular_granularity
    toggle = (toggle + 1) % 4
  end

  @cube_count.times do |count|
    MESHNET.each do |row|
      @face_list.push("f " + row.map{|x| x + (4 * count)} .join(" "))
```

```
      end
    end
    #join front and back faces.  Hope this works
    # MESHNET.each do |row|
    #   @face_list.push("f " + row.map{|x| (x + (4 * @cube_count)) % (4*
(@cube_count+1)) + 1}.join(" "))
    # end

    # Close off front face
    @face_list.push("f 1 2 3")
    @face_list.push("f 1 3 4")
    # close off back face
     s = "f "
    [0,-1,-2].each do |count|
      v = @vertex_list.size + count
      s = s + v.to_s + " "
    end
    @face_list.push(s)
    [0,-3,-2].each do |count|
      v = @vertex_list.size + count
      s = s + v.to_s + " "
    end
    @face_list.push(s)

    puts "@face_list size is #{@face_list.size}"
    puts "@vertex_list size is #{@vertex_list.size}"
    puts "@cube_count is #{@cube_count}"
    puts "4 * (@cube_count+1) is #{4 * (@cube_count+1)}"
  end

end




class GridToObj
  @@verbose = :verbose
  @@scaling = :linear
  # Set the verbose flag to the supplied symbol
  def GridToObj.verbose(sym)
    @@verbose = sym
  end

  def GridToObj.verbose?
    @@verbose == :verbose
  end

  # Read the data in a YAML file, and output the
  # grid of points as a .OBJ file.
  def GridToObj.process(*args)
    output_names = []
    if @@verbose == :verbose
      Logger.logwrite "called GridToObj.process(#{args.join(", ")})\n"
```

```
    end
    args.flatten!
    if args[0] == "--log"
      @@scaling = :logarithmic
      args.shift
    end
    args.each do |name|
      # Having the count overcomplicates things. Just follow
      # the Unix philosophy.
      # count = 1
      open(name, "r") do |fp|
        Logger.logwrite "process: About to create grid\n" if @@verbose ==
:verbose
        outname = name.sub(/.ya?ml$/, ".obj")
        Logger.logwrite "process: Will create #{outname}\n" if @@verbose
== :verbose
        YAML::load_documents(fp) do |yaml_data|
          grid = nil
          Logger.logwrite "yaml_data is \n#{yaml_data.inspect}" if
self.verbose?
          grid = self.create_grid(yaml_data)
          Logger.logwrite "About to write grid to #{outname}\n" if
self.verbose?
          grid.display_grid(outname)
          Logger.logwrite "grid created.\n" if self.verbose?
          output_names << outname
          # count += 1
        end
      end
    end
    return output_names
  end


  # Diagnostic routine for logging, principally.
  def self.inspect_data(raw_data)
    begin
      Logger.logwrite "create_grid: raw_data.class
is:\n#{raw_data.class}\n" if self.verbose?
      Logger.logwrite "create_grid: raw_data is:\n#{raw_data.inspect}\n"
if self.verbose?
    rescue => e
      Logger.logwrite "attempt to print raw_data.inspect failed with
#{e.message}"
      raise
    end
  end


  #
  def self.create_grid(raw_data)
    self.inspect_data(raw_data)
    Logger.logwrite "create_grid: call DataSet.new()..." if self.verbose?
    #Create the collection of points.
```

```
    data = DataSet.new()
    Logger.logwrite "create_grid: verify data is rectangle"
    data.check_is_rectangular(raw_data)
    data.add_array_to_dataset(raw_data,@@scaling)
    ysize = raw_data.size
    xsize = raw_data[0].size
    Logger.logwrite "create_grid: calling Grid.verbose()" if
self.verbose?
    Grid.verbose(@@verbose)
    Logger.logwrite "create_grid: calling Grid.new(...)" if self.verbose?
    grid = Grid.new(0, 0, xsize-1, ysize-1, 1)
    data.each do |point|
      Logger.logwrite "create_grid: point is #{point}" if self.verbose?
      grid.populate(BiPoint.new(point.x, point.y), point.z, :replace)
    end
    return grid
  end

end

class Logger
  @@logfile = nil
  def self.logwrite(*args)
    unless @@logfile.nil?
      open(@@logfile, "a") do |fp|
        fp.puts args
      end
    end
  end

  def self.set_logfile(file)
    @@logfile = file
  end
end

if __FILE__ == $0

  # Dimensions from slotted_ring_post_cst_advice....
  r = 5.0
  s = 1.0
  h = 1.0
  hg = 0.25
  wr = 0.45
  ws = 0.0

  r1 = r - ((1-s) * wr) - ws
  r0 = r1 - (s * wr)

  roughness = Roughness.new(r0, r1, h, h + hg, (s*wr)/20.0)
  roughness.set_roughness_params
  roughness.create_list_of_voxels
  roughness.("roughness_object.OBJ")

  roughness2 = Roughness2.new(r0, r1, h, h + hg, (s*wr)/20.0)
```

```
  roughness2.set_roughness_params
  roughness2.create_list_of_voxels
  roughness2.create_alias_wavefront_file("roughness_object2.OBJ")

  roughness3 = Roughness3.new(r0, r1, h, h + hg, (s*wr)/20.0)
  roughness3.set_roughness_params
  roughness3.create_list_of_voxels
  roughness3.create_alias_wavefront_file("roughness_object3.OBJ")
end
```